AEDC-TR-75-40
AFATL-TR-75-52
240136

EXPERIMENTAL MAGNUS AND STATIC STABILITY CHARACTERISTICS OF BALLISTIC PROJECTILES WITH VARIOUS BOATTAIL ANGLES AND LENGTHS AT MACH NUMBERS FROM 0.5 THROUGH 2.5

PROPULSION WIND TUNNEL FACILITY
ARNOLD ENGINEERING DEVELOPMENT CENTER
AIR FORCE SYSTEMS COMMAND
ARNOLD AIR FORCE STATION, TENNESSEE 37389

August 1975

Final Report for Period October 25 – 31, 1974

Prepared for

AIR FORCE ARMAMENT LABORATORY (DLDL)
EGLIN AFB, FLORIDA 32542

29

REPORT DOCUMENTATION PAGE		READ INSTRUCTIONS BEFORE COMPLETING FORM
1 REPORT NUMBER AEDC-TR-75-40 AFATL-TR-75-52	2 GOVT ACCESSION NO.	3. RECIPIENT'S CATALOG NUMBER
4 TITLE (and Subtitle) EXPERIMENTAL MAGNUS AND STATIC STABILITY CHARACTERISTICS OF BALLISTIC PROJECTILES WITH VARIOUS BOATTAIL ANGLES AND LENGTHS AT MACH NUMBERS FROM 0.5 THROUGH 2.5		5. TYPE OF REPORT & PERIOD COVERED Final Report - October 25-31, 1974 6. PERFORMING ORG. REPORT NUMBER
7 AUTHOR(s) Leroy M. Jenke and T. O. Shadow, ARO, Inc.		8. CONTRACT OR GRANT NUMBER(s)
9 PERFORMING ORGANIZATION NAME AND ADDRESS Arnold Engineering Development Center (XO) Air Force Systems Command Arnold Air Force Station, TN 37389		10. PROGRAM ELEMENT, PROJECT, TASK AREA & WORK UNIT NUMBERS Program Element 62602F Project 2547
11 CONTROLLING OFFICE NAME AND ADDRESS Air Force Armament Laboratory (DLDL) Eglin AFB, Florida 32542		12. REPORT DATE August 1975 13. NUMBER OF PAGES
14 MONITORING AGENCY NAME & ADDRESS(if different from Controlling Office)		15. SECURITY CLASS. (of this report) UNCLASSIFIED 15a. DECLASSIFICATION DOWNGRADING SCHEDULE N/A

16 DISTRIBUTION STATEMENT (of this Report)

Approved for public release; distribution unlimited.

DDC

17 DISTRIBUTION STATEMENT (of the abstract entered in Block 20, if different from Report)

18 SUPPLEMENTARY NOTES

Available in DDC

19 KEY WORDS (Continue on reverse side if necessary and identify by block number)

ballistics	Magnus effect
projectiles	static stability
geometry	transonic flow
spin-stabilized ammunition	wind tunnel tests

20 ABSTRACT (Continue on reverse side if necessary and identify by block number)

An experimental investigation was conducted to determine the effect of boattail angle, boattail length, and base diameter on the Magnus-force and moment characteristics of spin-stabilized projectiles. The models were tested at Mach numbers from 0.5 through 1.3 over an angle-of-attack range from -2 to 8 deg. Data were obtained at length Reynolds numbers of 5.7×10^6 and 9.6×10^6 and for spin parameter ($pd/2V_\infty$) values from 0.02 to 0.67 radians.

DD FORM 1 JAN 73 1473 EDITION OF 1 NOV 65 IS OBSOLETE

20. ABSTRACT Continued

Results of this test, as well as results for Mach numbers 1.5, 2.0, and 2.5 from previous tests, are presented showing the effects of Mach number, angle of attack, spin rate, and boattail geometry. The results show that with the exception of the configurations with a constant base diameter (0.7 calibers), increasing the boattail length or increasing the boattail angle generally decreased the slope of the normal-force coefficient curve (C_{N_α}) and the static stability, increased the magnitude of the Magnus-force coefficient derivative ($C_{Y_{p_\alpha}}$), and moved the Magnus center of pressure toward the model base.

NOTICES

When U. S. Government drawings specifications, or other data are used for any purpose other than a definitely related Government procurement operation, the Government thereby incurs no responsibility nor any obligation whatsoever, and the fact that the Government may have formulated, furnished, or in any way supplied the said drawings, specifications, or other data, is not to be regarded by implication or otherwise, or in any manner licensing the holder or any other person or corporation, or conveying any rights or permission to manufacture, use, or sell any patented invention that may in any way be related thereto.

Qualified users may obtain copies of this report from the Defense Documentation Center.

References to named commercial products in this report are not to be considered in any sense as an endorsement of the product by the United States Air Force or the Government.

This report has been reviewed by the Information Office (OI) and is releasable to the National Technical Information Service (NTIS). At NTIS, it will be available to the general public, including foreign nations.

APPROVAL STATEMENT

This technical report has been reviewed and is approved for publication.

FOR THE COMMANDER

LAMAR R. KISSLING
Lt Colonel, USAF
Chief Air Force Test Director, PWT
Directorate of Test

FRANK J. PASSARELLO
Colonel, USAF
Director of Test

PREFACE

The work reported herein was conducted by the Arnold Engineering Development Center (AEDC), Air Force Systems Command (AFSC), for the Naval Weapons Laboratory (NWL) under the sponsorship of the Air Force Armament Laboratory (AFATL), AFSC, under Project Element 62602F, Project 2547. The AFATL project monitor was Mr. E. Sears, and the NWL project monitor was Mr. Gil Graff. The results presented herein were obtained by ARO, Inc. (a subsidiary of Sverdrup & Parcel and Associates, Inc.), contract operator of AEDC, AFSC, Arnold Air Force Station, Tennessee. The tests were conducted under ARO Project No. P41C-52A. The authors of this report were Leroy M. Jenke and T. O. Shadow, ARO, Inc. The final data package was completed on December 20, 1974, and the manuscript (ARO Control No. ARO-PWT-TR-75-12) was submitted for publication on February 10, 1975.

CONTENTS

ILLUSTRATIONS

Figure | Page

1.0 INTRODUCTION

A wind tunnel investigation to obtain the Magnus-force and moment and static stability characteristics of several ballistic projectiles was conducted in the Aerodynamic Wind Tunnel (4T), Propulsion Wind Tunnel Facility (PWT). The tests were part of a continuing investigation (Refs. 1, 2, and 3) by the Naval Weapons Laboratory (NWL) on development of ballistic projectiles. The projectiles must be spin-stabilized, since they are statically unstable. The spin velocity required to stabilize the projectiles tends to induce Magnus effects which can lead to dynamic instabilities that influence the flight path. The objective of this investigation was to determine the effects of boattail angle, boattail length, and base diameter on the Magnus-force and moment characteristics of projectiles. A secondary objective was to obtain the static stability characteristics of each configuration. Data were obtained at Mach numbers from 0.5 to 1.3 at Reynolds numbers (based on a model length of 28.662 in.) of 5.7×10^6 and 9.6×10^6. Some additional results (Ref. 3) are presented for Mach numbers 1.5, 2.0, and 2.5. The angle of attack was varied from -2 to 8 deg, and the values of the spin parameter ($pd/2V_\infty$) ranged from 0.02 to about 0.67 radians.

2.0 APPARATUS AND PROCEDURE

2.1 TEST ARTICLES AND TEST MECHANISM

The aluminum models (Figs. 1 and 2) were supplied by NWL and were the same models used for tests reported in Ref. 3. The models consisted of one common nose section and ten afterbody sections with various boattail lengths and angles as well as various base diameters. All of the models were dynamically

balanced in roll at the VKF so that there would be no vibrational loads on the balance.

The models were mounted on the Magnus-force test mechanism shown in Fig. 3. Basically, the Magnus-force test mechanism has a sting-mounted, water-jacketed, four-component balance with a shell mounted on ball bearings over the water jacket. A two-stage, air-driven turbine is mounted near the forward end of the sting just aft of the model mounting shell. The turbine which can be engaged to the model mounting shell with an air-operated sliding clutch, spins the model to the desired speed, and then is disengaged with the clutch to allow the model to spin freely on the ball bearings. It is estimated that the turbine will produce a starting torque of 50 in.-lb and a developed torque of approximately 100 in.-lb. With this torque output, both finned and nonfinned models can be driven to high spin rates. An air-operated brake is mounted inside the model mounting shell. The brake will provide a static braking moment of 50 in.-lb and a dynamic braking moment of 30 in.-lb. The mechanism is designed to operate under normal-force loads up to 500 lb and axial loads of 125 lb and at maximum spin rates of approximately 25,000 rpm.

2.2 TEST FACILITY

Tunnel 4T is a closed-circuit, continuous flow, variable density tunnel. It is capable of being operated at Mach numbers from 0.20 to 1.30 with a variable stagnation pressure from 2.1 to 23.6 psia at all Mach numbers. The test section is 4 ft square and 12.5 ft long with variable porosity walls (0 to 10 percent). The test section is completely enclosed in a plenum chamber from which the air can be evacuated, thus allowing part of the tunnel airflow to be removed through the

test section walls. This design allows control of wave attenuation and blockage effects. Further control of wall interference effects can be accomplished by converging or diverging the top and bottom test section walls by as much as 0.5 deg. The tunnel model support system consists of a pitch sector, strut, and sting attachment receptacle, and the system has a pitch capability from -12 to 28 deg with respect to the tunnel centerline.

2.3 INSTRUMENTATION

Model forces and moments were measured with the VKF four-component, moment-type, strain-gage balance shown in Fig. 4. The small outrigger side beams of the balance, with semiconductor strain gages, were used to obtain the sensitivity required to measure small side loads while maintaining adequate balance stiffness for the larger pitch loads. When a yawing moment is imposed on the balance, secondary bending moments are induced in the side beams. Thus, the outrigger beams act as mechanical amplifiers, and a normal-force to side-force capability ratio of 20 was achieved for a 500-lb normal-force loading. The uncertainties listed below represent bands for 95 percent of the measurement residuals based on the balance calibration results.

Balance Component	Design Load	Measurement Uncertainty
Normal force, lb	500	±0.13
Pitching moment*, in.-lb	2500	±0.60
Side force, lb	25	±0.07
Yawing moment*, in.-lb	125	±0.20

*About the balance forward moment bridge

The transfer distance to the model moment reference was measured with a precision of ±0.005 in.

The rotational speed of the model was computed from the electrical pulses produced by a ring with reflective surfaces passing two internally mounted infrared-emitting diodes and phototransistors. Only one sensor is required to determine the spin rate; however, with two sensors the roll direction may be determined. This tachometer system can measure spin rates from 0 to 25,000 rpm.

2.4 TEST PROCEDURE

The model was positioned at the desired attitude with the tunnel pitch mechanism and then spun with the turbine. When the desired spin rate was achieved, the air to the turbine was shut off, the clutch was disengaged, and data were recorded as the model spin rate decayed. In most cases, after some data had been taken the data acquisition system was stopped, the brake was applied for a short period of time and released, and then the data acquisition system was again turned on. By using the brake in this manner, the amount of time required to take a set of data was considerably reduced. The model spin rate was monitored using the internally mounted tachometer described in Section 2.3.

3.0 TEST CONDITIONS AND DATA PRECISION

3.1 TEST CONDITIONS

The nominal test conditions for this test are listed below and a complete test summary of the configurations tested is presented in Table 1.

M_∞	p_o, psia	T_o, °R	q_∞, psia	V_∞, ft/sec	$Re \times 10^{-6}$, ft^{-1}
0.50	20.5	560	3.02	566	4.03
0.80	8.8	↓	2.59	873	2.36
0.80	14.9		4.38	873	3.99
0.90	14.1		4.73	968	3.98
0.95	13.9		4.91	1014	4.00
1.00	8.0		2.96	1059	2.34
1.00	13.7		5.07	1059	4.00
1.05	13.5		5.19	1102	3.99
1.10	13.5		5.36	1145	4.02
1.30	8.0		3.42	1303	2.40
1.30	13.5		5.76	1303	4.04

3.2 DATA PRECISION

Uncertainties (bands which include 95 percent of the calibration data) in the basic tunnel parameters, p_o, T_o, and M_∞, were estimated from repeat calibrations of the instrumentation and from the repeatability and uniformity of the test section flow during tunnel calibration. These uncertainties were then used to estimate uncertainties in other free-stream properties using the Taylor series method of error propagation. The uncertainties for the primary test conditions are:

M_∞	$Re \times 10^{-6}$, ft^{-1}	Uncertainty, percent					
		M_∞	p_o	T_o	q_∞	V_∞	Re
0.50	4.03	0.45	0.10	0.39	0.76	0.47	0.62
0.80	3.99	0.32	0.10	0.39	0.40	0.35	0.54
0.90	3.98	0.34	0.10	0.39	0.36	0.35	0.53
0.95	4.00	0.36	0.10	0.39	0.35	0.36	0.53
1.00	4.00	0.40	0.10	0.39	0.35	0.39	0.53
1.05	3.99	0.47	0.10	0.39	0.36	0.43	0.53
1.10	4.02	0.55	0.10	0.39	0.36	0.48	0.53
1.30	4.04	1.14	0.10	0.39	0.28	0.87	0.54

Measurements of the model pitch attitude, including the model-balance deflection, are precise within ±0.07 deg based on repeat calibration. The spin rate precision is estimated to be ±0.5 radians/sec.

The balance uncertainties listed in Section 2.3 were combined with uncertainties in the tunnel parameters, assuming a Taylor series error propagation, to estimate the precision of the aerodynamic coefficients. The following uncertainties are those that were computed for the test conditions ($Re_\ell = 9.6 \times 10^{-6}$) at which almost all of the data were obtained.

COEFFICIENT, PRECISION

		Uncertainty						
M_∞	α, deg	C_N	C_m	C_Y	C_n	C_{Y_p}, rad^{-1}	C_{n_p}, rad^{-1}	$pd/2V_\infty^*$
0.50	0	±0.0018	±0.0015	±0.00098	±0.00051	---	---	±0.5
	8	±0.0031	±0.0055	±0.00117	±0.00062	±0.015	±0.008	
0.80	0	±0.0013	±0.0011	±0.00067	±0.00035	---	---	±0.4
	8	±0.0018	±0.0029	±0.00074	±0.00040	±0.010	±0.005	
0.90	0	±0.0012	±0.0010	±0.00062	±0.00033	---	---	±0.4
	8	±0.0017	±0.0027	±0.00067	±0.00035	±0.009	±0.005	
0.95	0	±0.0011	±0.0009	±0.00060	±0.00031	---	---	±0.4
	8	±0.0022	±0.0027	±0.00068	±0.00044	±0.009	±0.006	
1.00	0	±0.0011	±0.0009	±0.00058	±0.00030	---	---	±0.4
	8	±0.0016	±0.0027	±0.00065	±0.00043	±0.009	±0.006	
1.10	0	±0.0010	±0.0009	±0.00055	±0.00029	---	---	±0.5
	8	±0.0020	±0.0027	±0.00060	±0.00036	±0.009	±0.005	
1.30	0	±0.0010	±0.0008	±0.00051	±0.00027	---	---	±0.9
	8	±0.0015	±0.0021	±0.00054	±0.00031	±0.008	±0.004	

*For p > 300 radians/sec in percent

DERIVATIVE COEFFICIENT PRECISION

	Uncertainty			
M_∞	C_{N_α}, deg^{-1}	C_{m_α}, deg^{-1}	$C_{Y_{p_\alpha}}$, rad^{-2}	$C_{n_{p_\alpha}}$, rad^{-2}
0.50	±0.00099	±0.0018	±0.140	±0.082
0.80	±0.00082	±0.0018	±0.121	±0.058
0.90	±0.00079	±0.0018	±0.113	±0.055
0.95	±0.00081	±0.0019	±0.115	±0.057
1.00	±0.00088	±0.0019	±0.116	±0.059
1.10	±0.00090	±0.0019	±0.115	±0.058
1.30	±0.00096	±0.0017	±0.097	±0.040

It should be noted that the data repeatability, which is a measure of the random errors, was generally within the maximum propagated uncertainties quoted.

4.0 RESULTS AND DISCUSSION

The current tests were conducted primarily to determine the effect of varying the boattail geometry of ballistic shell configurations on their Magnus-force and moment characteristics at subsonic and transonic Mach numbers. Data were obtained at Mach numbers of 0.5 through 1.3 for angles of attack from -2 to 8 deg. The spin rate parameter ($pd/2V_\infty$) ranged from 0.02 to 0.67 radians. Some results from Ref. 3 for Mach numbers 1.5, 2.0, and 2.5 are also presented.

The variations of normal force (C_N) and pitching moment (C_m) with angle of attack (for $p < 700$ radians/sec) are presented in Fig. 5. There is no measurable effect of spin rate of C_N and C_m for $p < 700$ radians/sec and only small effects (less than 10 percent) for p values up to 1700 radians/sec. These small variations in C_N and C_m are not presented in this report. All of the configurations were statically unstable, as expected, since this type of projectile is spin stabilized. Both C_N and C_m are essentially linear functions of angle of attack for angles up to 6 deg. Figure 6 shows the variation of C_{N_α}, C_{m_α}, and the center of pressure [$(X_{cp}/d)_N$] with Mach number. The data from Tunnel A ($M_\infty = 1.5 \rightarrow 2.5$) and from Tunnel 4T ($M_\infty = 0.5 \rightarrow 1.3$) show excellent agreement. The results show that as the boattail angle increases ($\delta_{BT} = 0 \rightarrow 7.5$ deg, Fig. 6a) or the boattail length increases ($\ell_{BT} = 0 \rightarrow 1.7$, Fig. 6b), which in effect decreases the projectile planform area aft of the moment references, C_{N_α} decreases, C_{m_α} increases, and $(X_{cp}/d)_N$ moves forward as would be expected. Maintaining a constant base diameter and increasing the boattail length (Fig. 6c) did not produce the same systematic variations. Configuration 7 with a short 18.4-deg boattail has trends very different from

the other configurations for $M_\infty < 1.3$. For the other configurations (6, 8, and 9) increasing the boattail length decreases C_{m_α} at $M_\infty \leq 1.0$ but increases C_{m_α} at $M_\infty \geq 1.3$. Increasing the boattail length produces little effect on C_{N_α} at $M_\infty \leq 1.1$.

Figure 7 presents the typical variation of side force (C_Y) and yawing moment (C_n) with $pd/2V_\infty$ for Configuration 8 at Mach number 0.5. The data typify the type of data, the amount of scatter, and the number of points that were obtained as the model spin rate changed. The gaps in the data indicate where the brake was used to slow the model. The data presented hereafter in this report show a computer fairing through the data points (least-squares curve fit) instead of a symbol for each data point. The complete C_Y and C_n versus $pd/2V_\infty$ results at a length Reynolds number of 9.6×10^6 are presented in Figs. 8 through 17. Generally, the results indicate that both C_Y and C_n are nonlinear with $pd/2V_\infty$ at the higher angles of attack ($\alpha > 4$ deg) and higher spin rates ($pd/2V_\infty > 0.15$). In addition, the usual negative C_Y and positive C_n for positive values of $pd/2V_\infty$ and α were obtained for all configurations except 0, 1, and 7 (Figs. 8, 9, and 15). For Configurations 0 and 1, the Magnus center of pressure $[(X_{cp}/d)_Y]$ is generally forward of or very near the model moment reference point at the lower angles of attack. For Configuration 7, both C_Y and C_n exhibited unusual trends with spin rate for $\alpha > 4$ deg. This was probably a result of flow separation on the boattail ($\delta_{BT} = 18.4$ deg).

To examine the effects of angle of attack, the partial derivatives of C_Y and C_n with respect to $pd/2V_\infty$ were computed using the linear portion of the data in Figs. 8 through 17 ($pd/2V_\infty < 0.15$ when $\alpha < 4$ deg and $pd/2V_\infty < 0.10$ when $\alpha \geq 4$ deg) and the results (Cy_p and C_{n_p}) are presented

in Fig. 18 as a function of angle of attack. These results show that the magnitudes of both C_{Y_p} and C_{n_p} generally increase continuously with angle of attack with the exception of Configurations 0, 1, and 7. The value of C_{n_p} was generally negative or near zero at the lower Mach numbers and angles of attack for Configurations 0 and 1 as a result of the Magnus center-of-pressure location with respect to the model moment reference point. The erratic results for Configuration 7 (Fig. 18h) indicate separated flow in the boattail region.

To analyze the Mach number effects on the Magnus characteristics, the partial derivatives of C_{Y_p} and C_{n_p} with respect to angle of attack were computed using the linear portion of the data in Fig. 18 (-2.5 deg $< \alpha < 2.5$ deg) and the results ($C_{Y_{p_\alpha}}$ and $C_{n_{p_\alpha}}$) are presented in Fig. 19. Increasing the boattail angle and maintaining a constant boattail length (Fig. 19a) produces a more positive $C_{n_{p_\alpha}}$, increases the magnitude of $C_{Y_{p_\alpha}}$, and shifts $(X_{cp}/d)_Y$ toward the model base. Increasing the boattail length and maintaining a constant boattail angle of 5 deg (Fig. 19b) generally increases $C_{n_{p_\alpha}}$ and the magnitude of $C_{Y_{p_\alpha}}$ except in the vicinity of $M_\infty = 1.0$. The center-of-pressure location is essentially the same for $\ell_{BT} \geq 1.0$ over the Mach number range tested. Figure 19c presents the results of increasing the boattail length and maintaining a constant base diameter of 0.7 calibers. The results show that the magnitude of both $C_{Y_{p_\alpha}}$ and $C_{n_{p_\alpha}}$ decreases with increasing boattail length and that $(X_{cp}/d)_Y$ moves forward for $M_\infty < 1.3$ (excluding Configuration 7). The variations for Configuration 7 are very erratic for $M_\infty < 1.5$ and no data are

presented at M_∞ = 1.1 and 1.3 because of the nonlinearity of the C_Y and C_n versus $pd/2V_\infty$ data (Figs. 15e and f).

It should be noted that Configuration 3 was also tested at a Reynolds number of 5.7×10^6 at Mach numbers 0.8, 1.0, and 1.3. These results are not presented in this report since the variation of C_Y and C_n with $pd/2V_\infty$ are essentially identical to the variations obtained at the higher Reynolds number ($Re_\ell = 9.6 \times 10^6$).

5.0 CONCLUDING REMARKS

An experimental investigation was conducted to determine the effects of boattail geometry on the Magnus-force and moment characteristics of ballistic shells at subsonic and transonic Mach numbers. The tests were conducted at Mach numbers from 0.5 through 1.3 and angles of attack from -2 to 8 deg. The spin rate parameter ($pd/2V_\infty$) ranged from 0.02 to 0.67 radians. The results of these tests as well as results for Mach numbers 1.5, 2.0, and 2.5 from previous tests are summarized below:

1. All configurations are statically unstable. (These are spin-stabilized projectiles.)

2. Except for the configurations with a constant base diameter, increasing the boattail length or angle decreases C_{N_α} and increases C_{m_α}.

3. Both C_Y and C_n are nonlinear with $pd/2V_\infty$ at the higher angles of attack ($\alpha > 4$ deg) and higher spin rates ($pd/2V_\infty > 0.15$).

4. Increasing the boattail angle while maintaining a constant boattail length produces an increase

in the magnitude of $C_{Y_{p_\alpha}}$ and moves the Magnus center-of-pressure $[(X_{cp}/d)_Y]$ toward the model base.

5. Increasing the boattail length while maintaining a constant boattail angle produces an increase in the magnitude of $C_{Y_{p_\alpha}}$, except in the region of $M_\infty = 1.0$ and has little effect on $(X_{cp}/d)_Y$.

6. A short, large angle boattail ($\ell_{BT} = 0.45$, $\delta_{BT} = 18.4$ deg) produces very nonlinear variations in C_Y and C_n with $pd/2V_\infty$ and erratic variations in C_{N_α}, C_{m_α}, $C_{Y_{p_\alpha}}$, and $C_{n_{p_\alpha}}$ with Mach number for $M_\infty < 1.5$.

7. Increasing the boattail length ($\ell_{BT} > 0.85$) while maintaining a constant base diameter decreases the magnitude of $C_{Y_{p_\alpha}}$ and moves $(X_{cp}/d)_Y$ toward the nose for $M_\infty < 1.3$; however, for $M_\infty > 1.3$ the magnitude of $C_{Y_{p_\alpha}}$ increases and $(X_{cp}/d)_Y$ is unaffected.

REFERENCES

1. Jenke, Leroy M. and Carman, Jack B. "Experimental Magnus Characteristics of Ballistic Projectiles with Anti-Magnus Vanes at Mach Numbers 0.7 through 2.5." AEDC-TR-73-126, AFATL-TR-73-150 (AD773383), December 1973.

2. Jenke, Leroy M. "Experimental Magnus Characteristics of Ballistic Projectiles with and without Anti-Magnus Vanes at Mach Numbers 1.5 through 2.5." AEDC-TR-73-162, AFATL-TR-73-188 (AD771807), December 1973.

3. Jenke, Leroy M. "Experimental Magnus Characteristics of Several Ballistic Projectiles with Various Boattail Angles and Lengths at Mach Numbers 1.5, 2.0, and 2.5." AEDC-TR-74-78, AFATL-TR-74-118 (AD785346), September 1974.

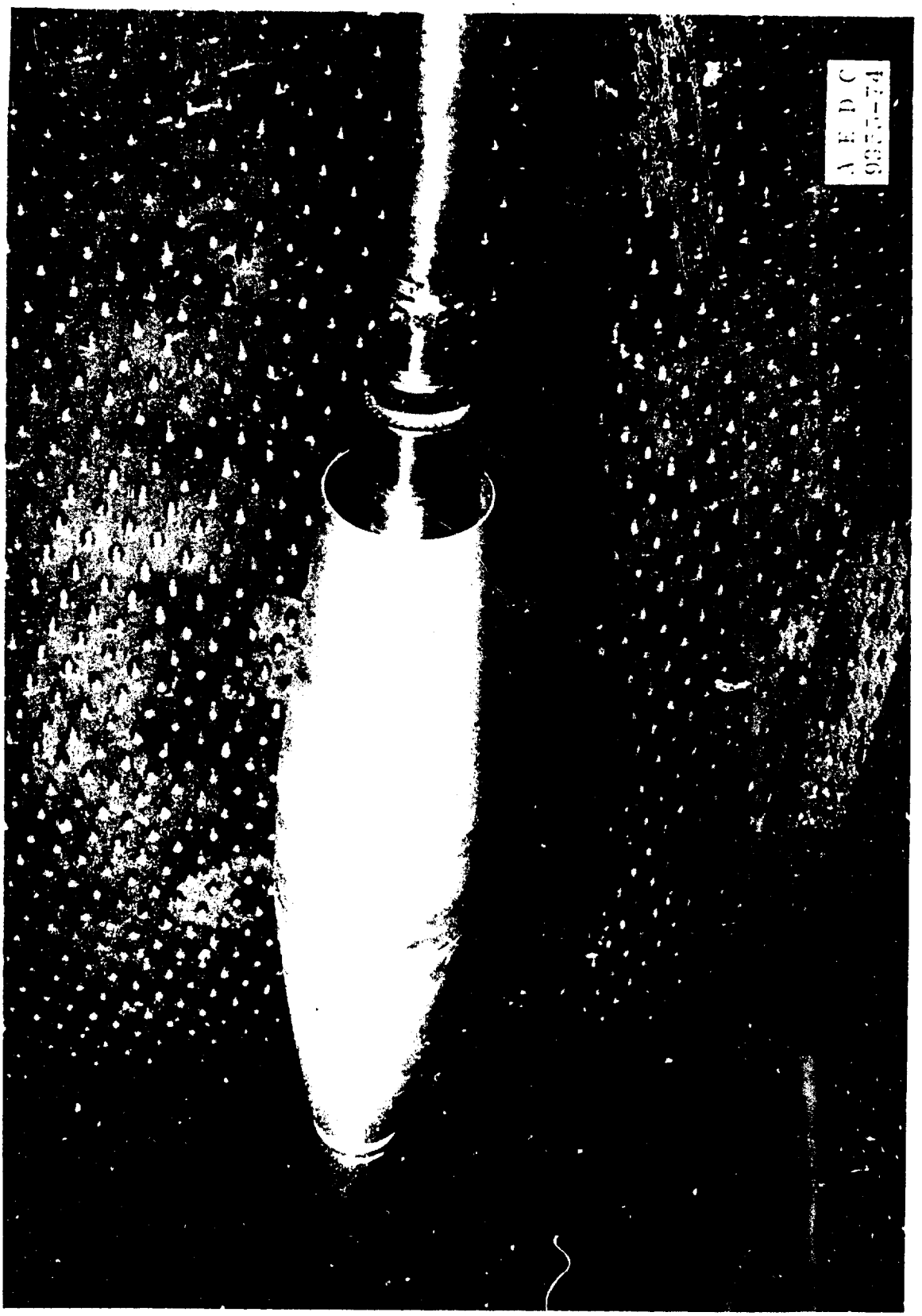

a. Tunnel installation (Configuration 6)

Figure 1. Photographs of the models.

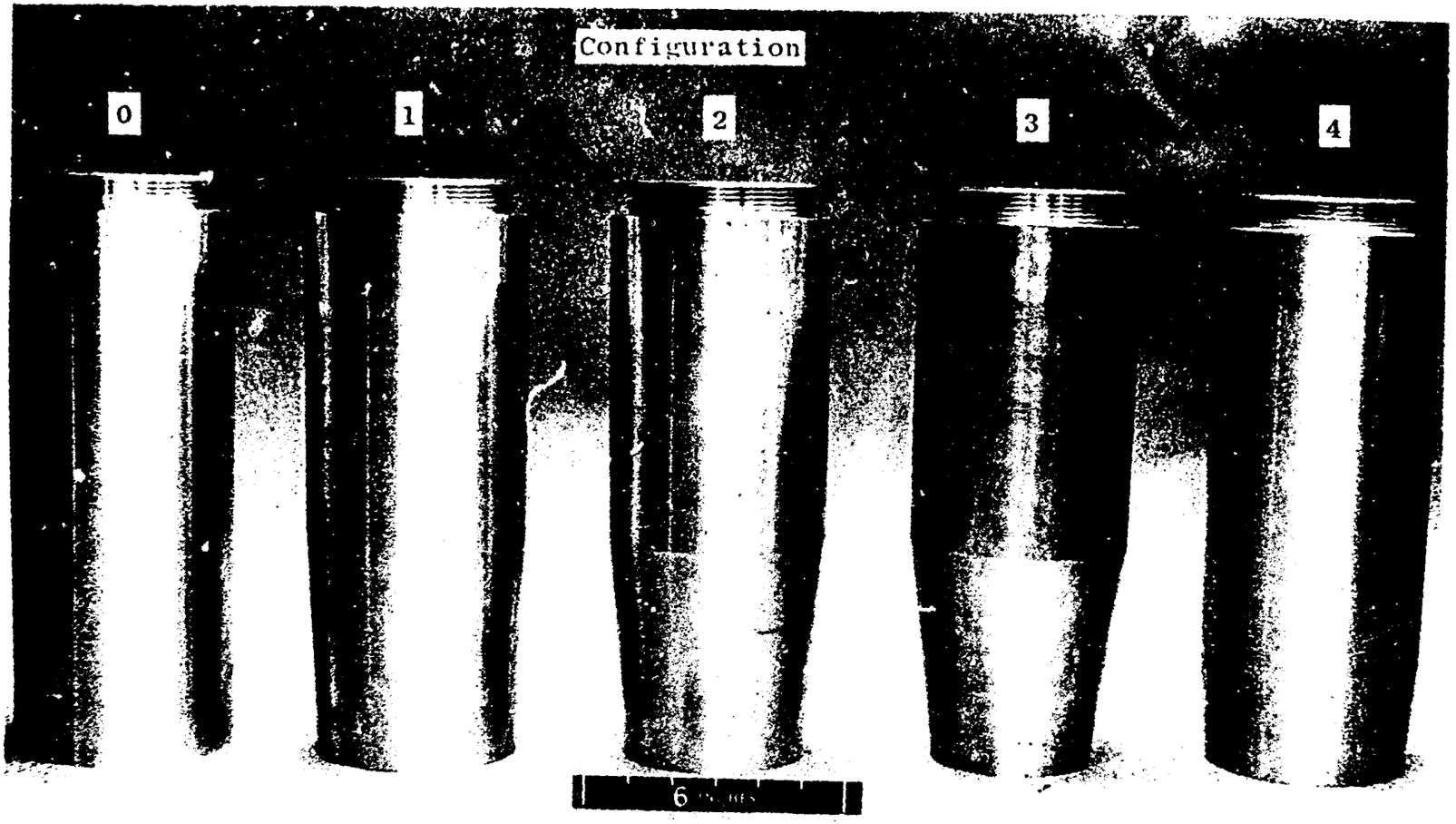

A E D C
2607-74

b. Boattail configurations
Figure 1. Continued.

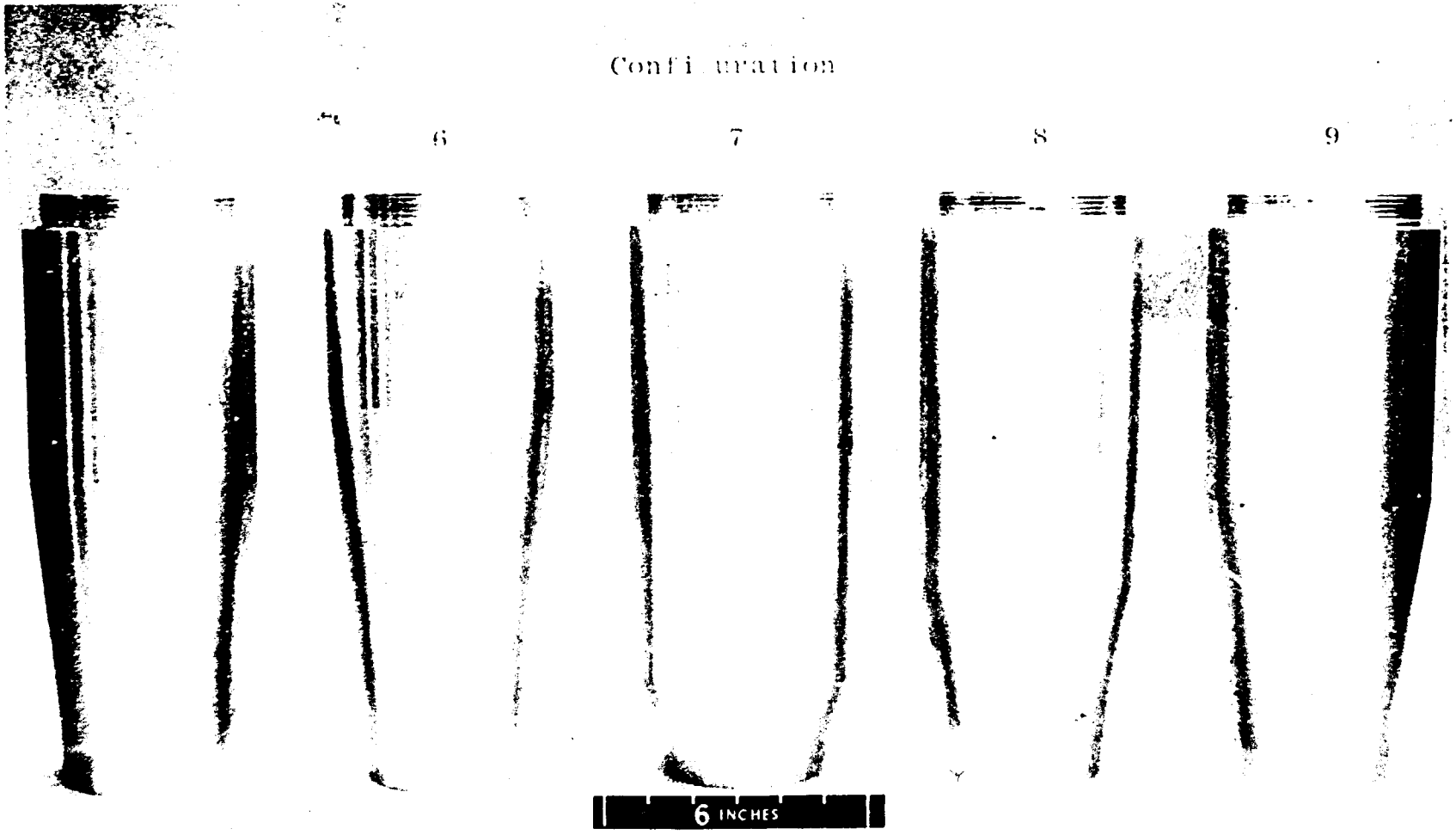

A E D C
2606-74

b. Concluded
Figure 1. Concluded.

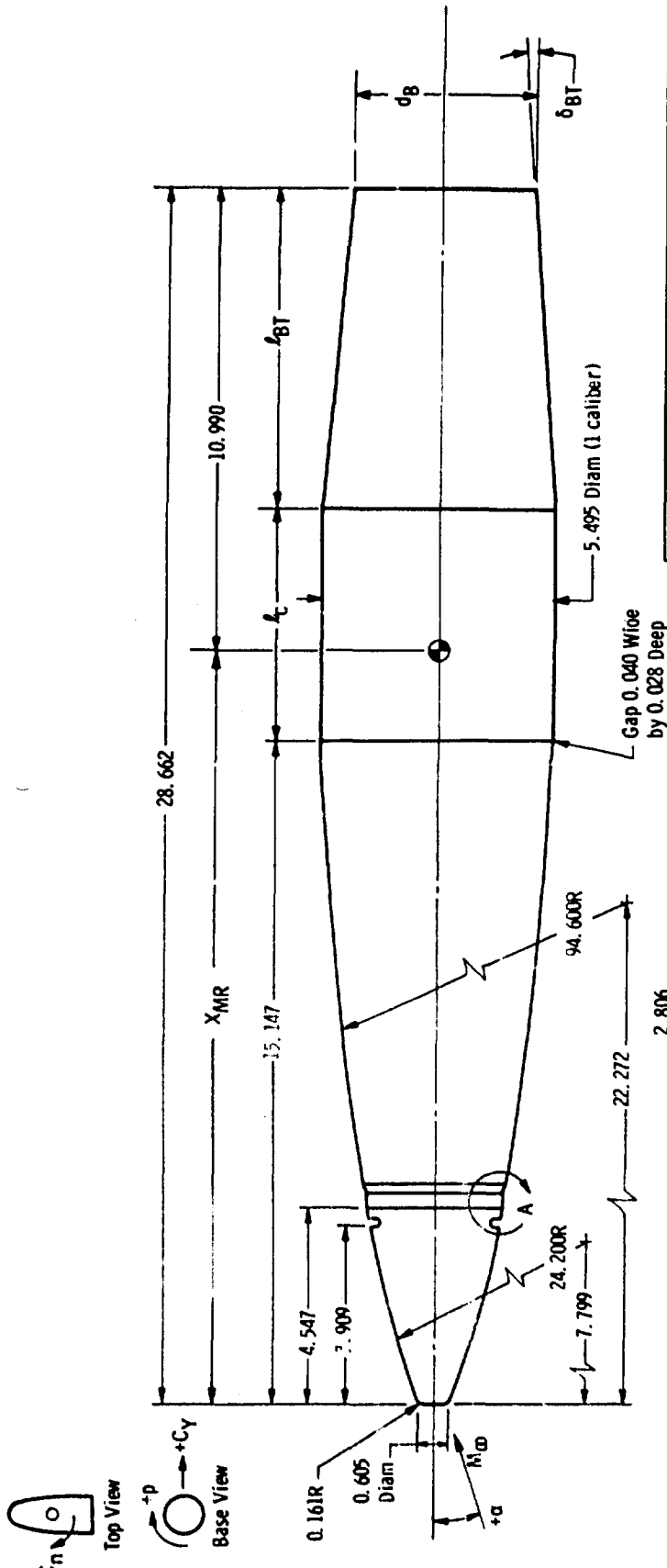

Configuration	l_{BT}, calibers	δ_{BT}, deg	d_B, calibers	l_c, calibers
0	0	0	1.0000	2.460
1	1.00	2.5	0.9126	1.460
2	1.00	5.0	0.8249	1.460
3	1.00	7.5	0.7366	1.460
4	0.50	5.0	0.9124	1.959
5	1.35	5.0	0.7637	1.110
6	1.70	5.0	0.7024	0.759
7	0.45	18.4	0.7000	2.009
8	0.85	10.0	0.7000	1.609
9	1.25	6.9	0.7000	1.205

Figure 2. Model details.

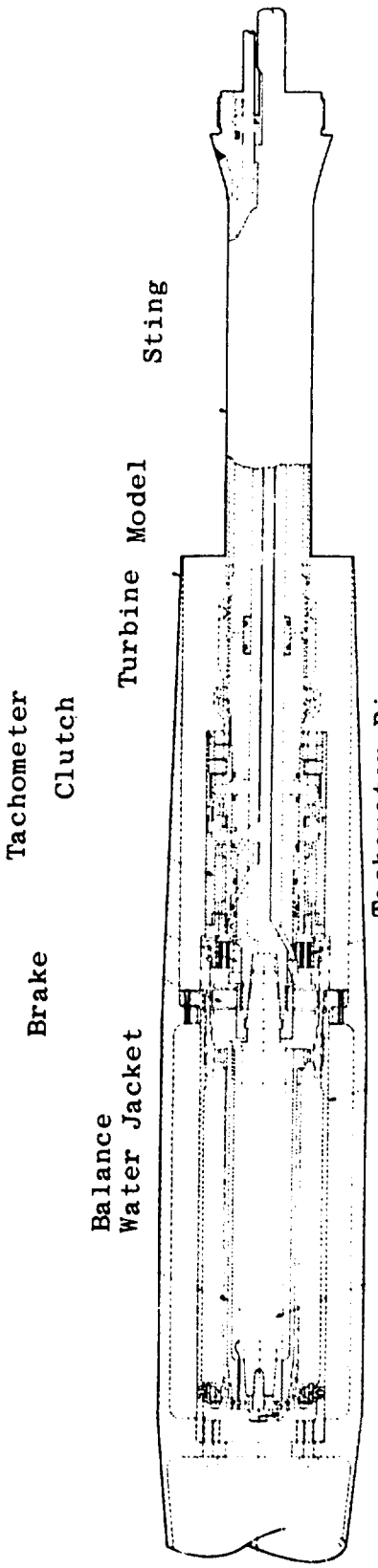

Figure 5. Magnus-force test mechanism.

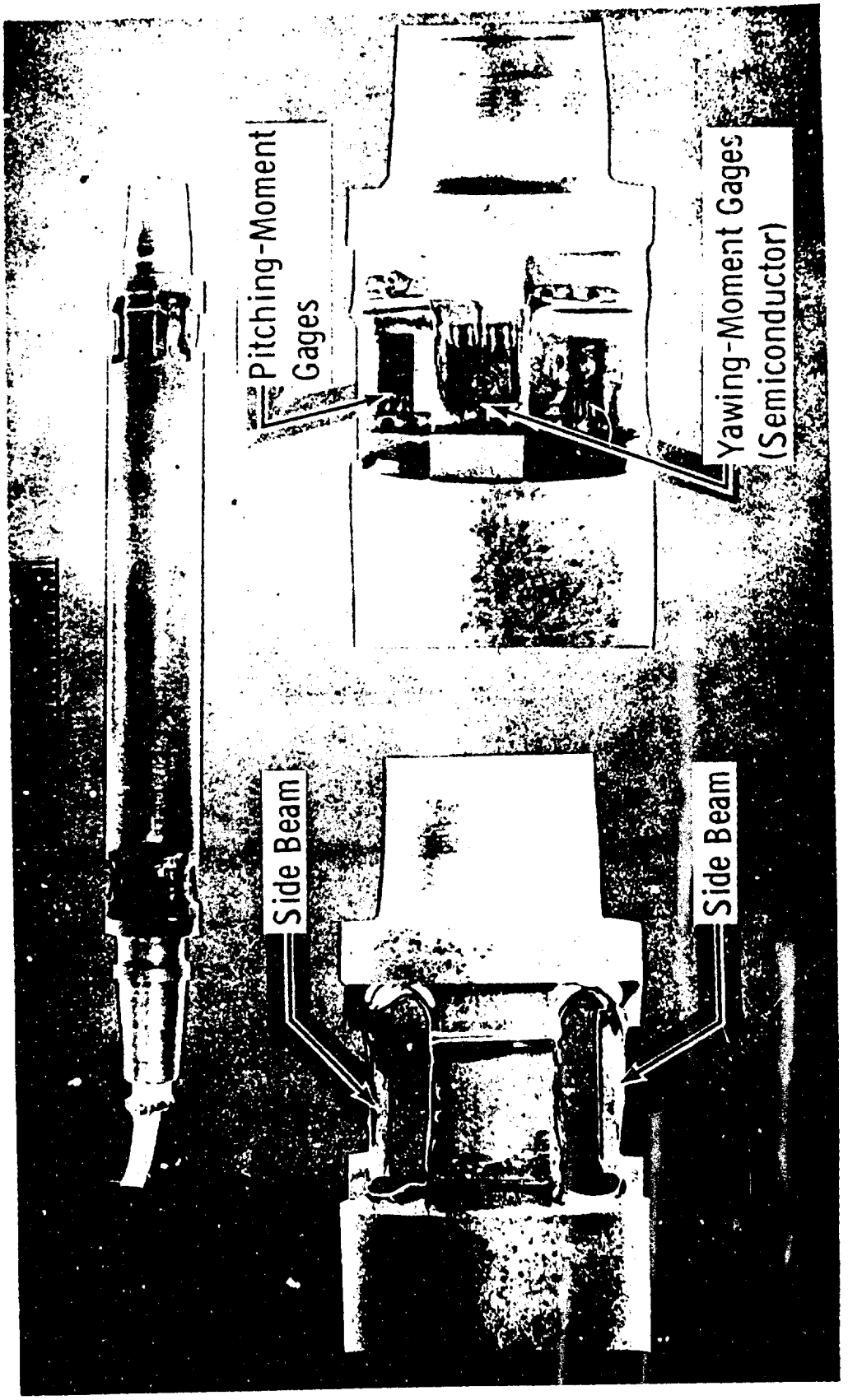

Figure 4. Balance details.

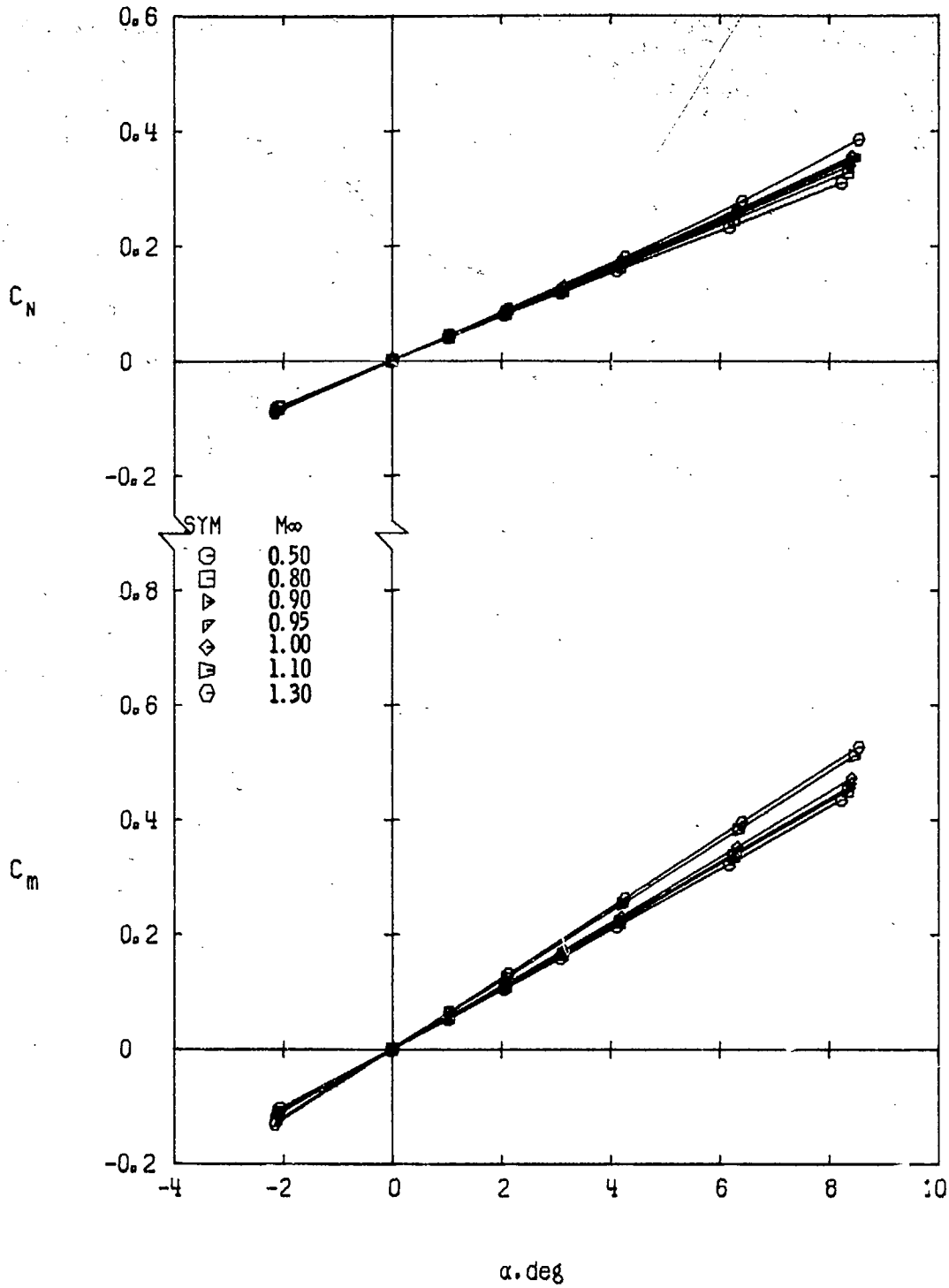

a. Configuration 0

Figure 5. Variation of C_N and C_m with angle of attack, $Re_\ell = 9.6 \times 10^6$.

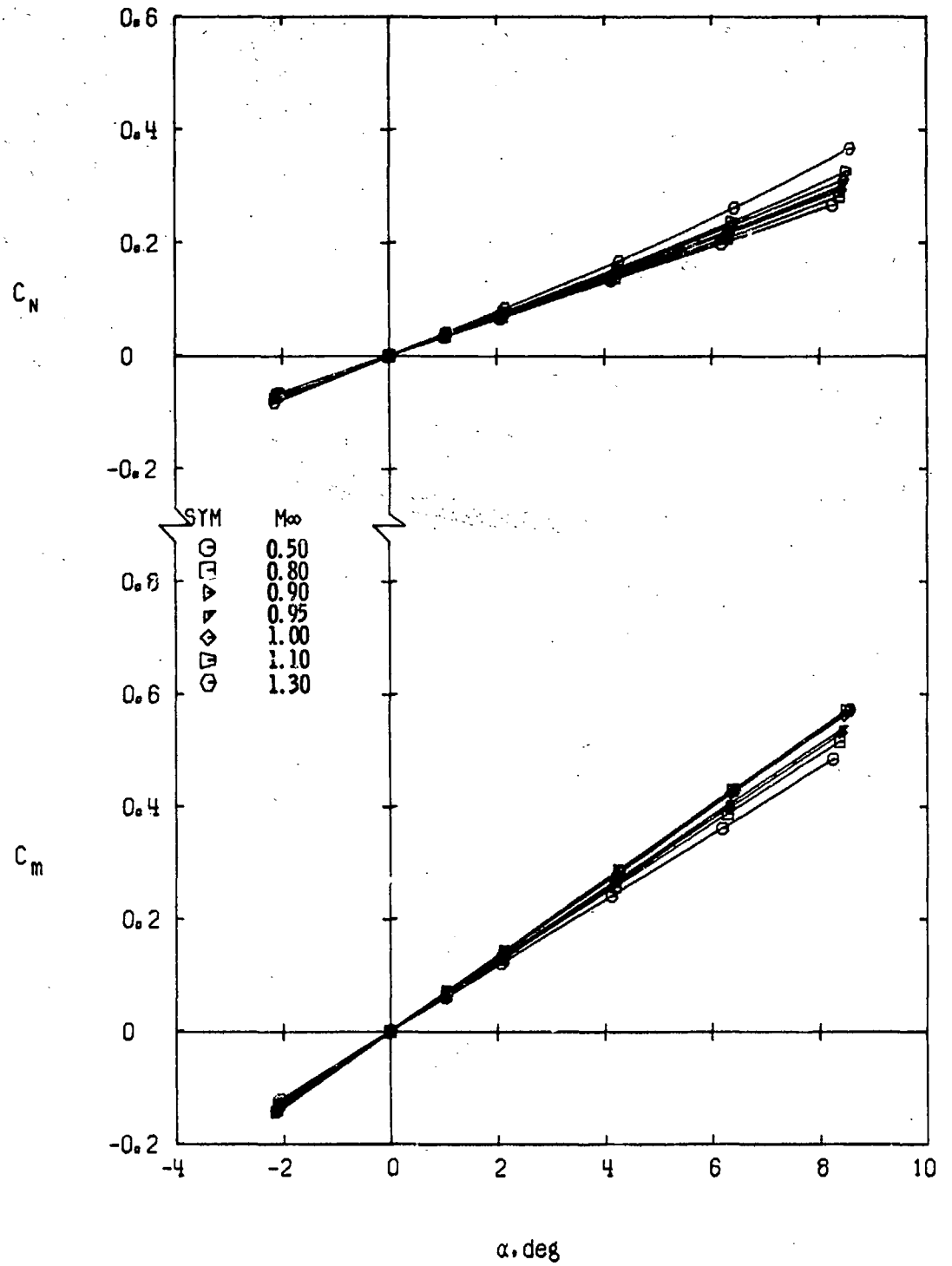

b. Configuration 1
Figure 5. Continued.

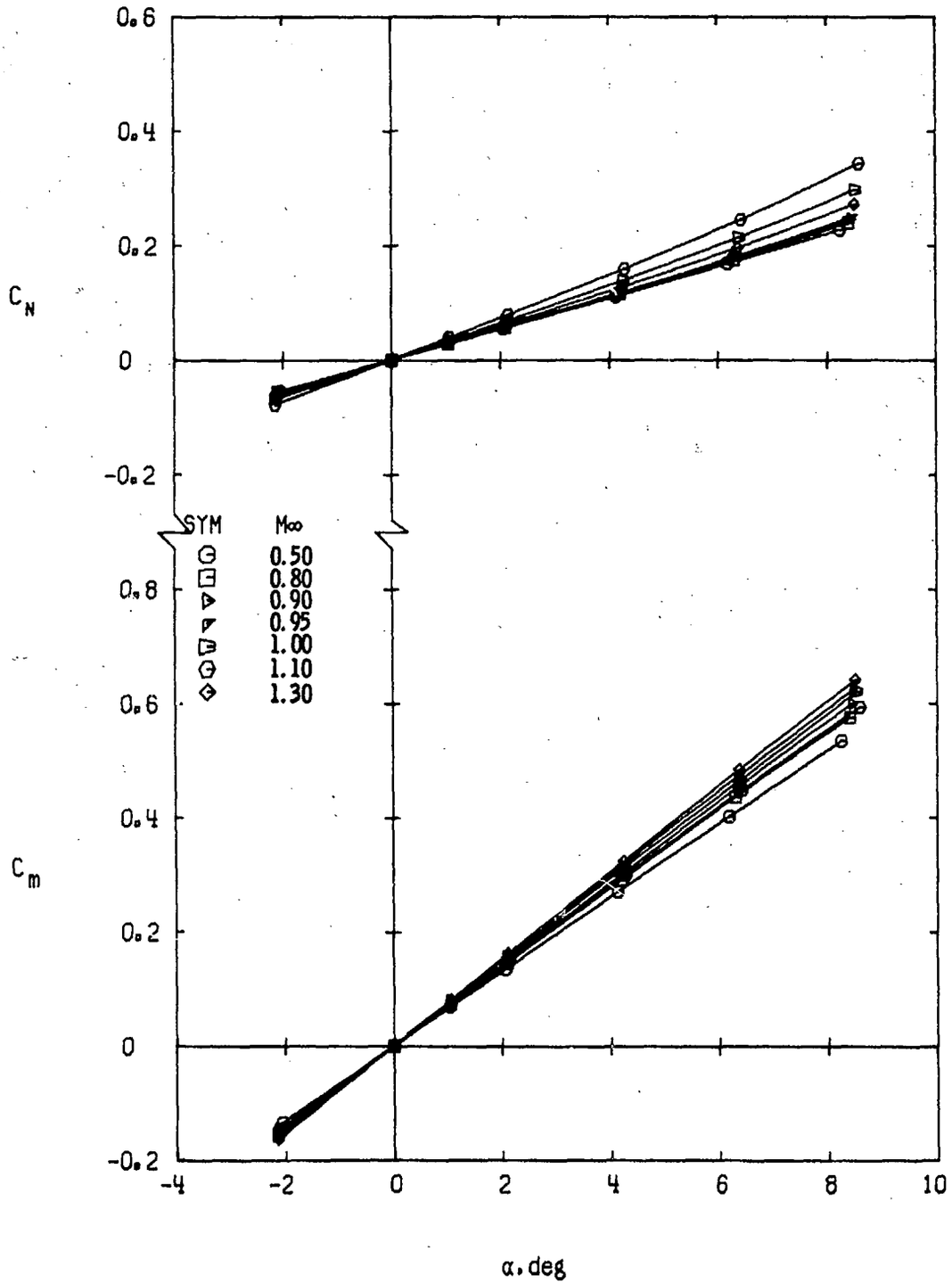

c. Configuration 2
Figure 5. Continued.

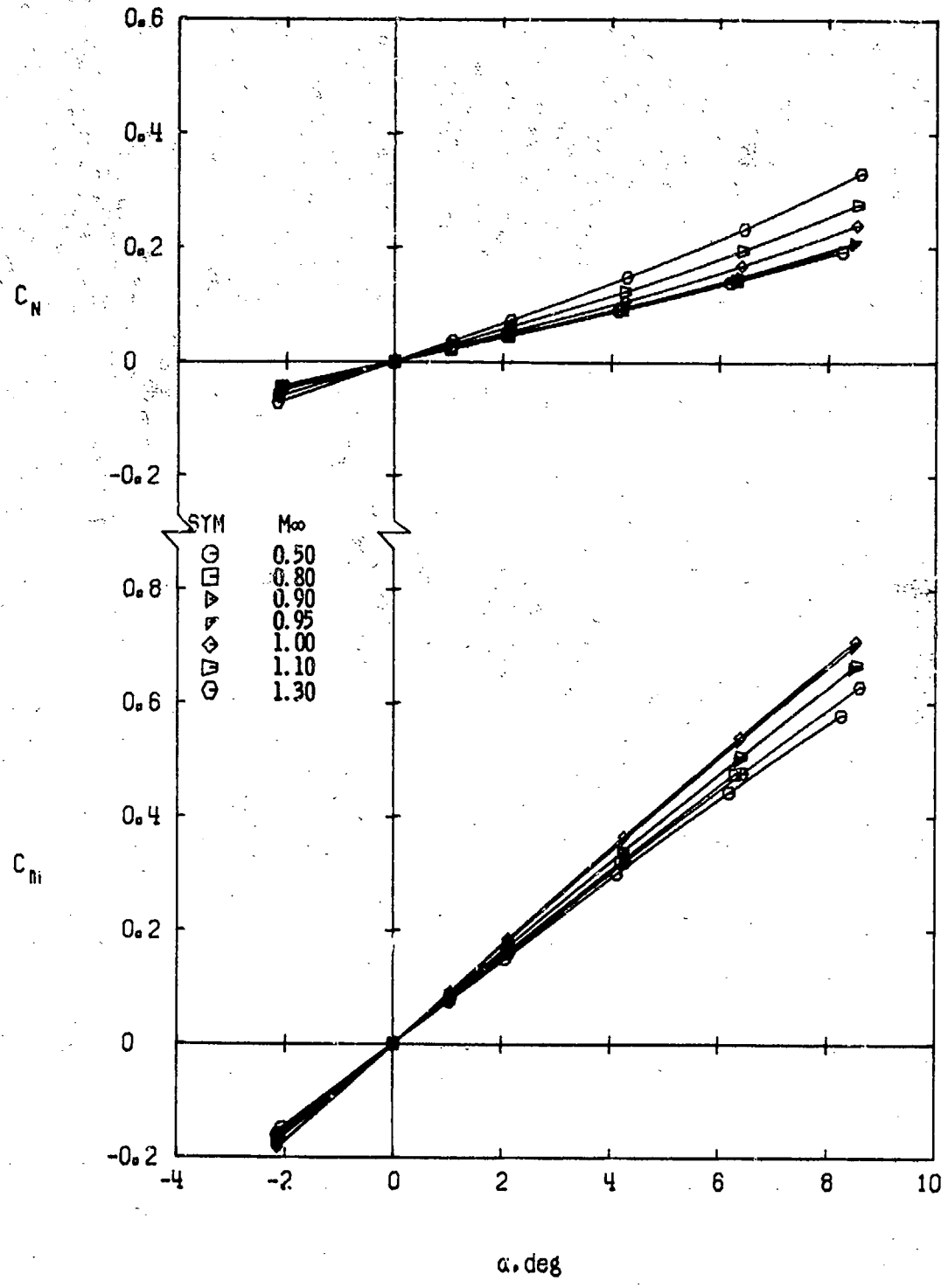

d. Configuration 3
Figure 5. Continued.

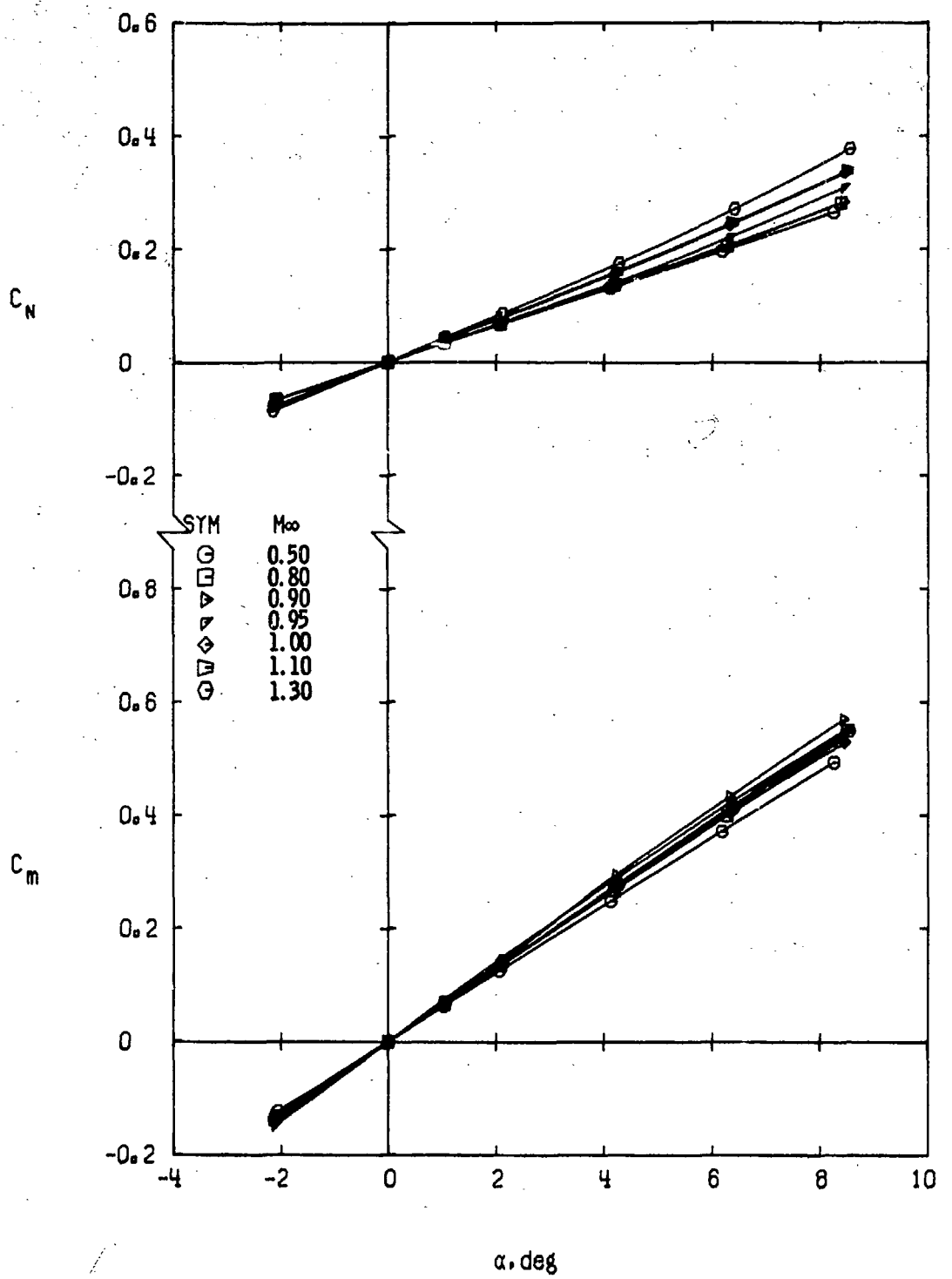

e. Configuration 4
Figure 5. Continued.

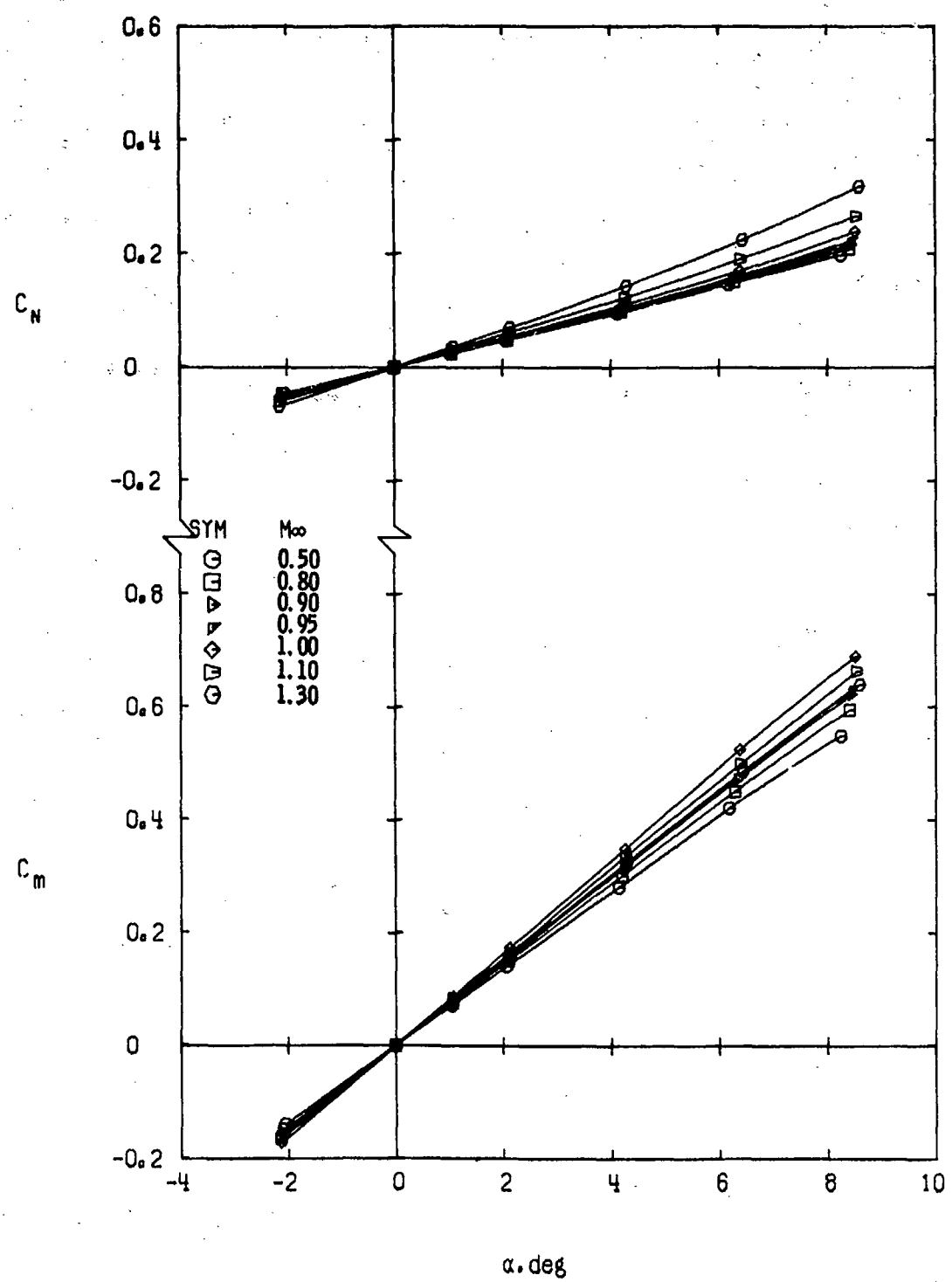

f. Configuration 5
Figure 5. Continued.

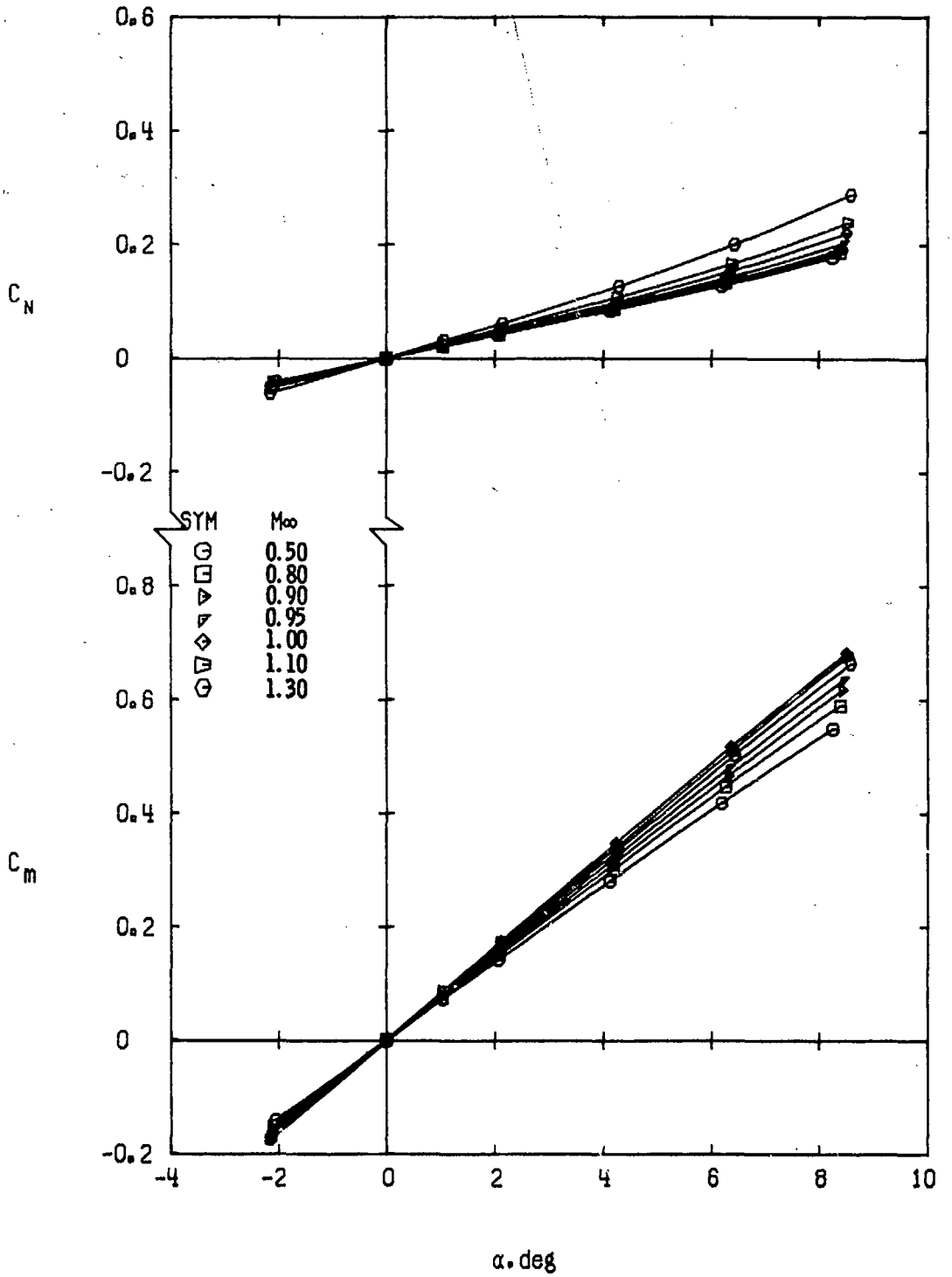

g. Configuration 6
Figure 5. Continued.

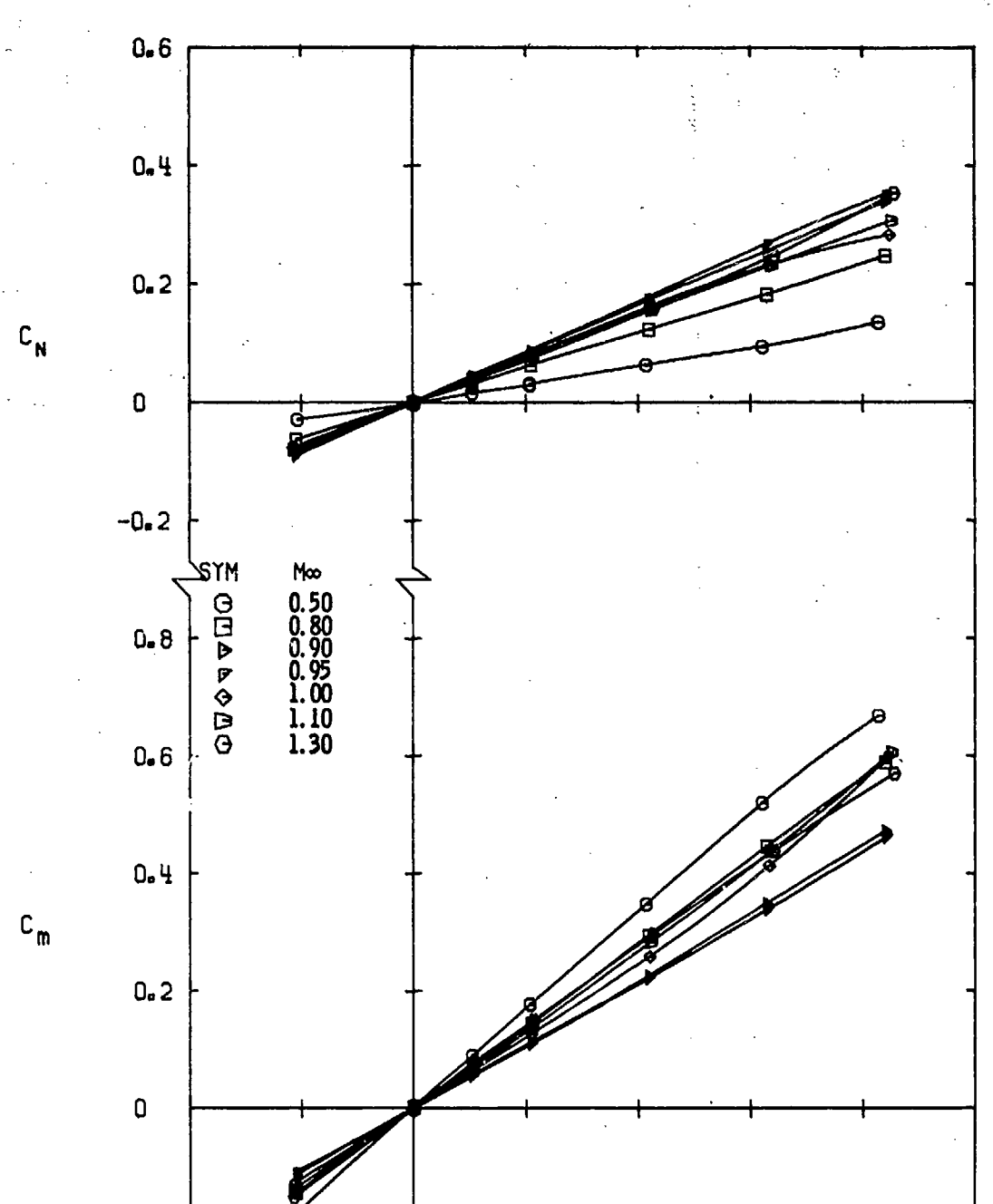

h. Configuration 7
Figure 5. Continued.

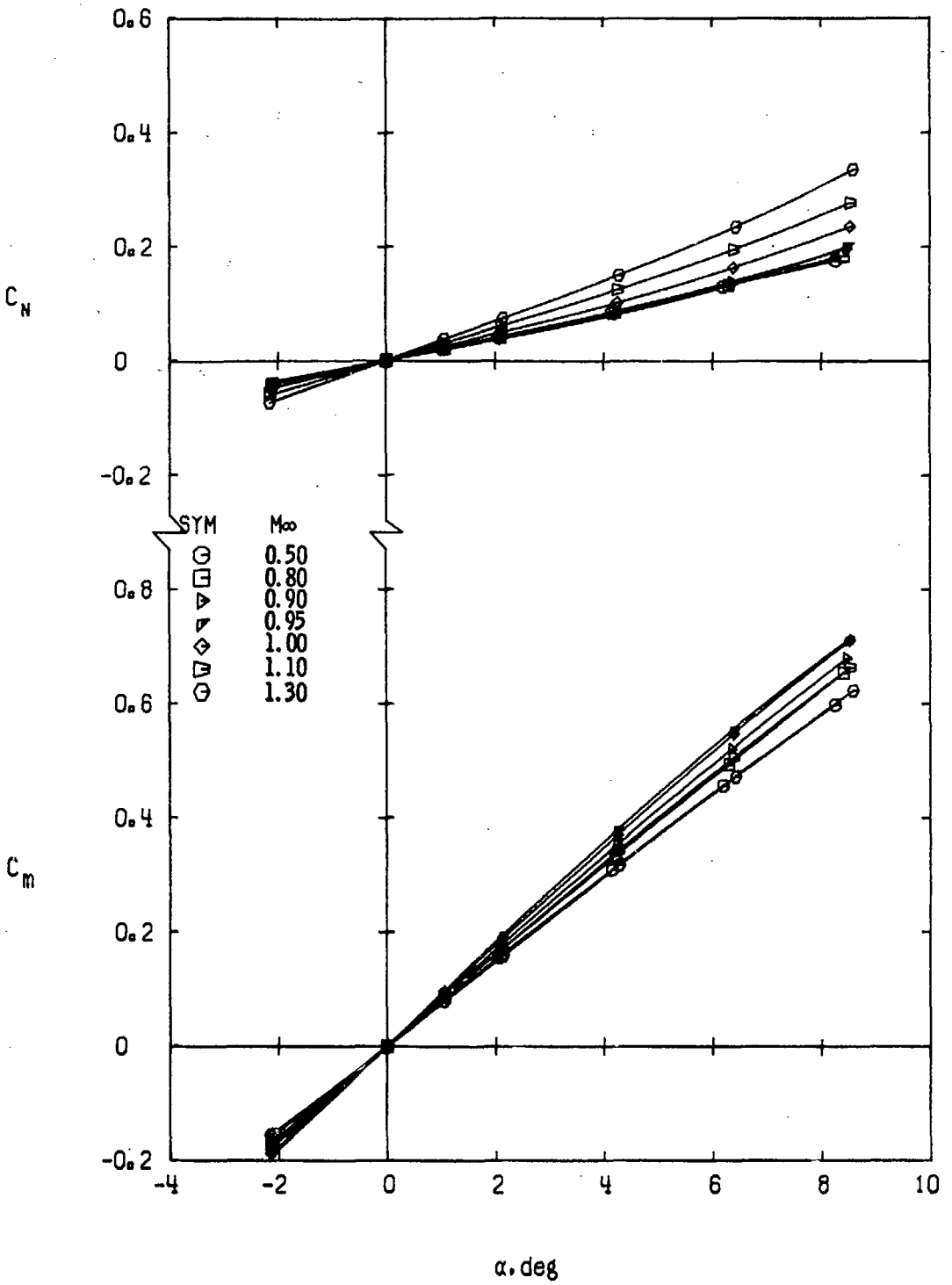

i. Configuration 8
Figure 5. Continued.

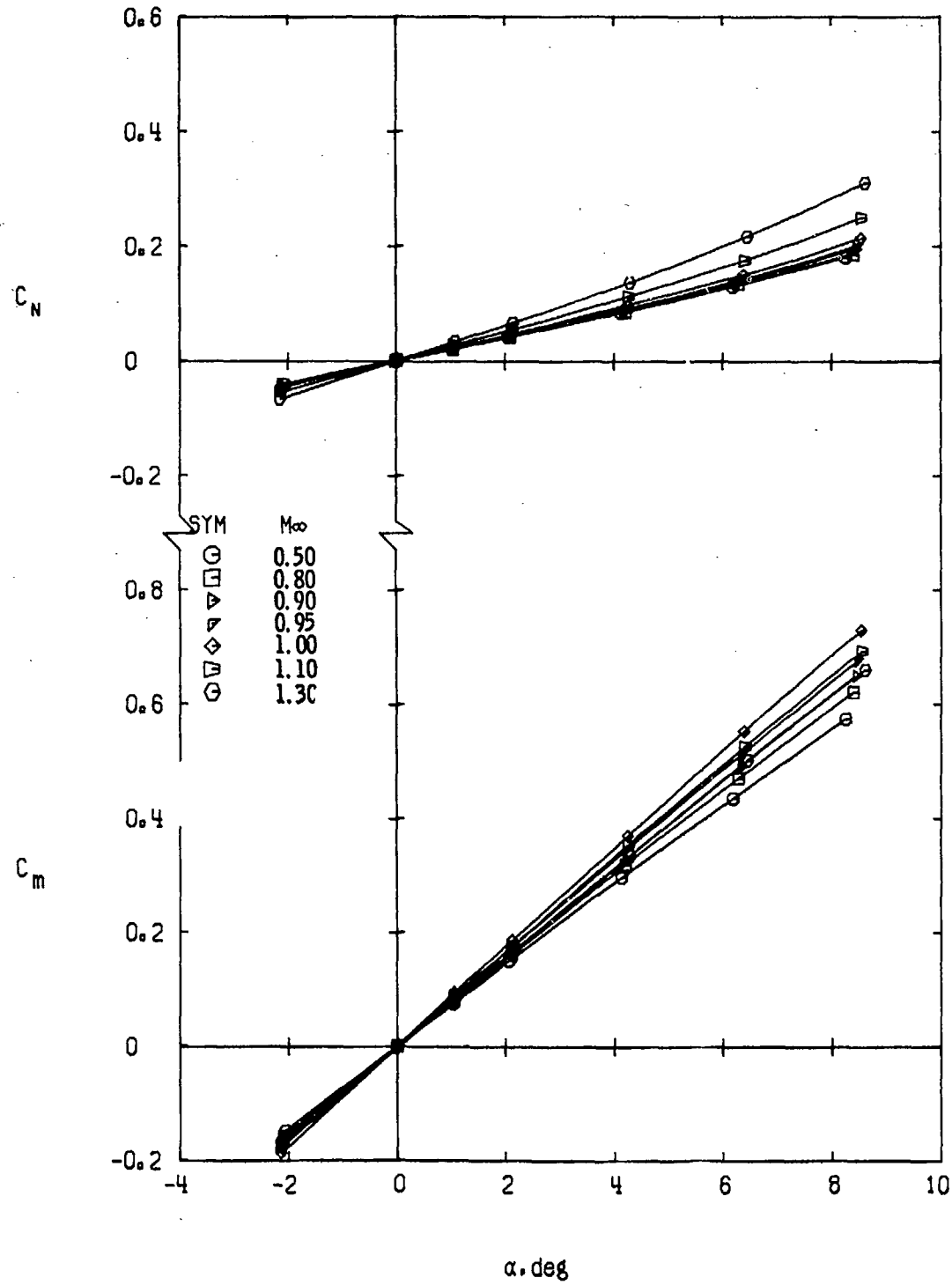

j. Configuration 9
Figure 5. Concluded.

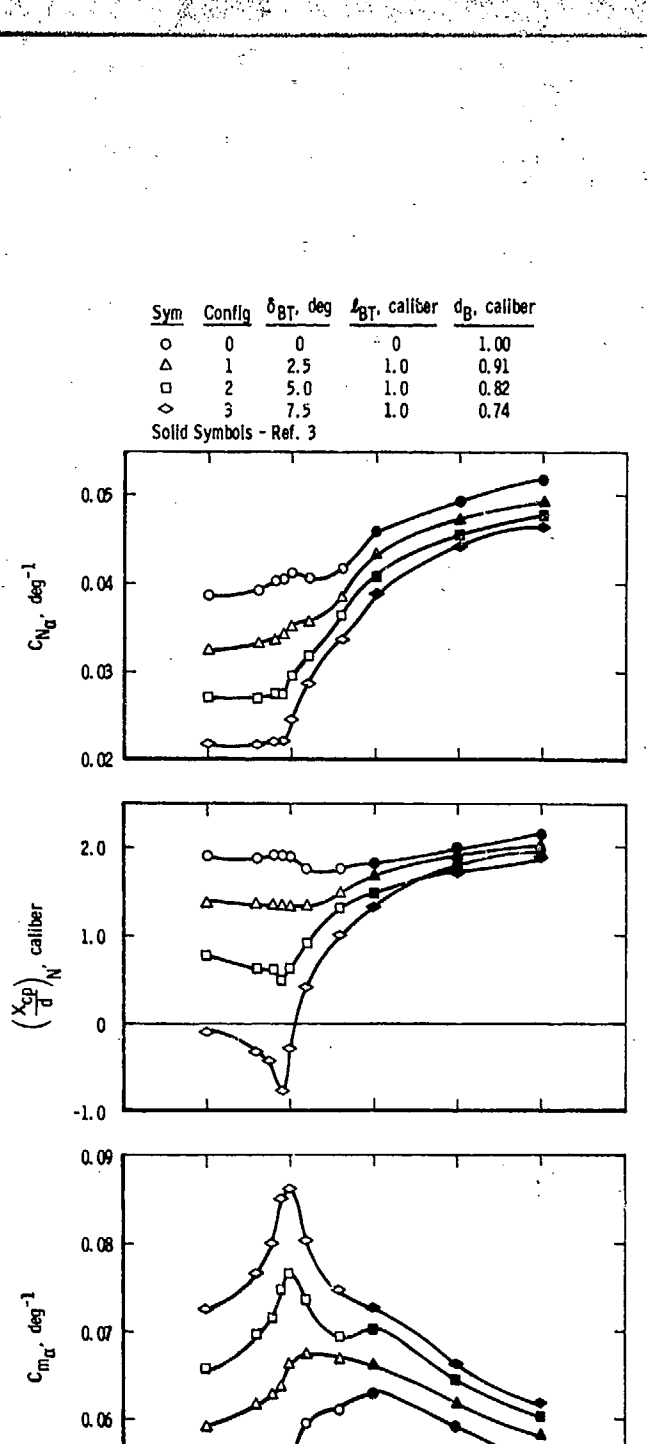

a. Effect of boattail angle with a constant boattail length

Figure 6. Variation of C_{N_α}, C_{m_α}, and $(X_{cp}/d)_N$ with Mach number, $Re_\ell = 9.6 \times 10^6$.

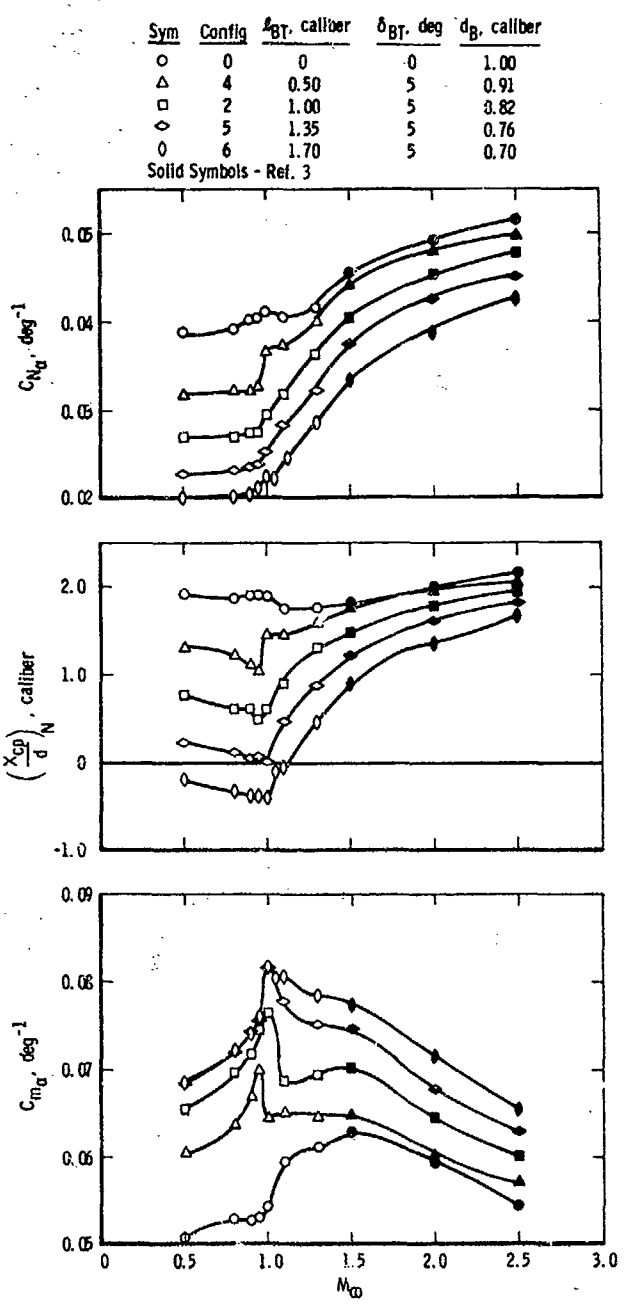

b. Effect of boattail length with a constant boattail angle
Figure 6. Continued.

Sym	Config	ℓ_{BT}, caliber	d_B, caliber	δ_{BT}, deg
△	7	0.45	0.7	18.4
□	8	0.85	0.7	10.0
◇	9	1.25	0.7	6.9
○	6	1.70	0.7	5.0

Solid Symbols - Ref. 3

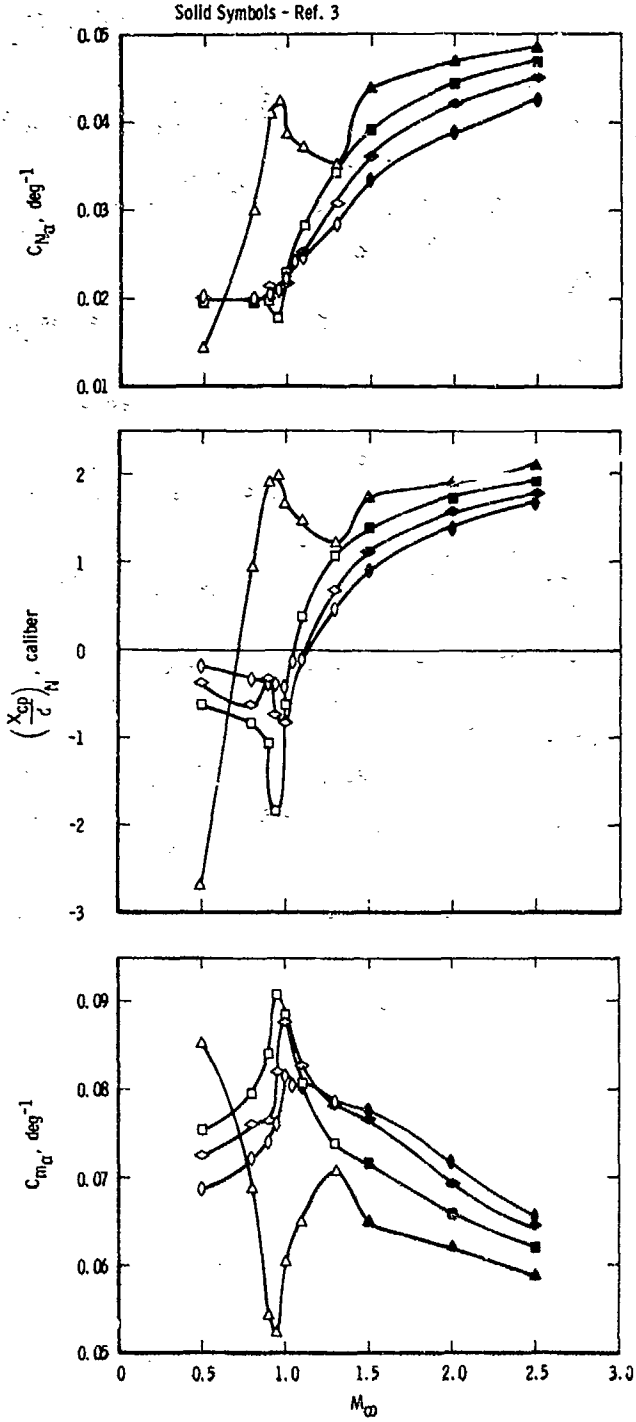

c. Effect of boattail length with a constant base diameter

Figure 6. Concluded.

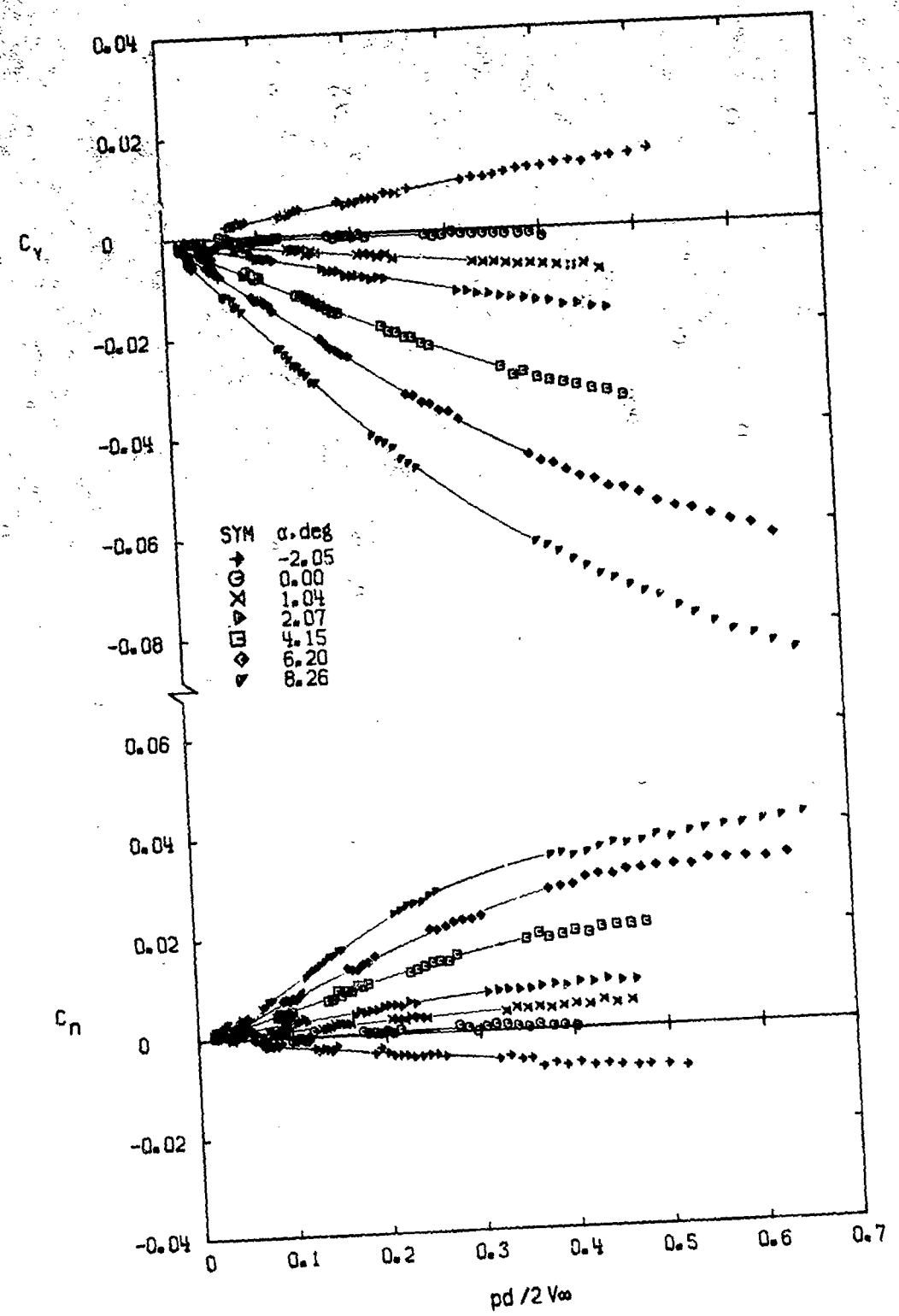

Figure 7. Typical variation of C_Y and C_n with $pd/2V_\infty$, Configuration 8, $M_\infty = 0.50$.

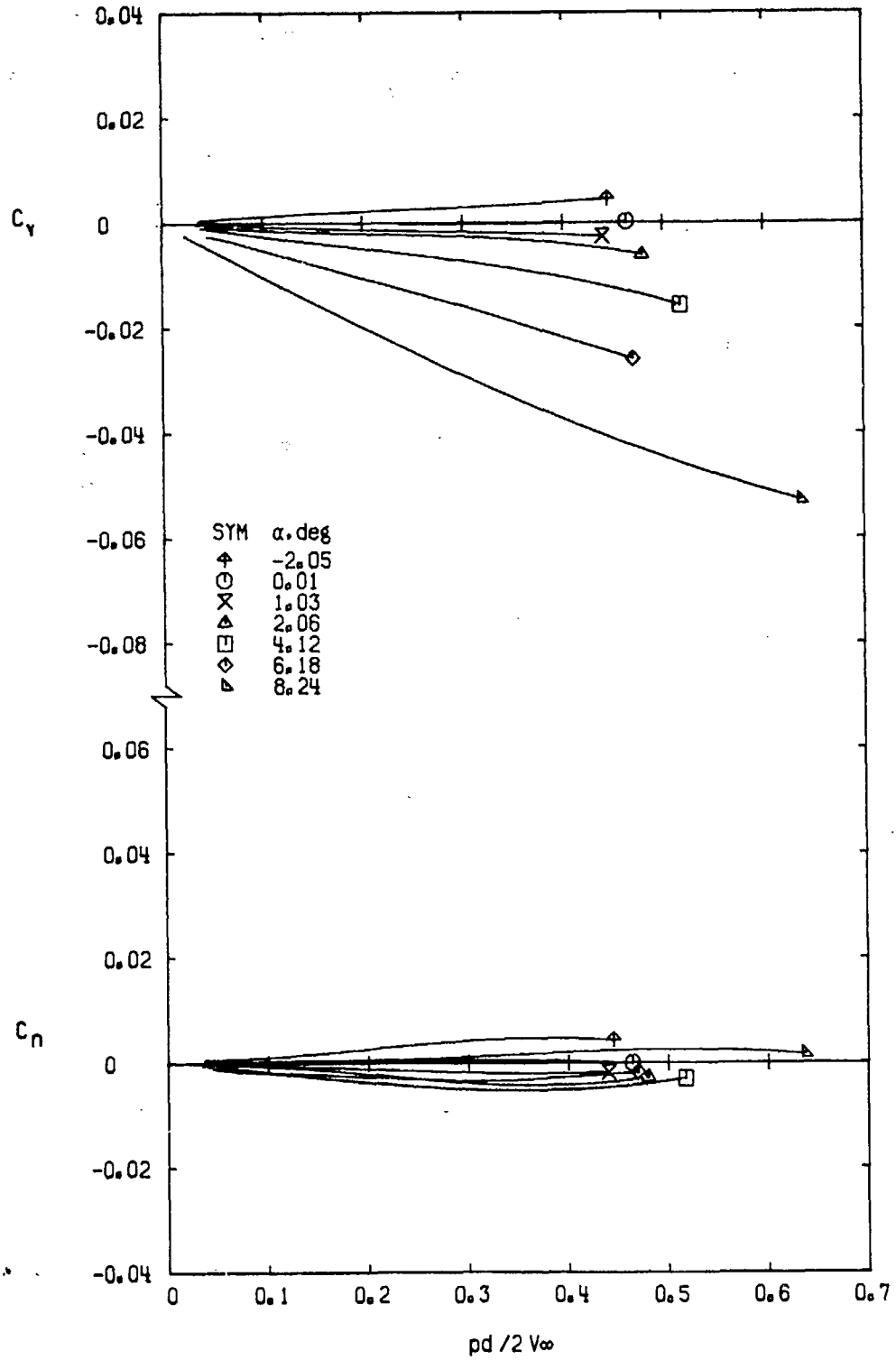

a. $M_\infty = 0.50$

Figure 8. Variation of C_Y and C_n with $pd/2V_\infty$ for Configuration 0.

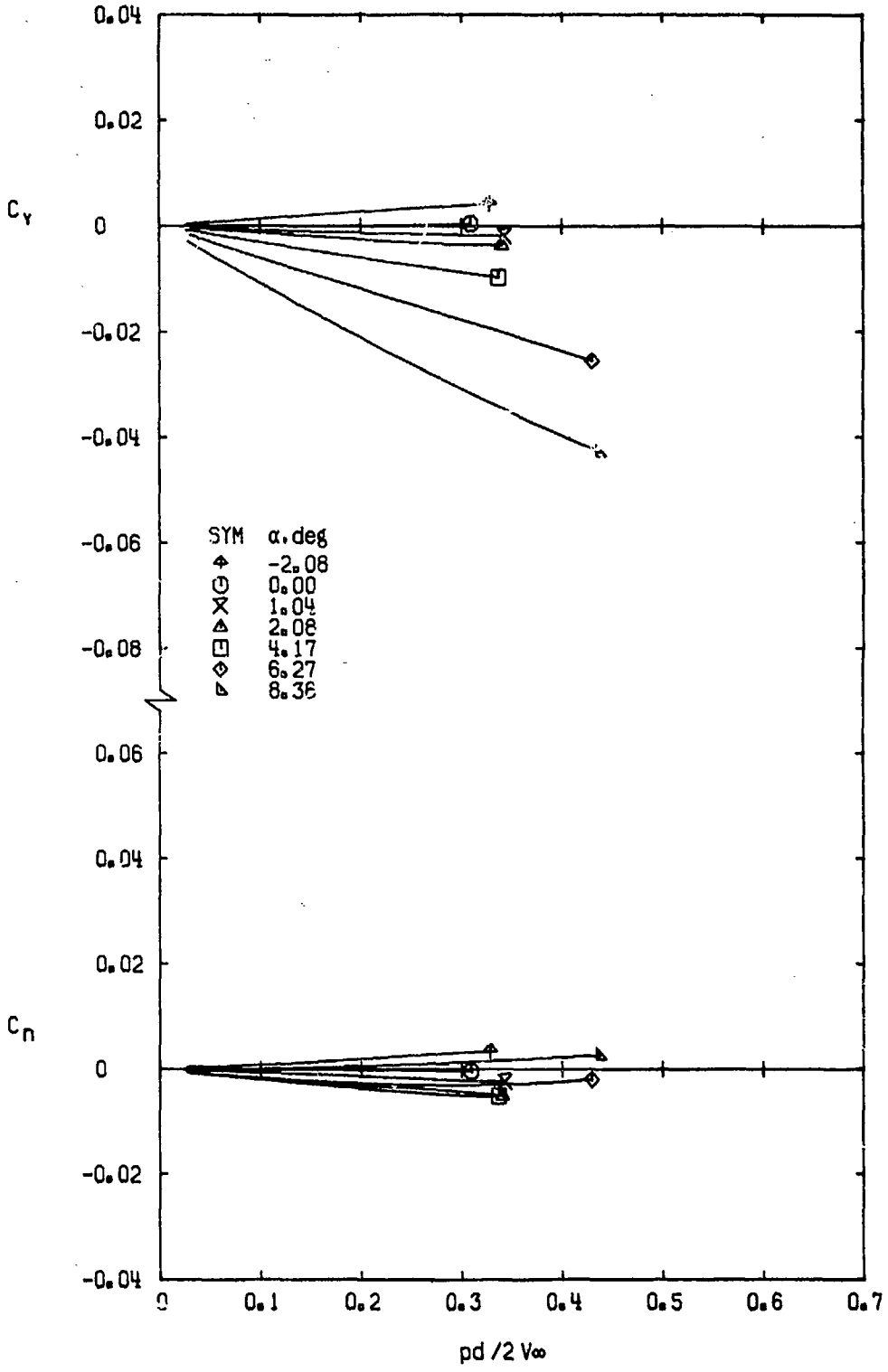

b. M_∞ = 0.80

Figure 8. Continued.

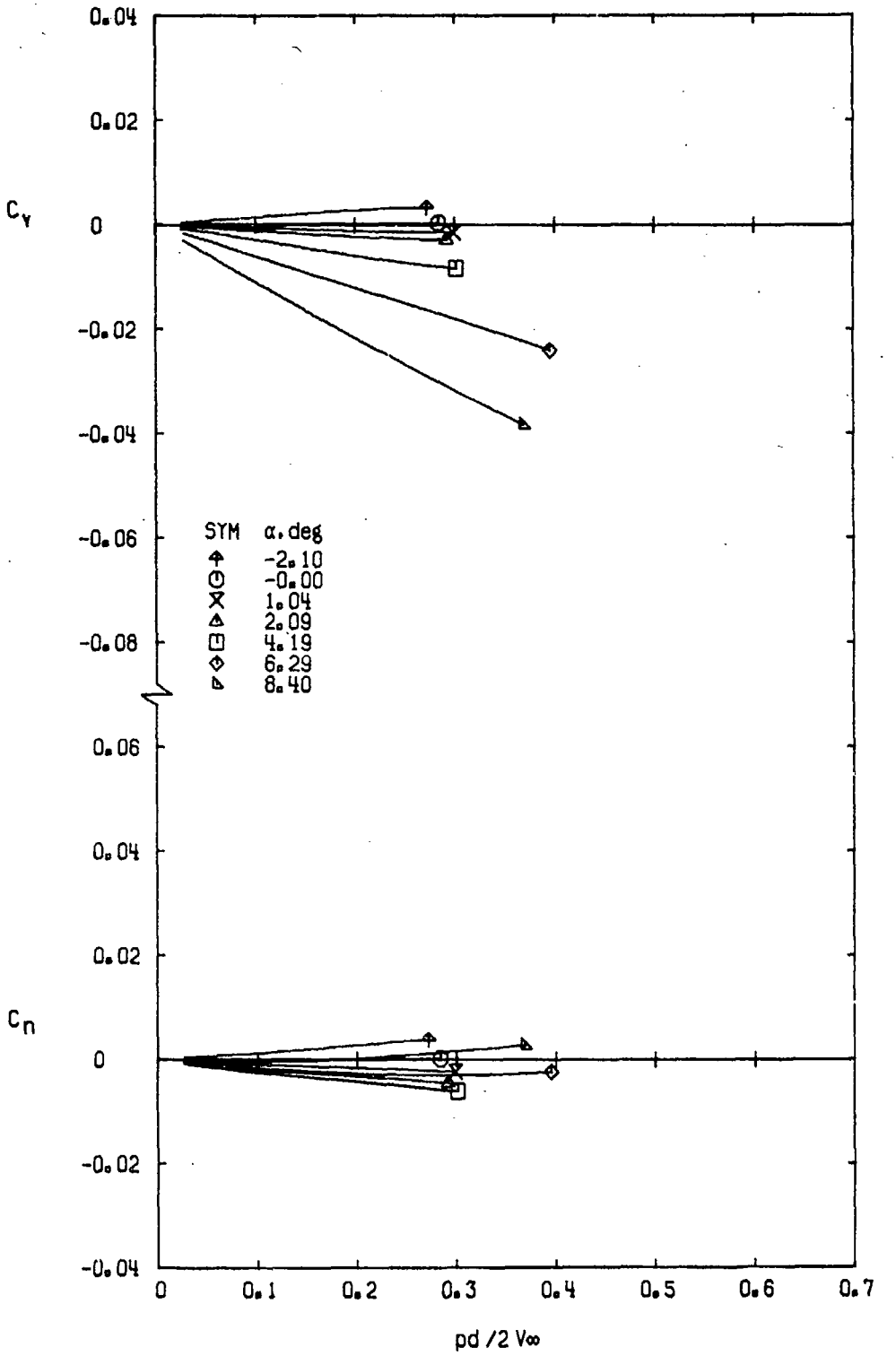

c. $M_\infty = 0.90$

Figure 8. Continued.

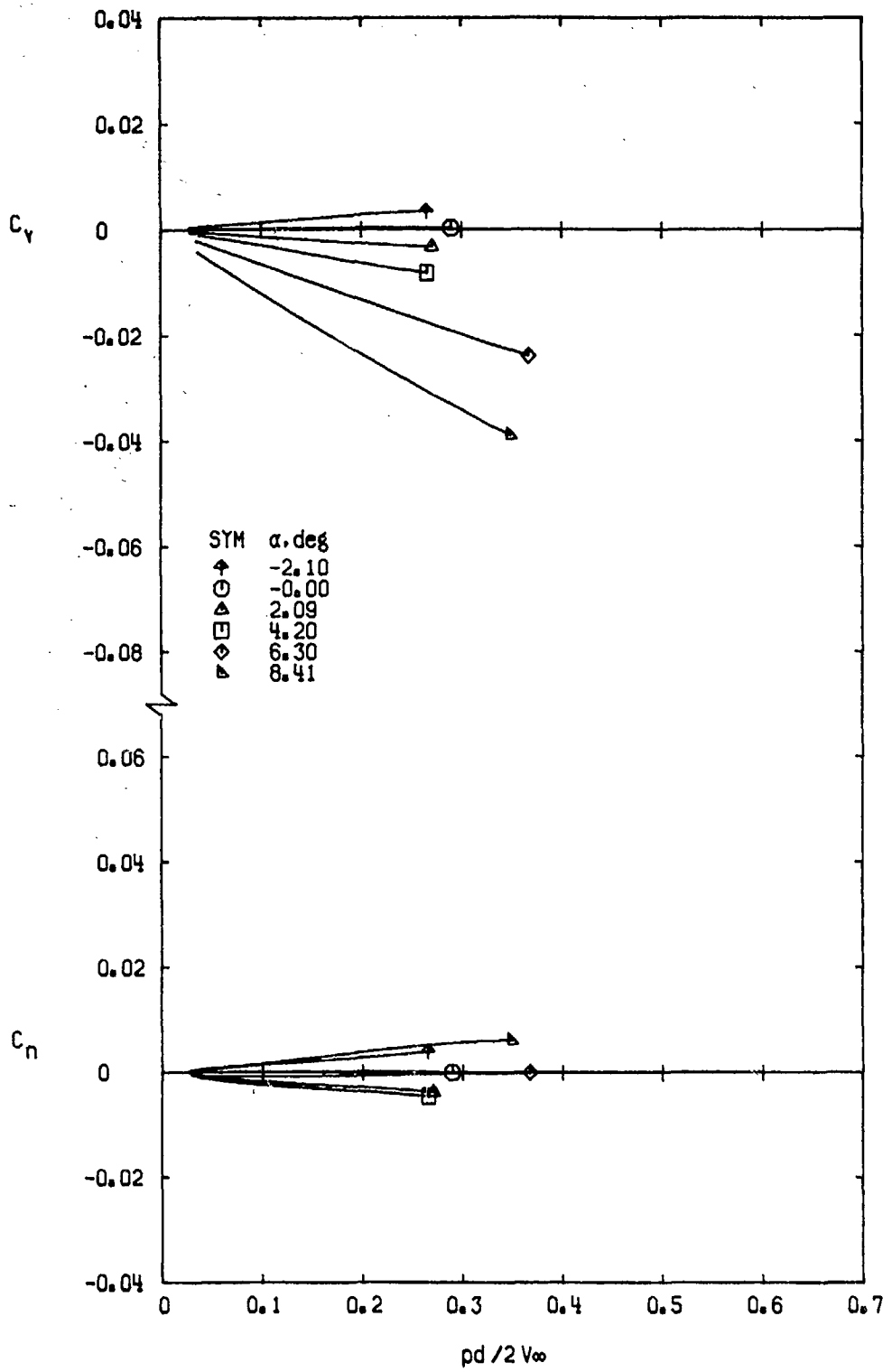

d. $M_\infty = 0.95$

Figure 8. Continued.

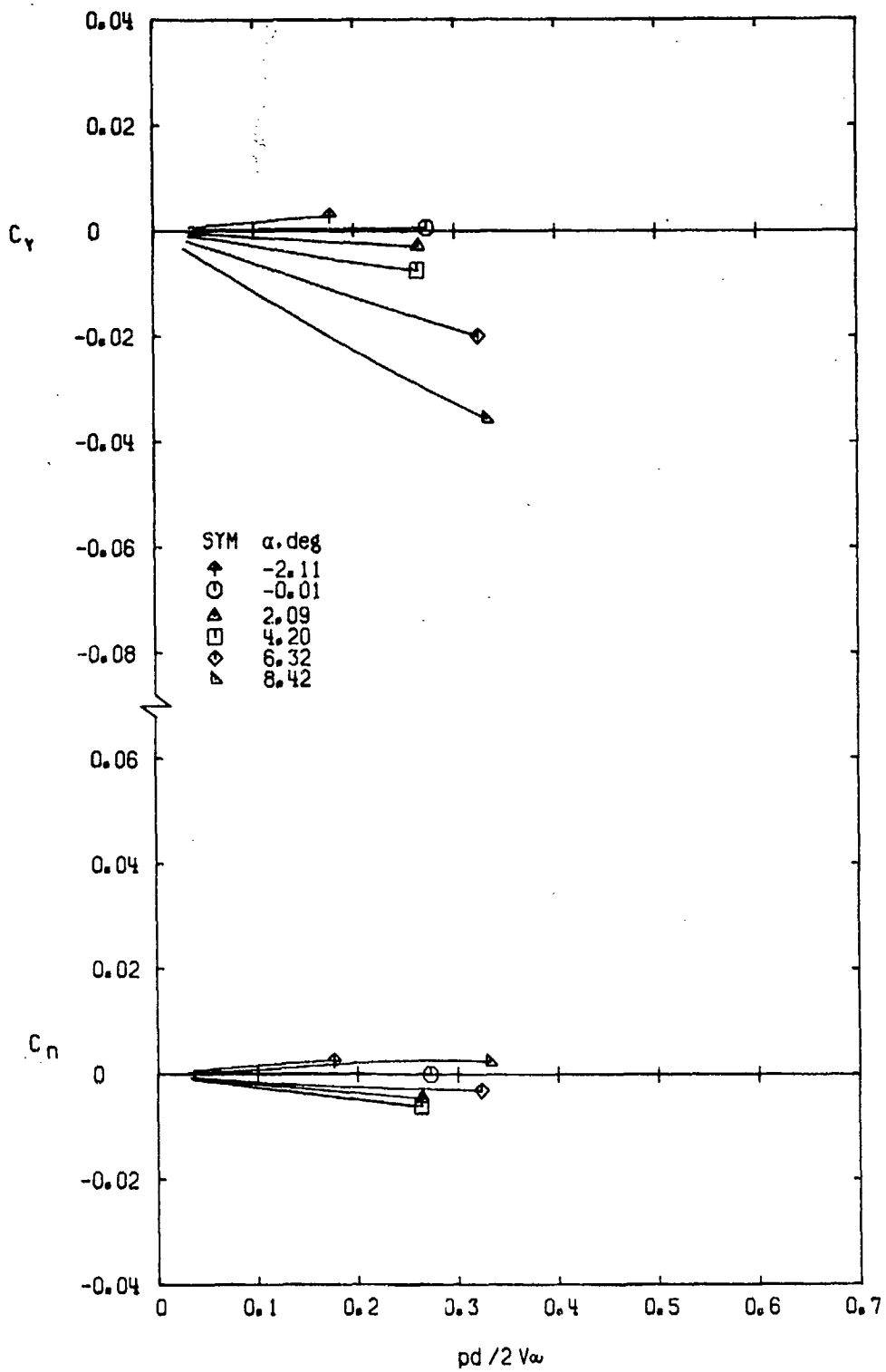

e. $M_\infty = 1.00$

Figure 8. Continued.

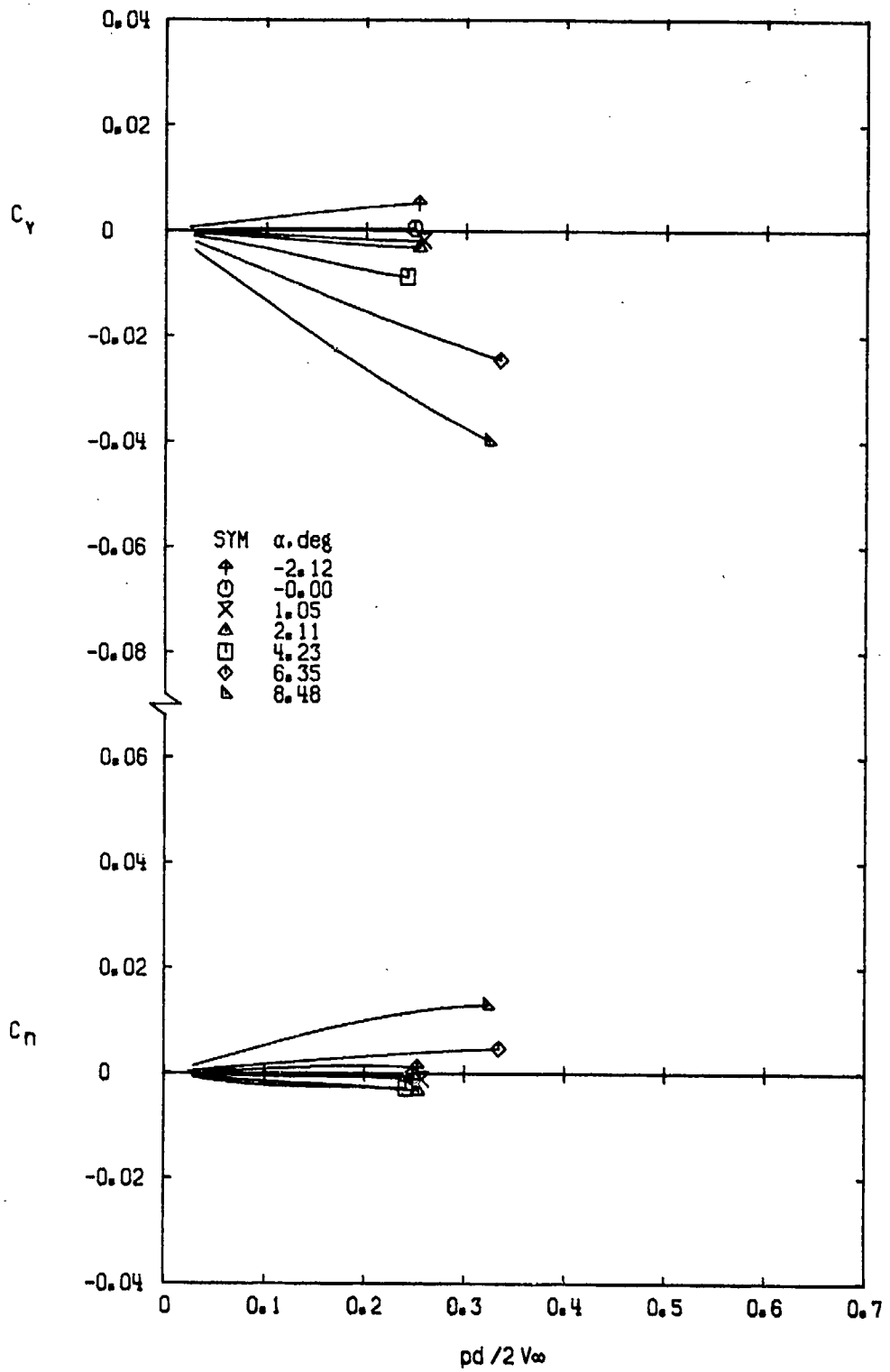

f. $M_\infty = 1.10$

Figure 8. Continued.

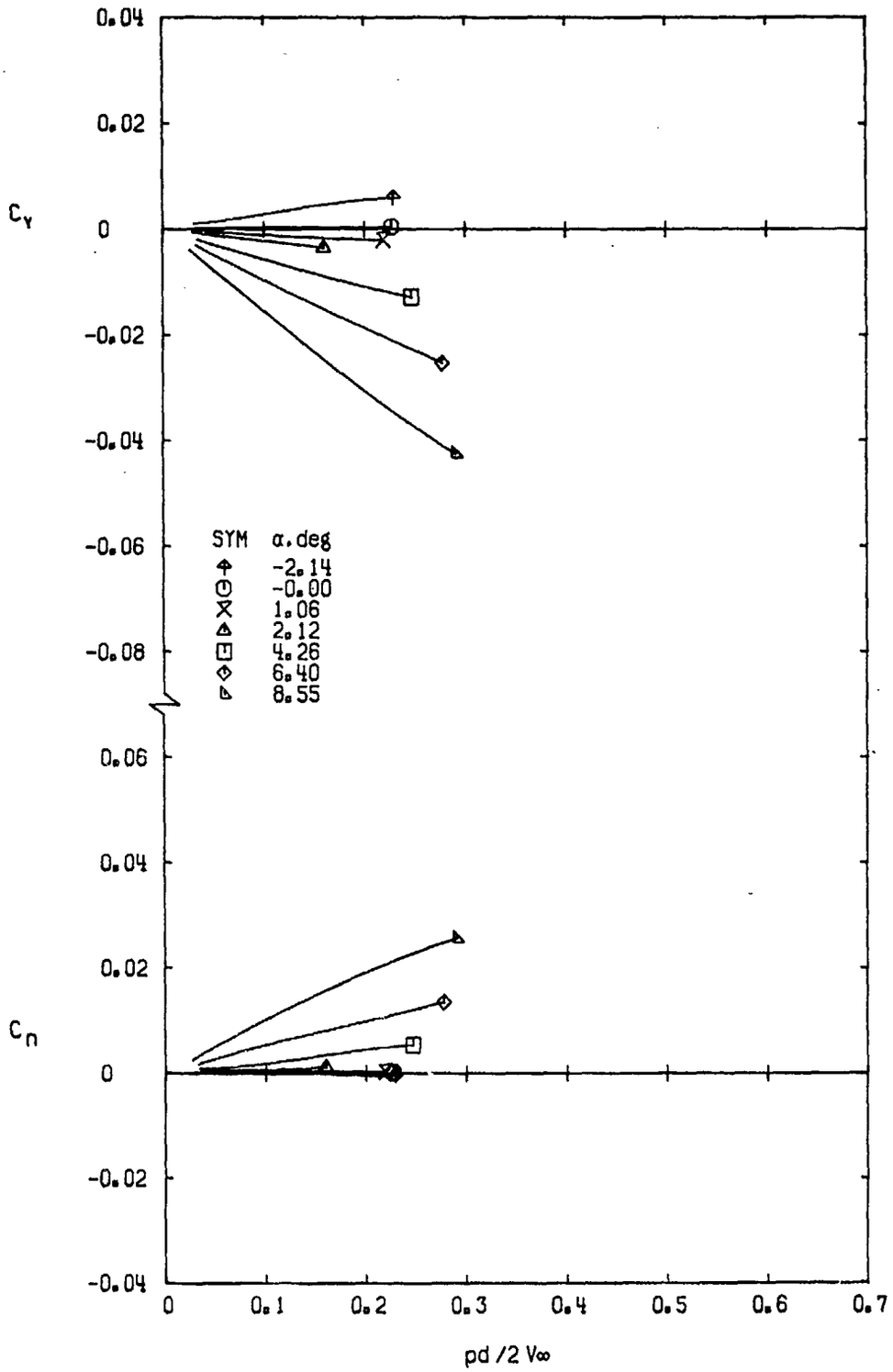

g. $M_\infty = 1.30$

Figure 8. Concluded.

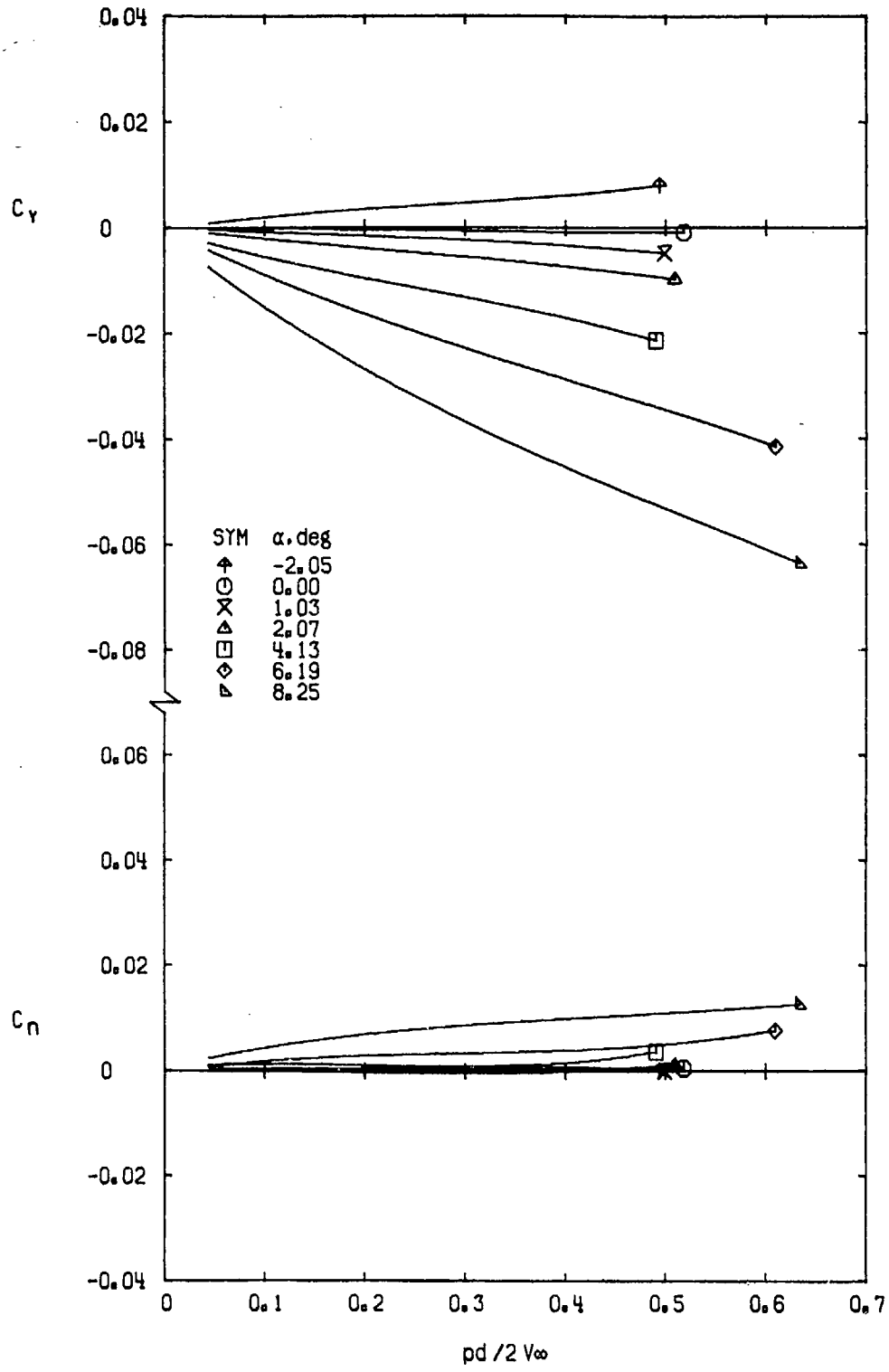

a. $M_\infty = 0.50$

Figure 9. Variation of C_Y and C_n with $pd/2V_\infty$ for Configuration 1.

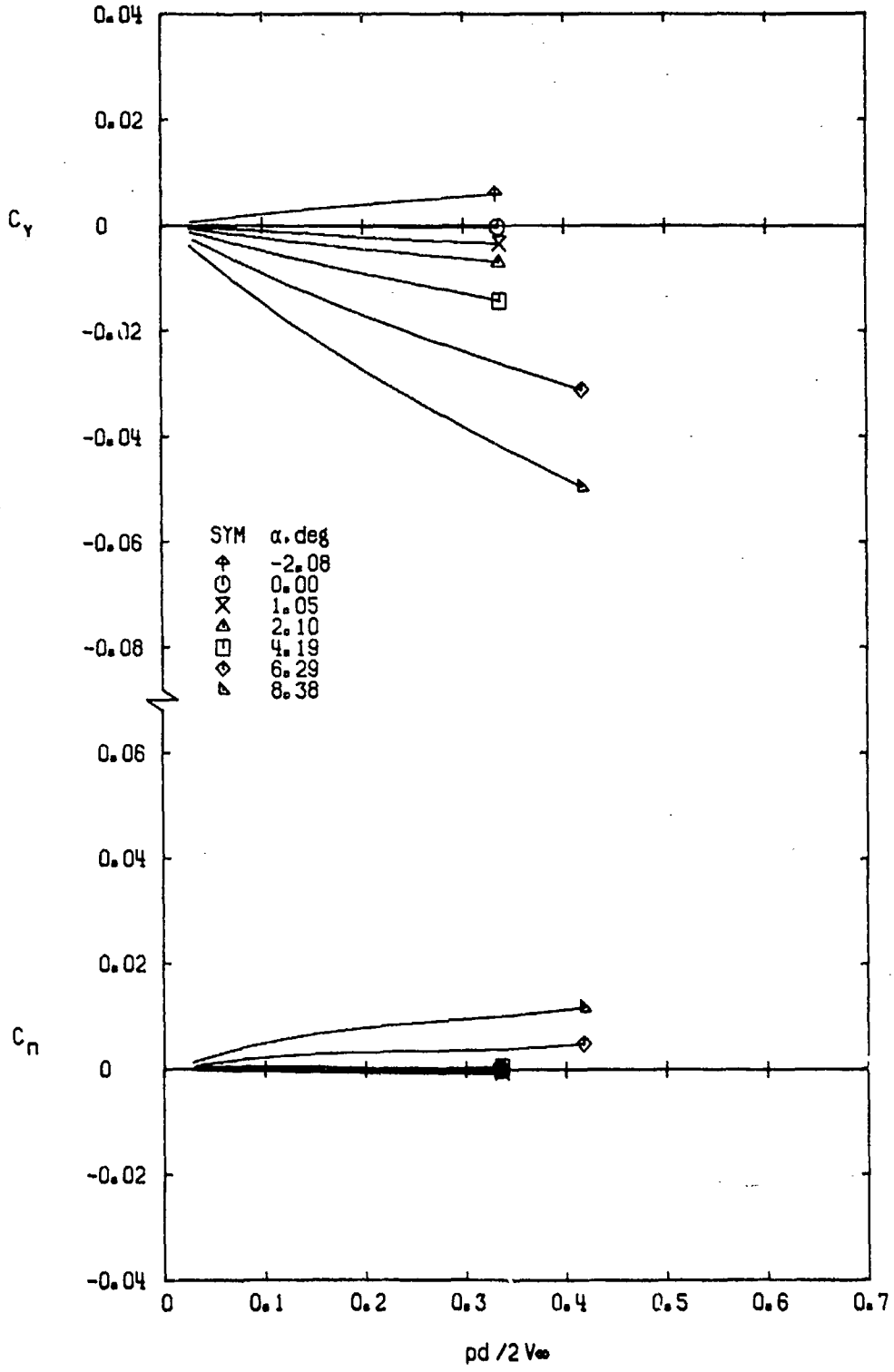

b. $M_\infty = 0.80$

Figure 9. Continued.

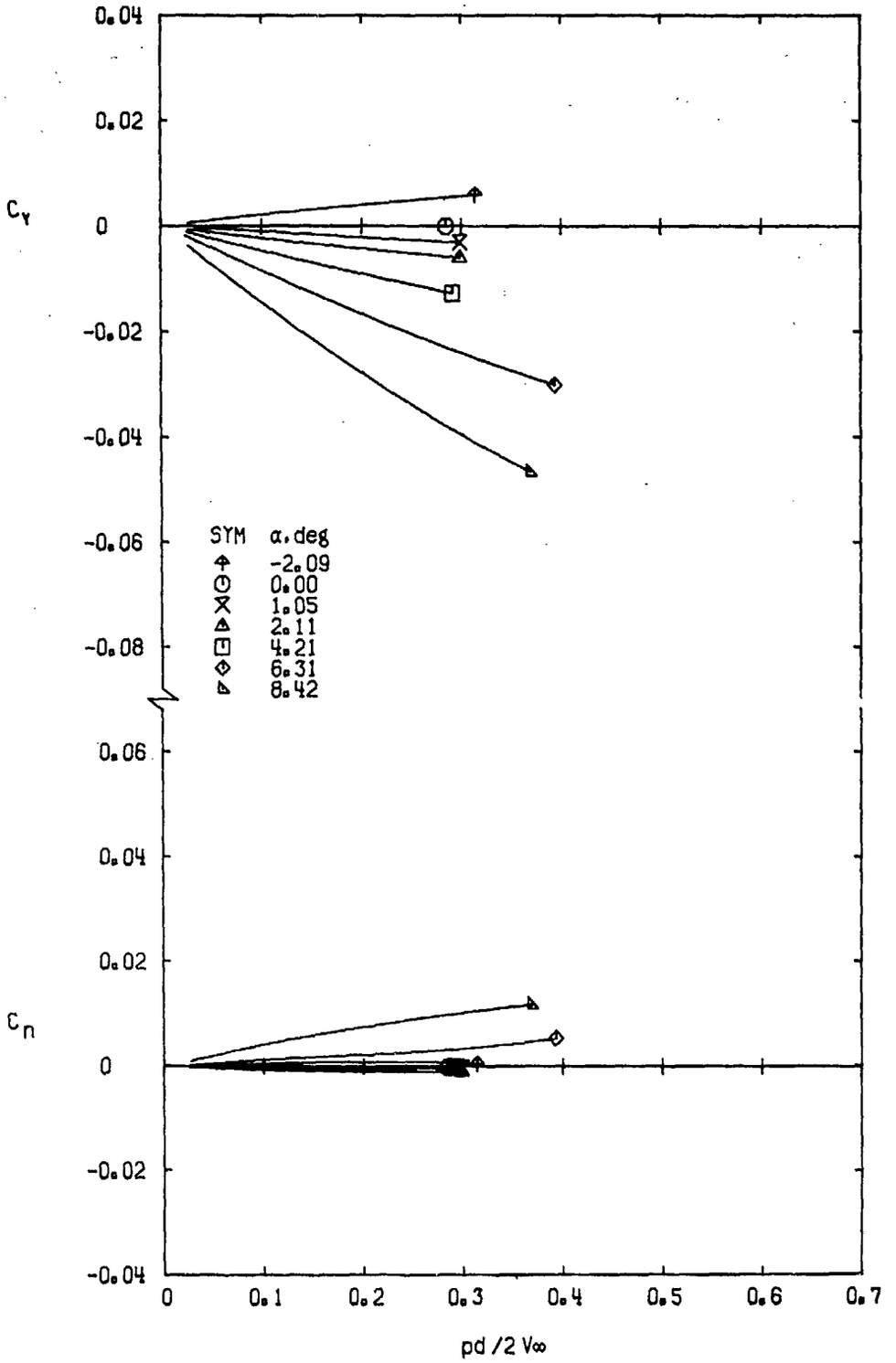

c. $M_\infty = 0.90$

Figure 9. Continued.

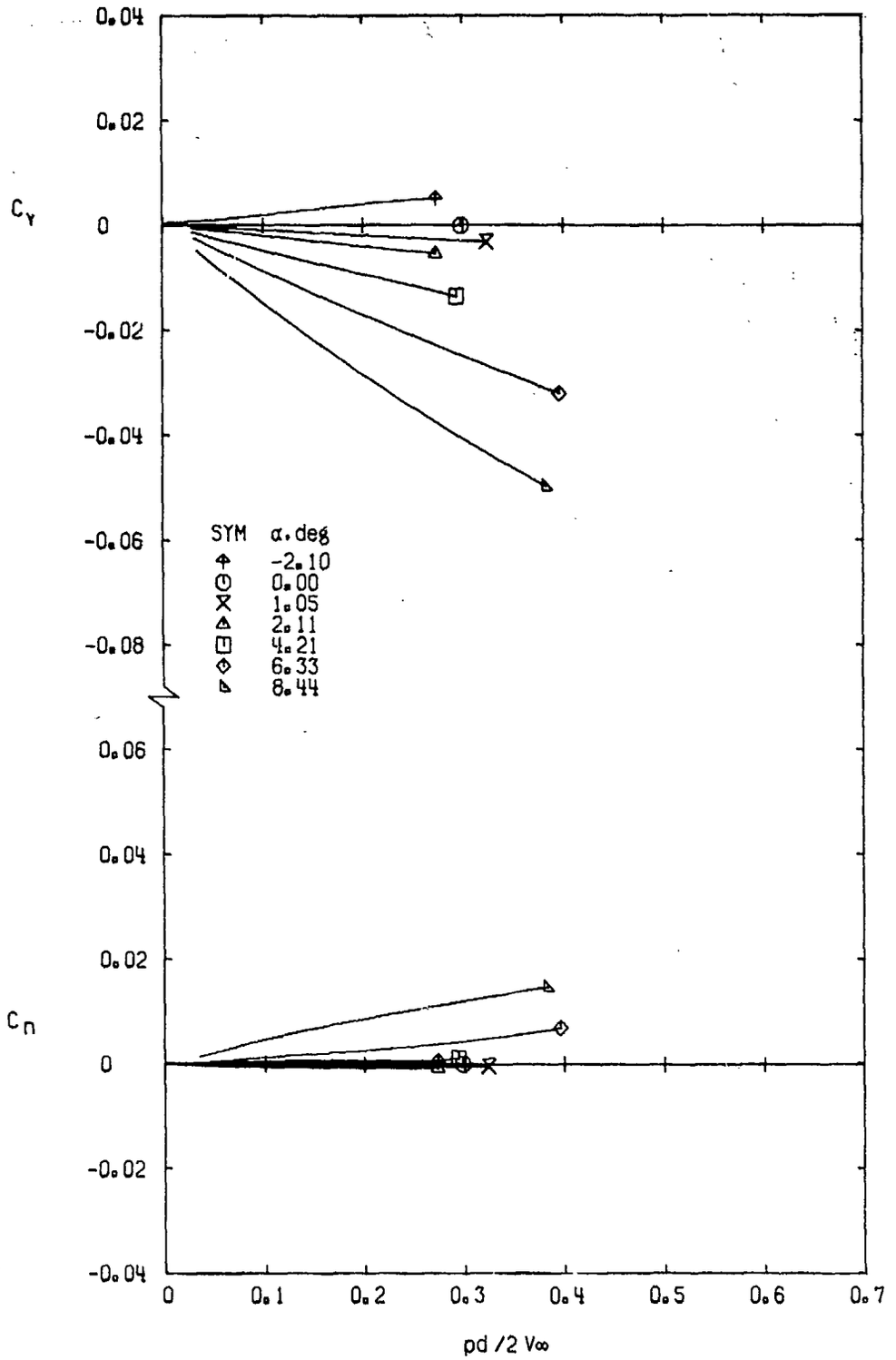

d. $M_\infty = 0.95$

Figure 9. Continued.

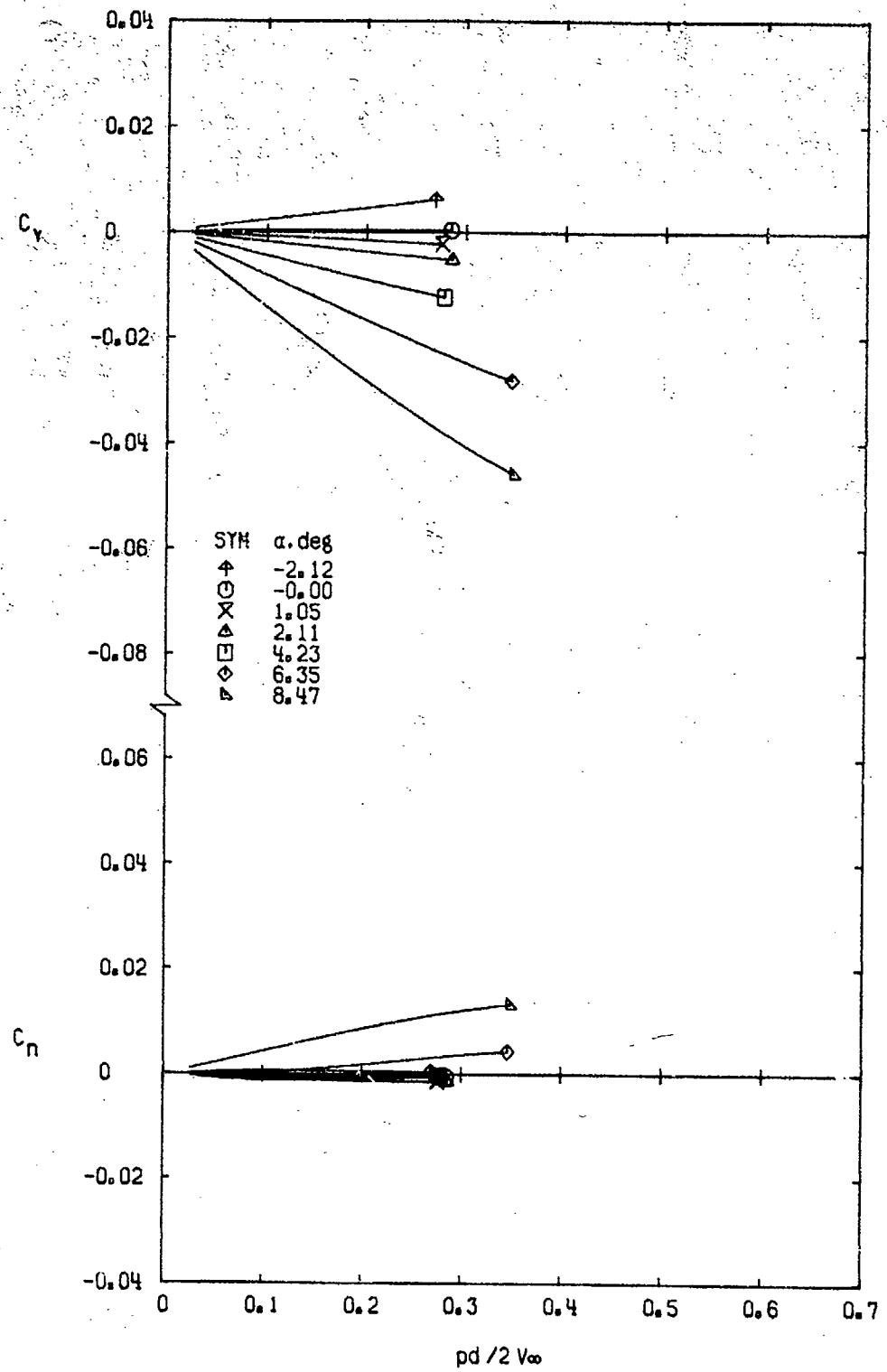

e. $M_\infty = 1.00$

Figure 9. Continued.

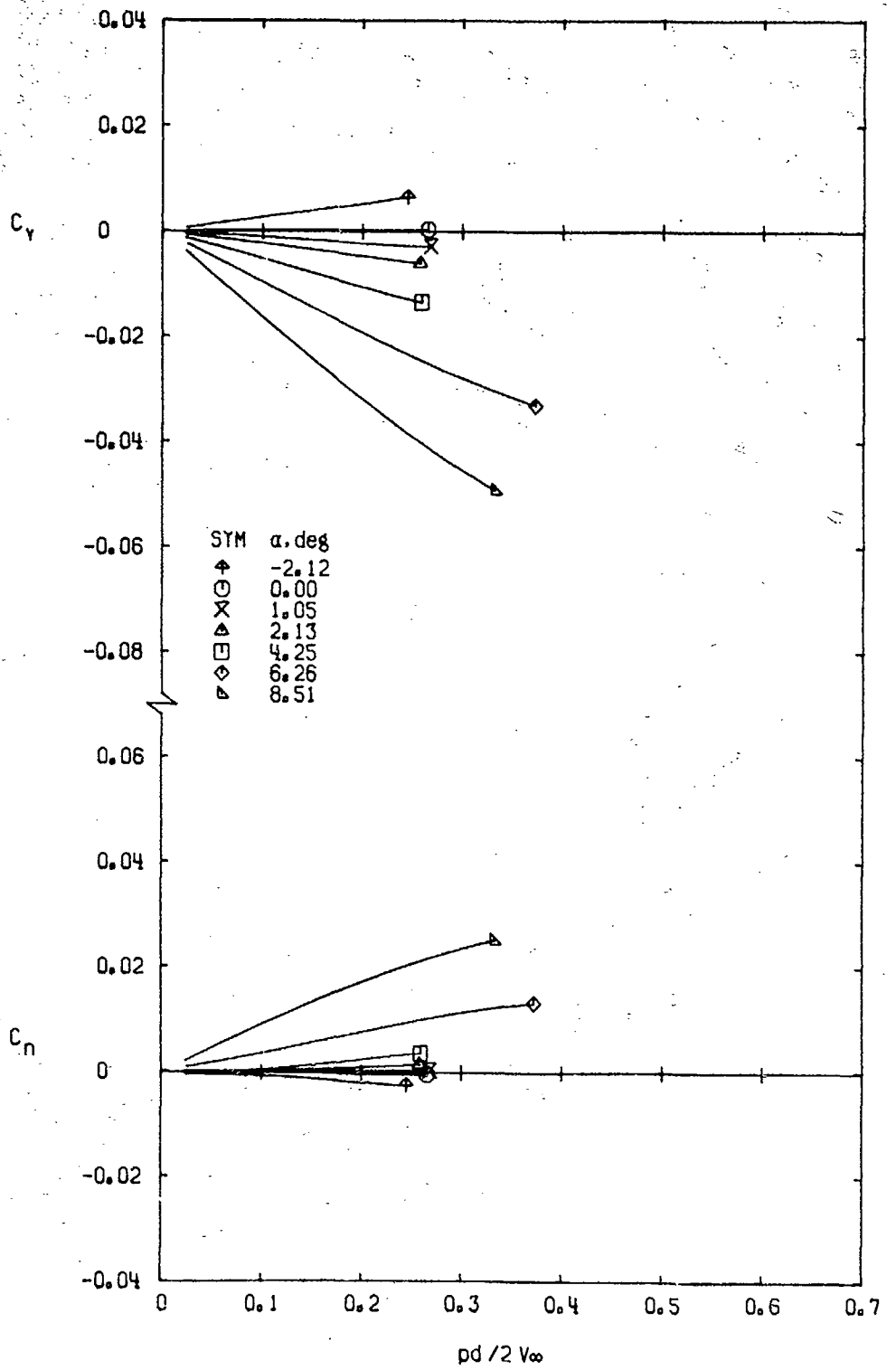

f. $M_\infty = 1.10$

Figure 9. Continued.

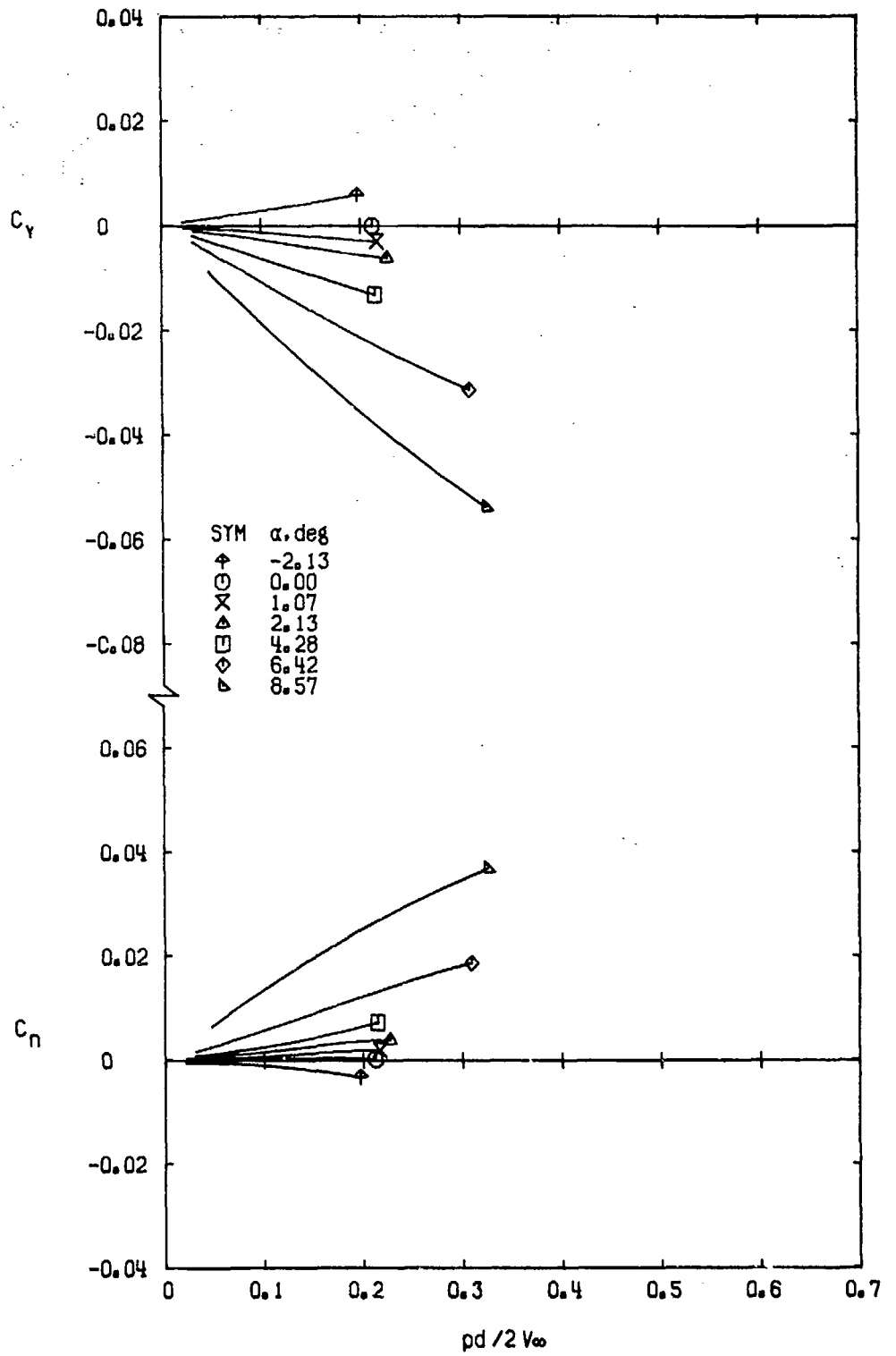

g. $M_\infty = 1.30$

Figure 9. Concluded.

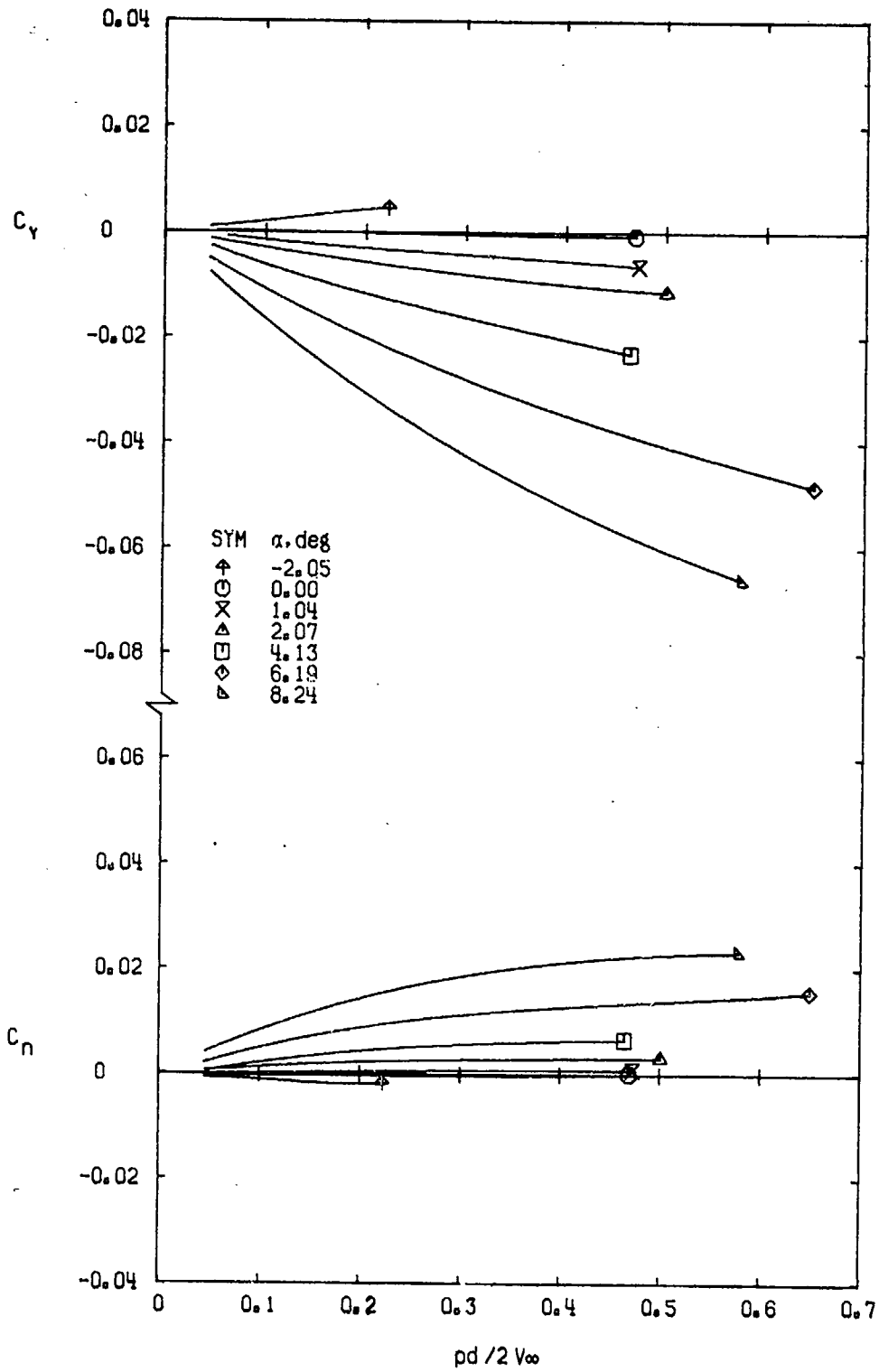

a. $M_\infty = 0.50$

Figure 10. Variation of C_Y and C_n with $pd/2V_\infty$ for Configuration 2.

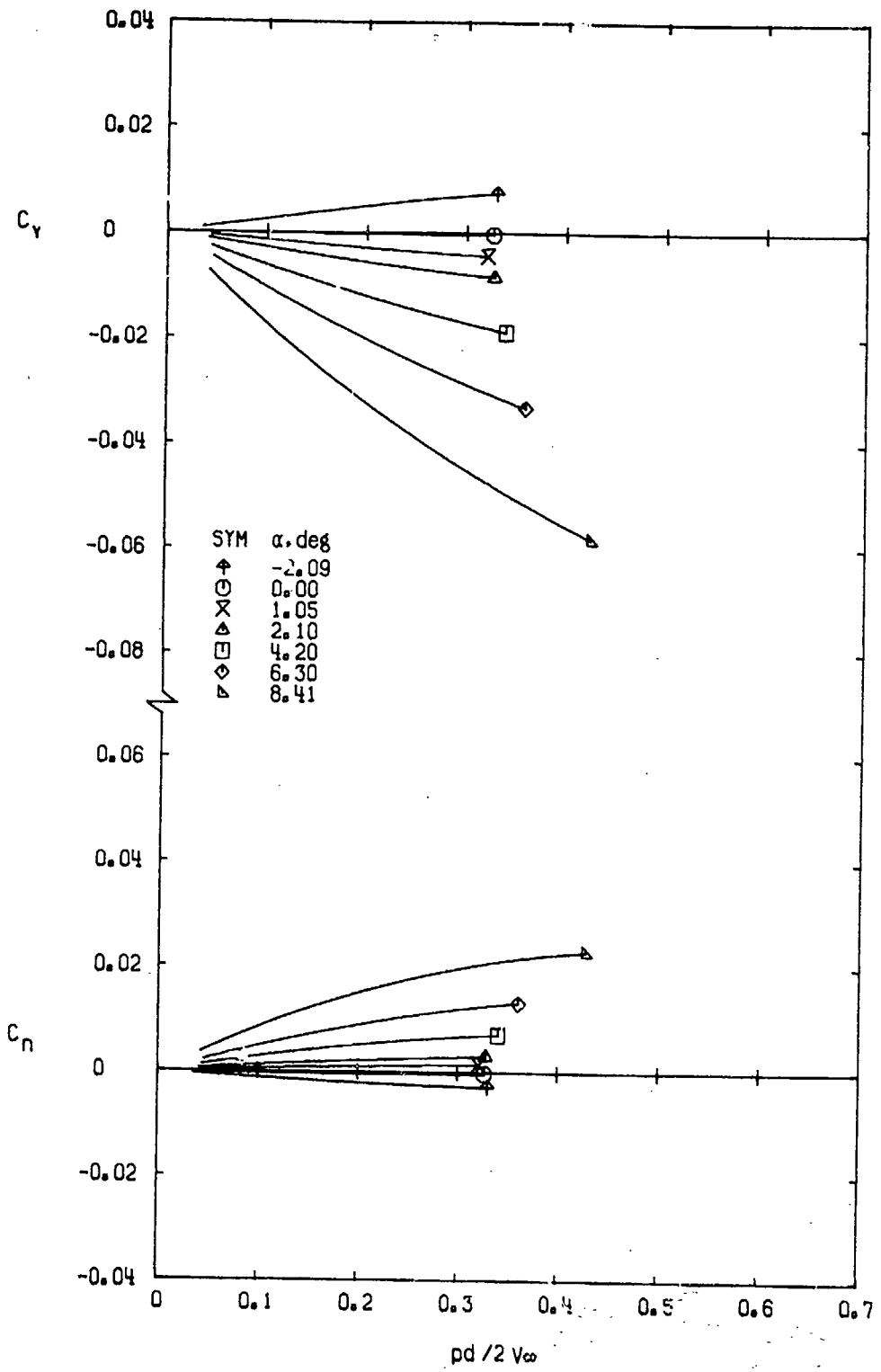

b. $M_\infty = 0.80$

Figure 10. Continued.

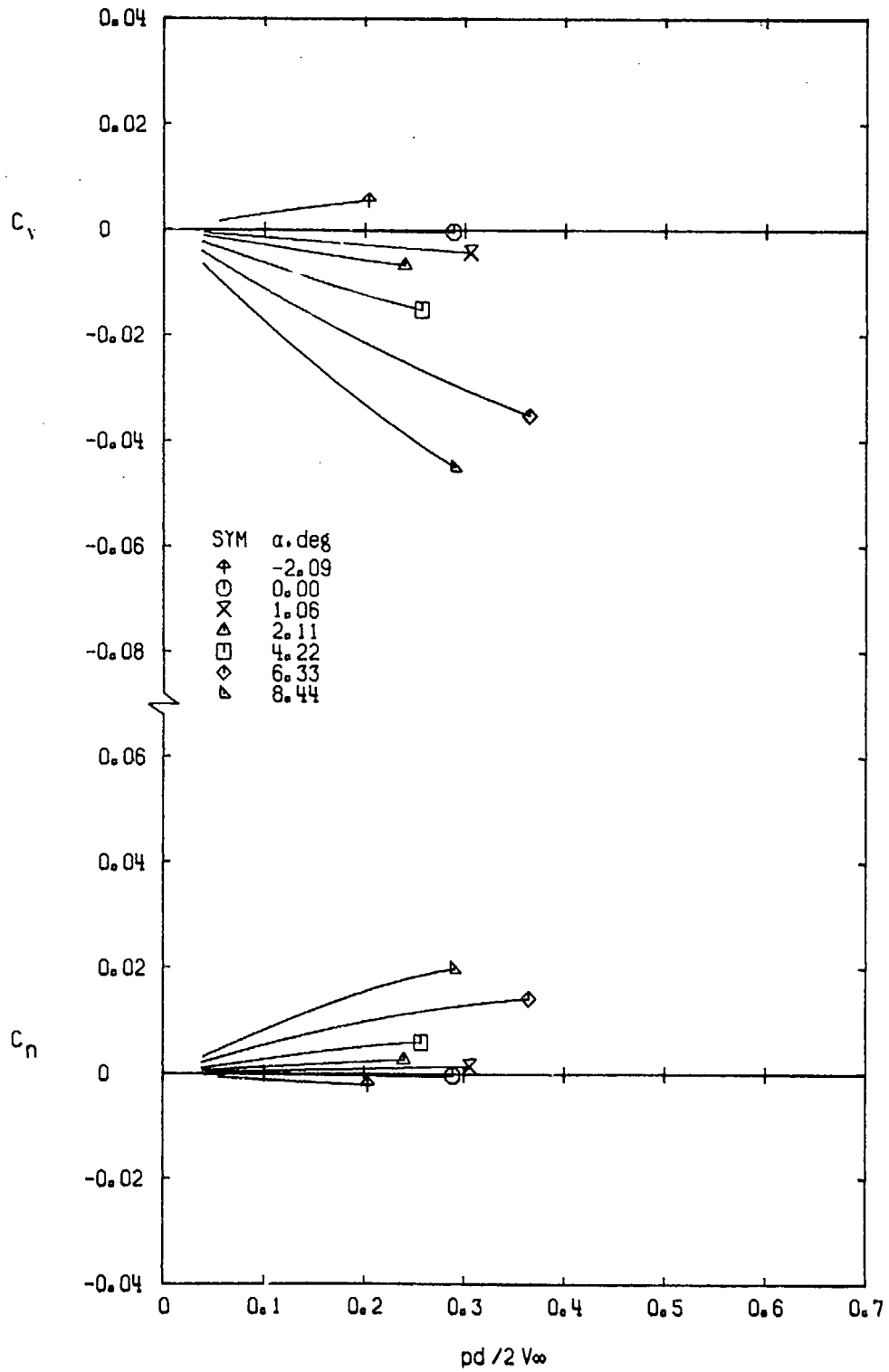

c. M_∞ = 0.90

Figure 10. Continued.

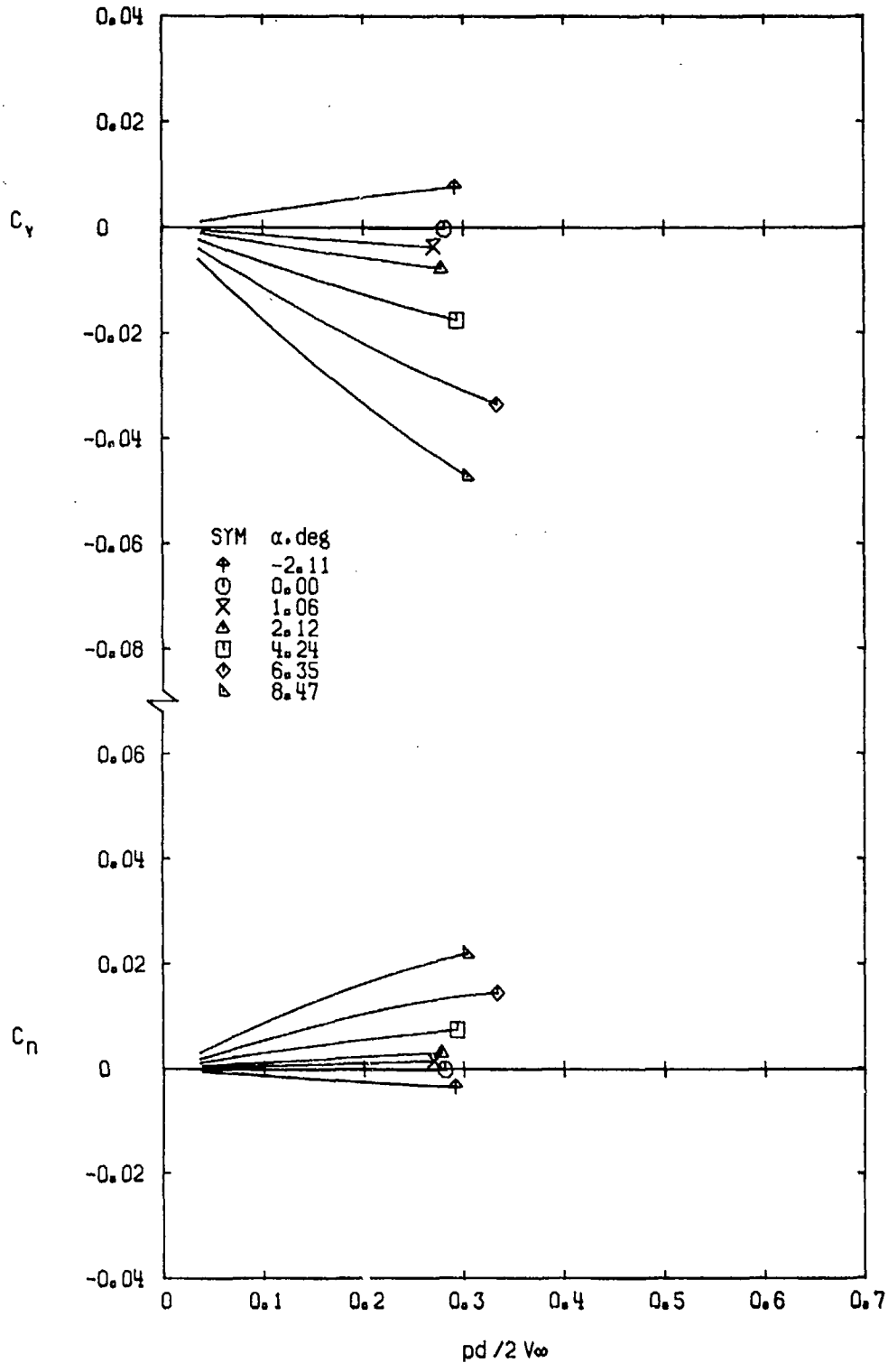

d. $M_\infty = 0.95$

Figure 10. Continued.

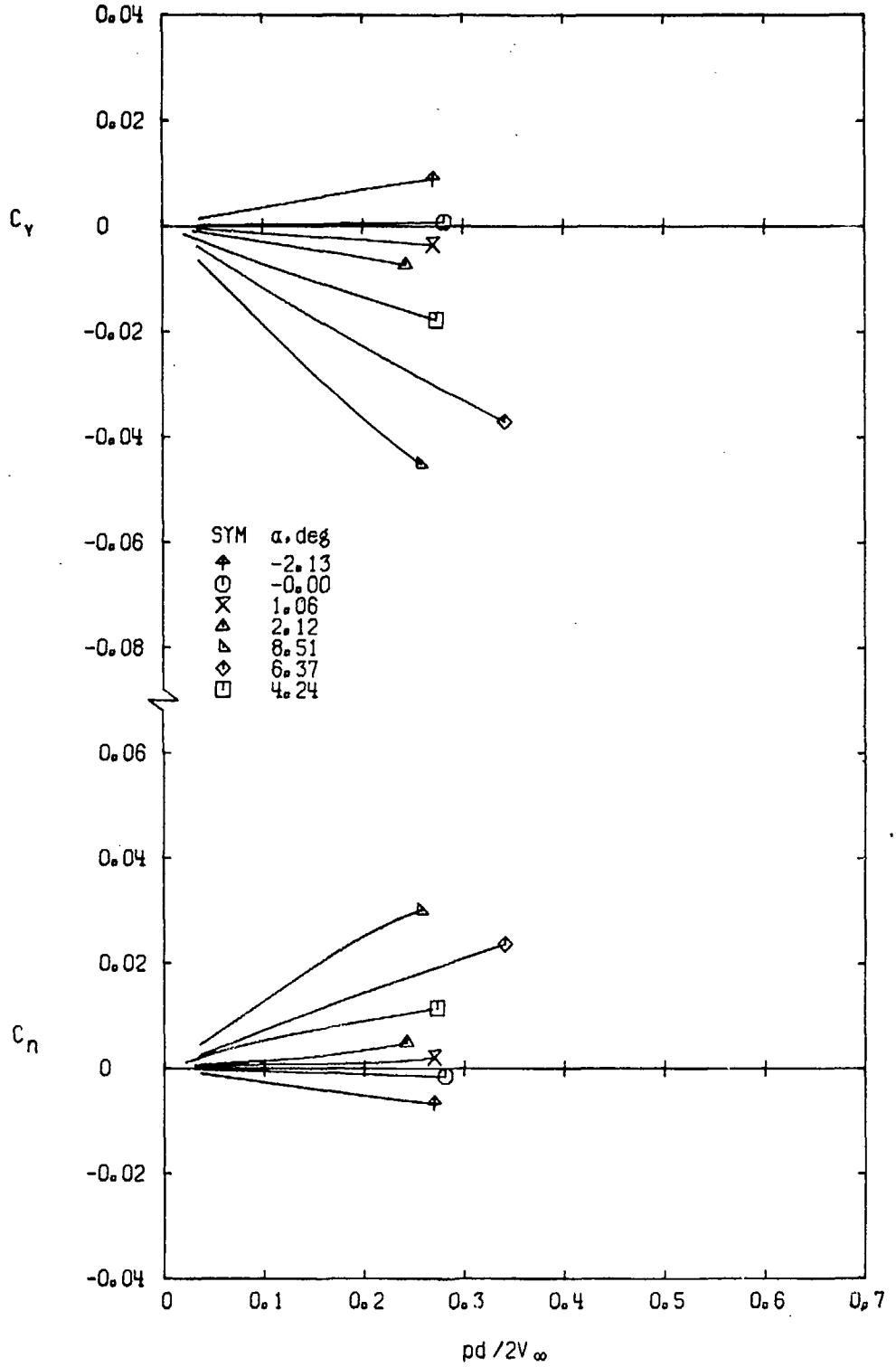

e. M_∞ = 1.00

Figure 10. Continued.

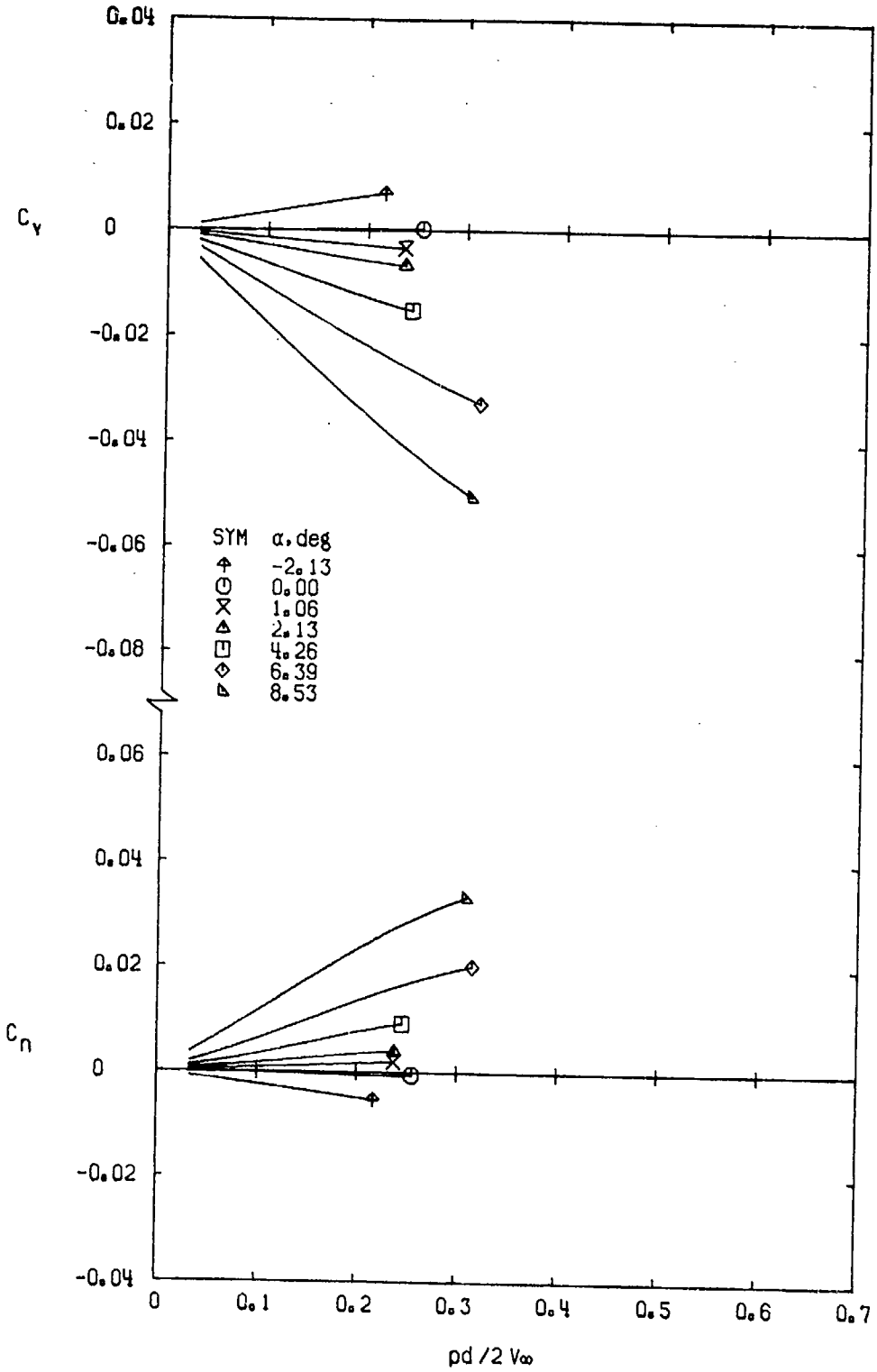

f. $M_\infty = 1.10$

Figure 10. Continued.

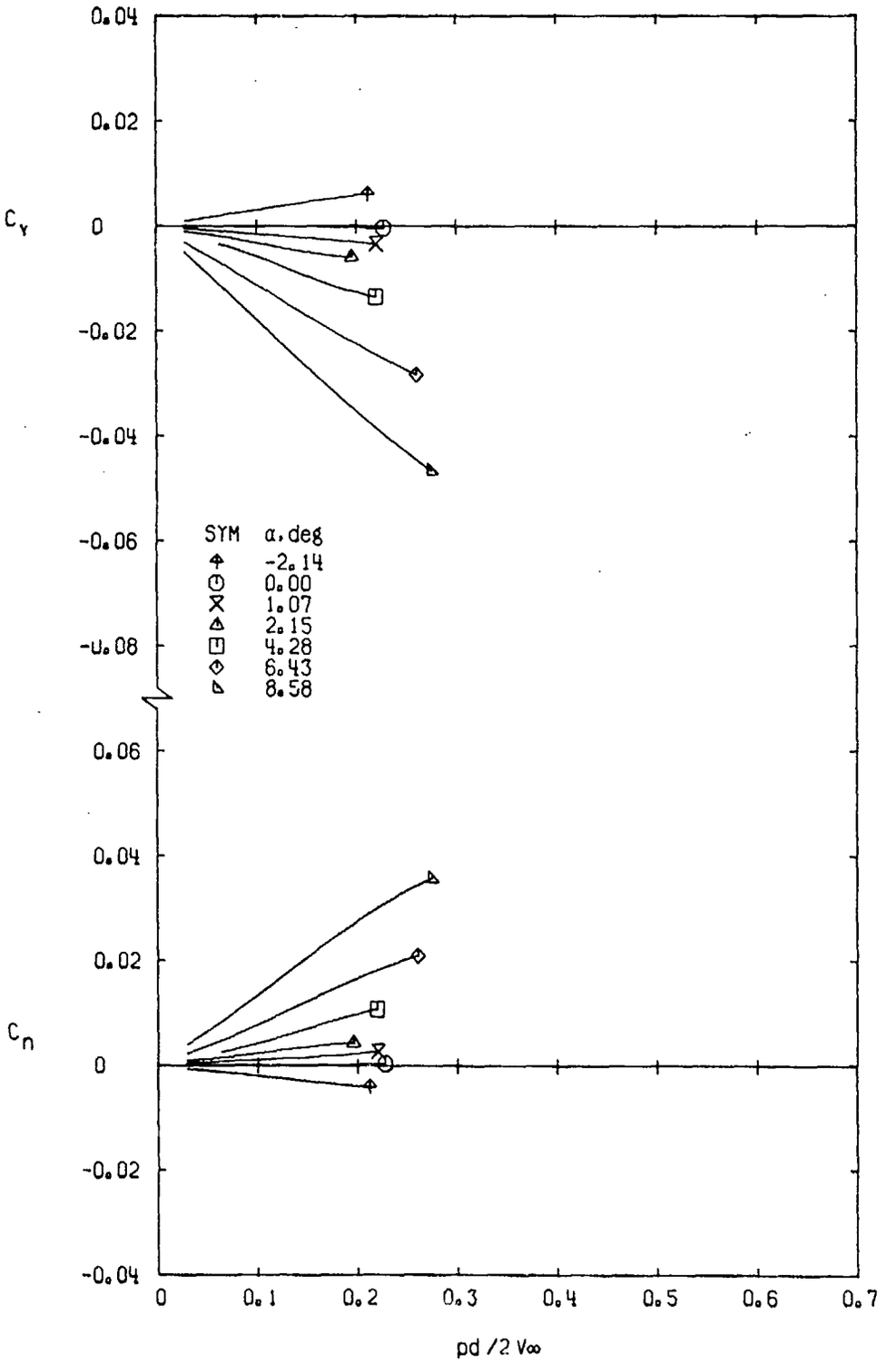

g. M_∞ = 1.30

Figure 10. Concluded.

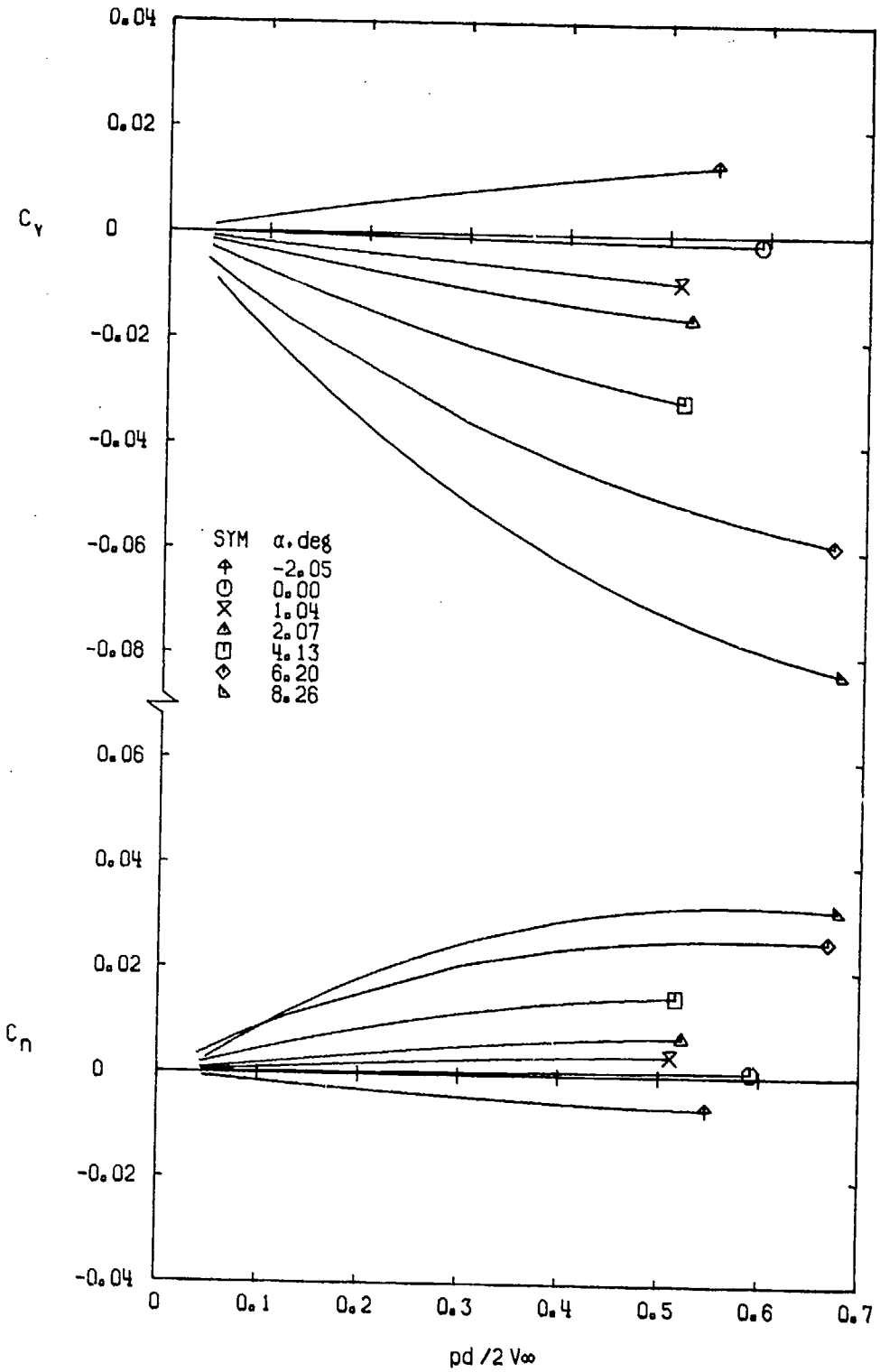

a. $M_\infty = 0.50$

Figure 11. Variation of C_Y and C_n with $pd/2V_\infty$ for Configuration 3.

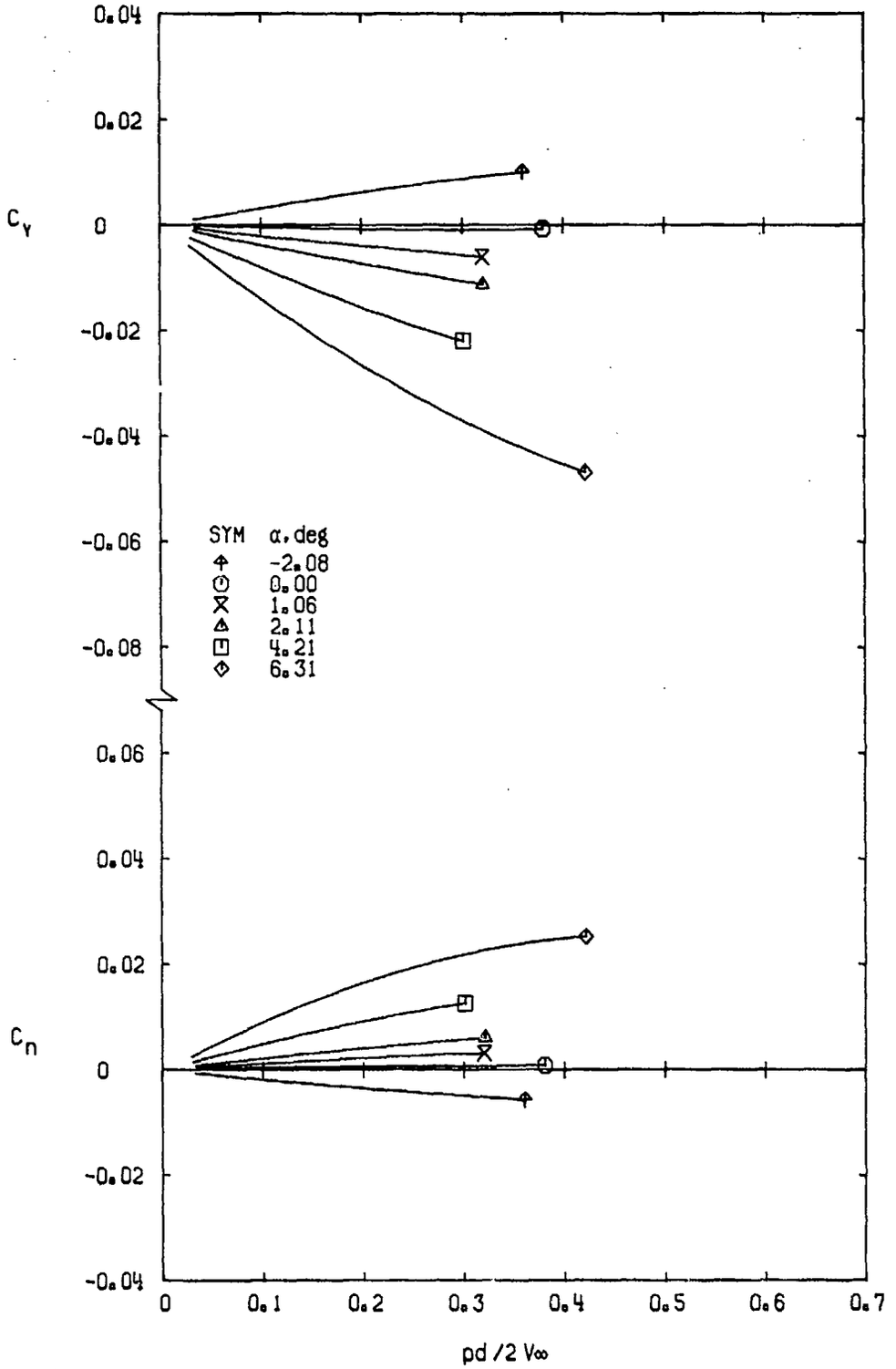

b. M_∞ = 0.80

Figure 11. Continued.

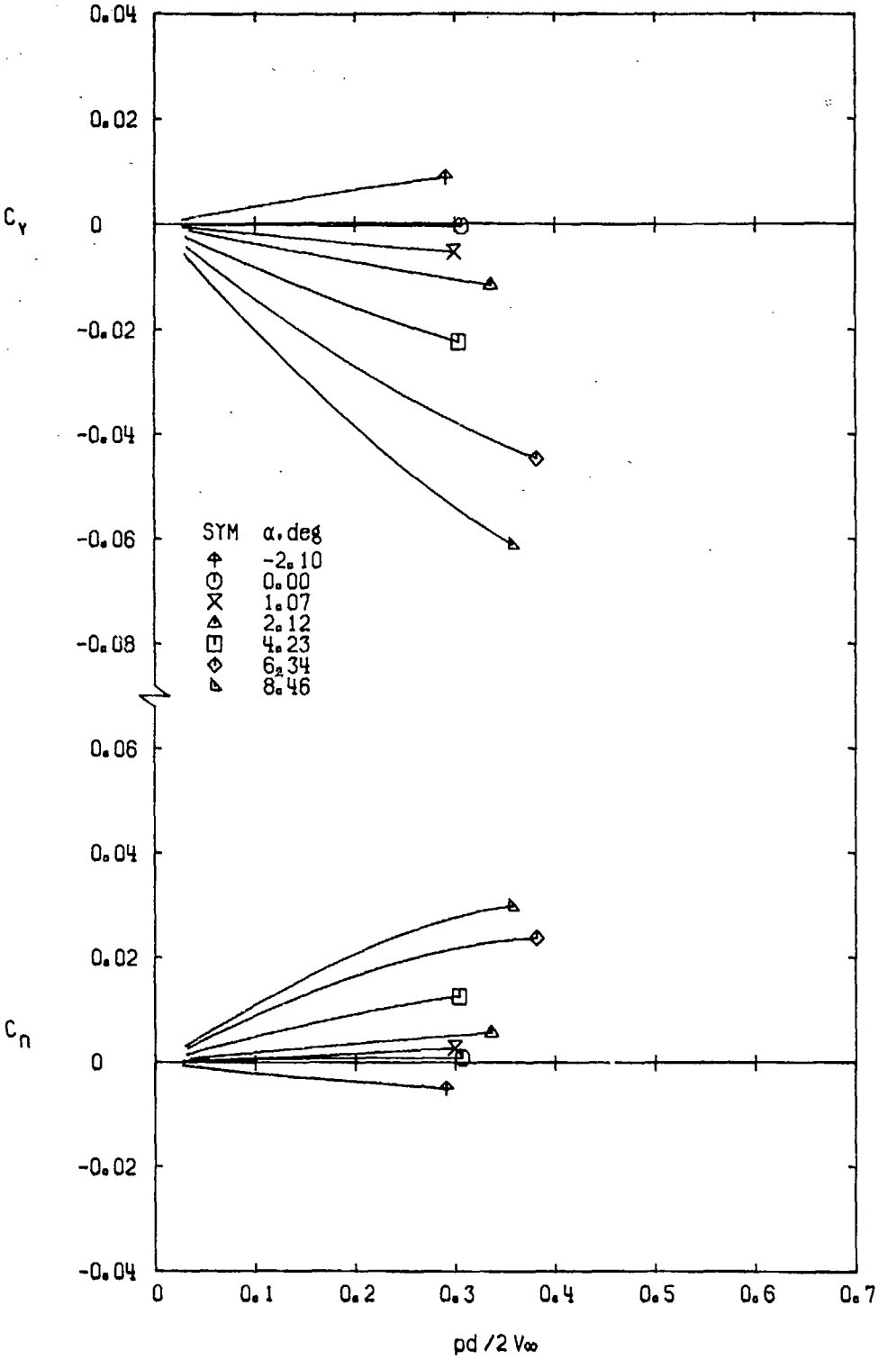

c. $M_\infty = 0.90$

Figure 11. Continued.

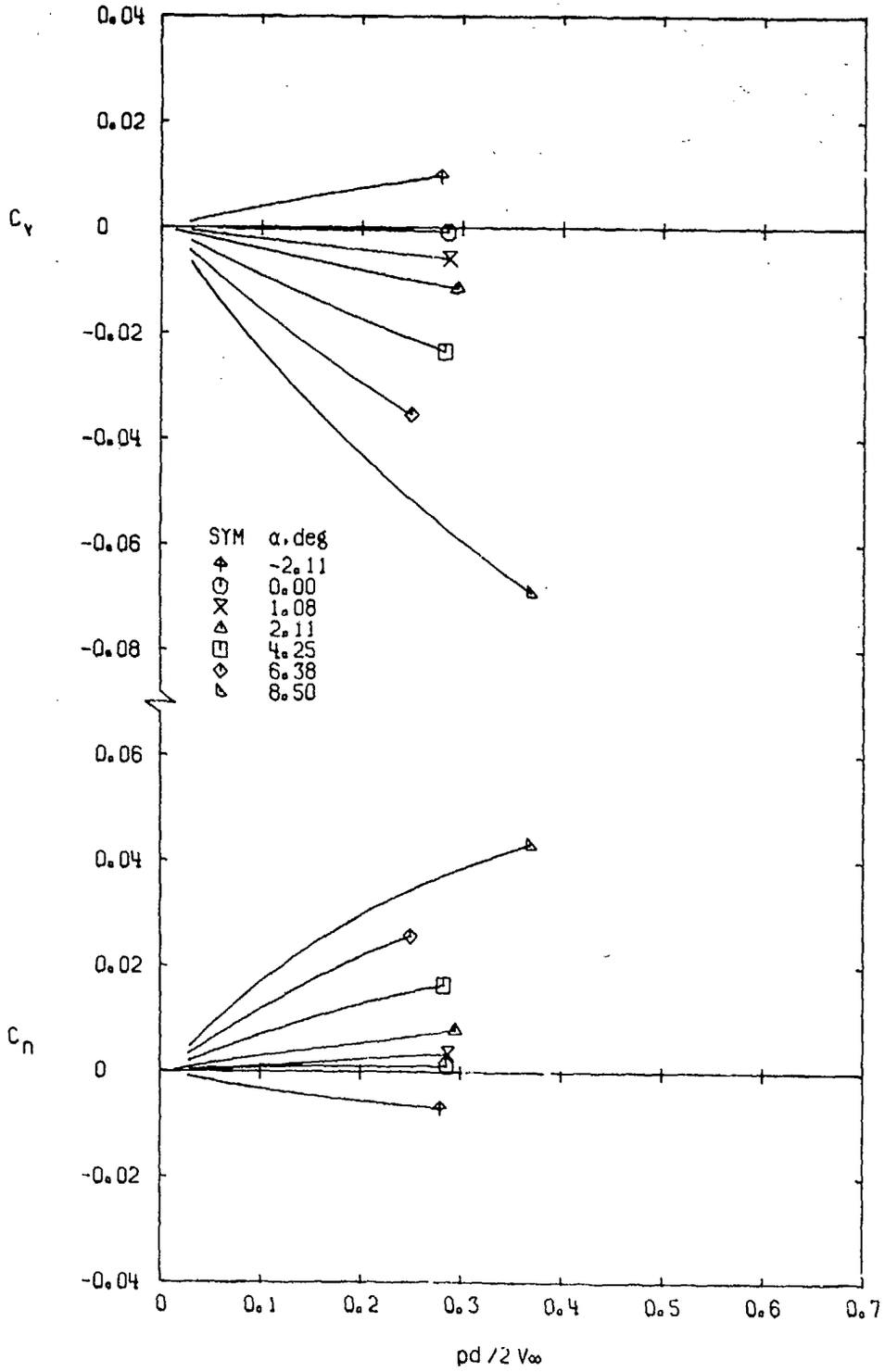

d. $M_\infty = 0.95$

Figure 11. Continued.

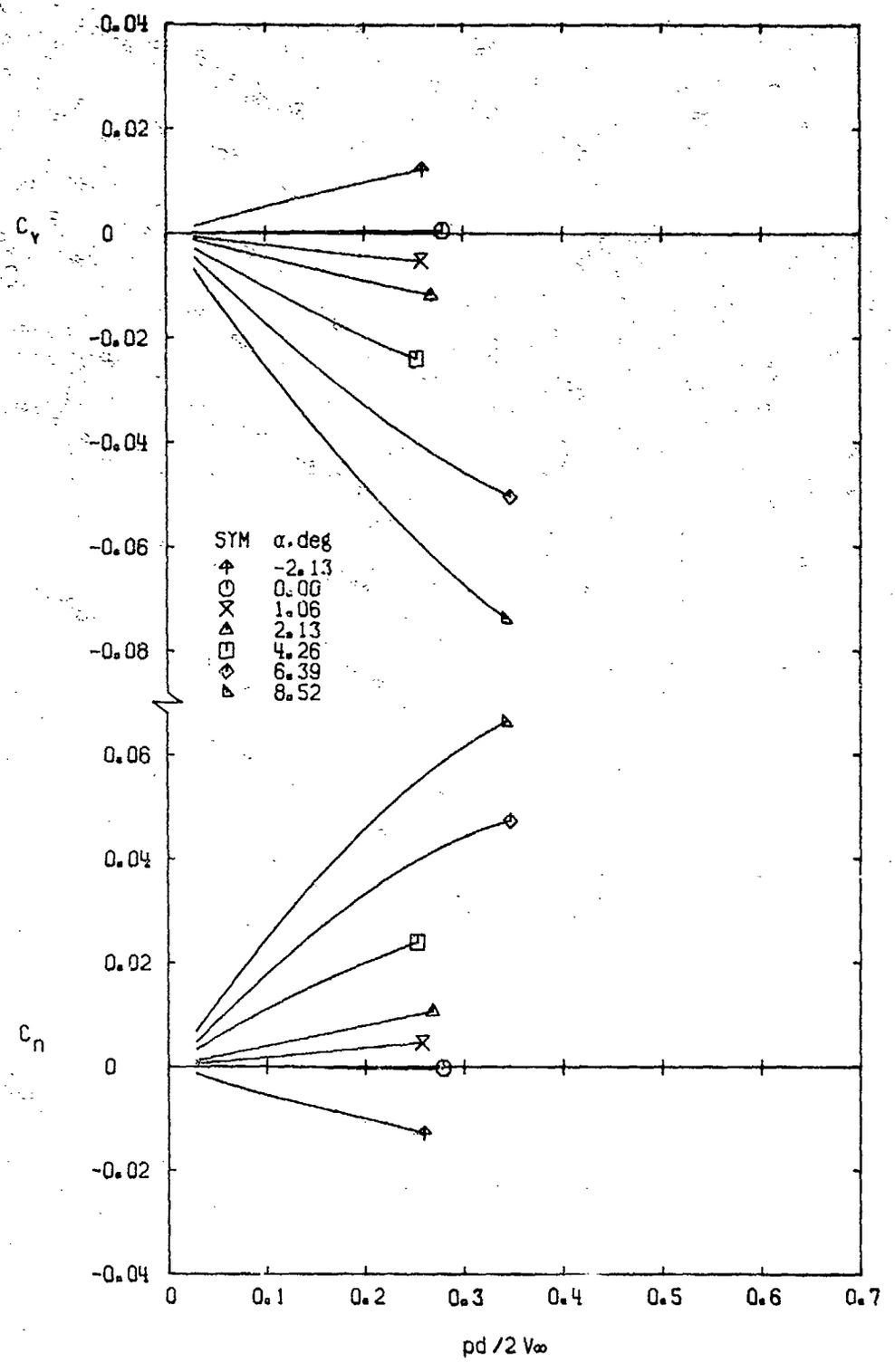

e. $M_\infty = 1.00$

Figure 11. Continued.

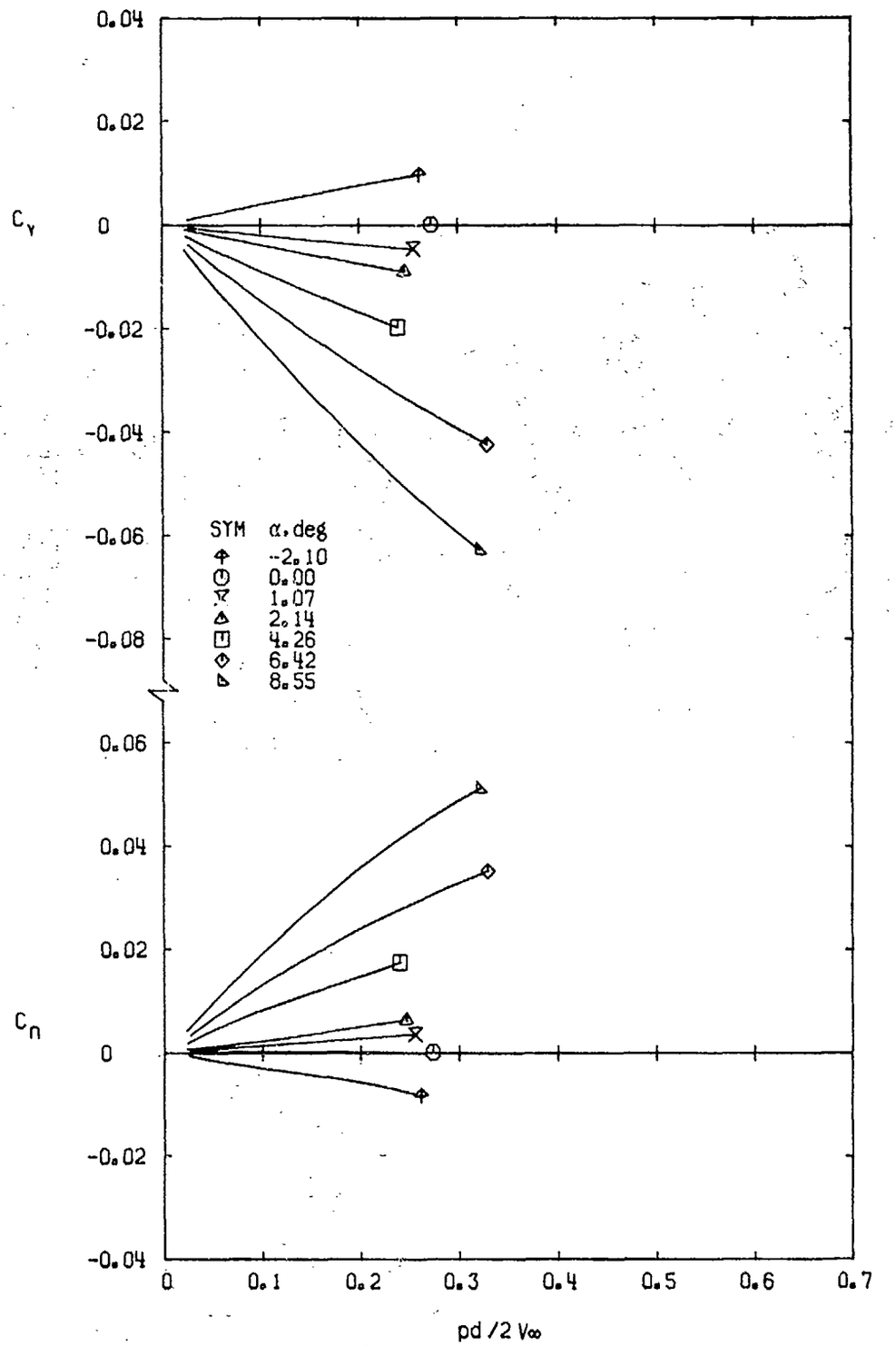

f. $M_\infty = 1.10$

Figure 11. Continued.

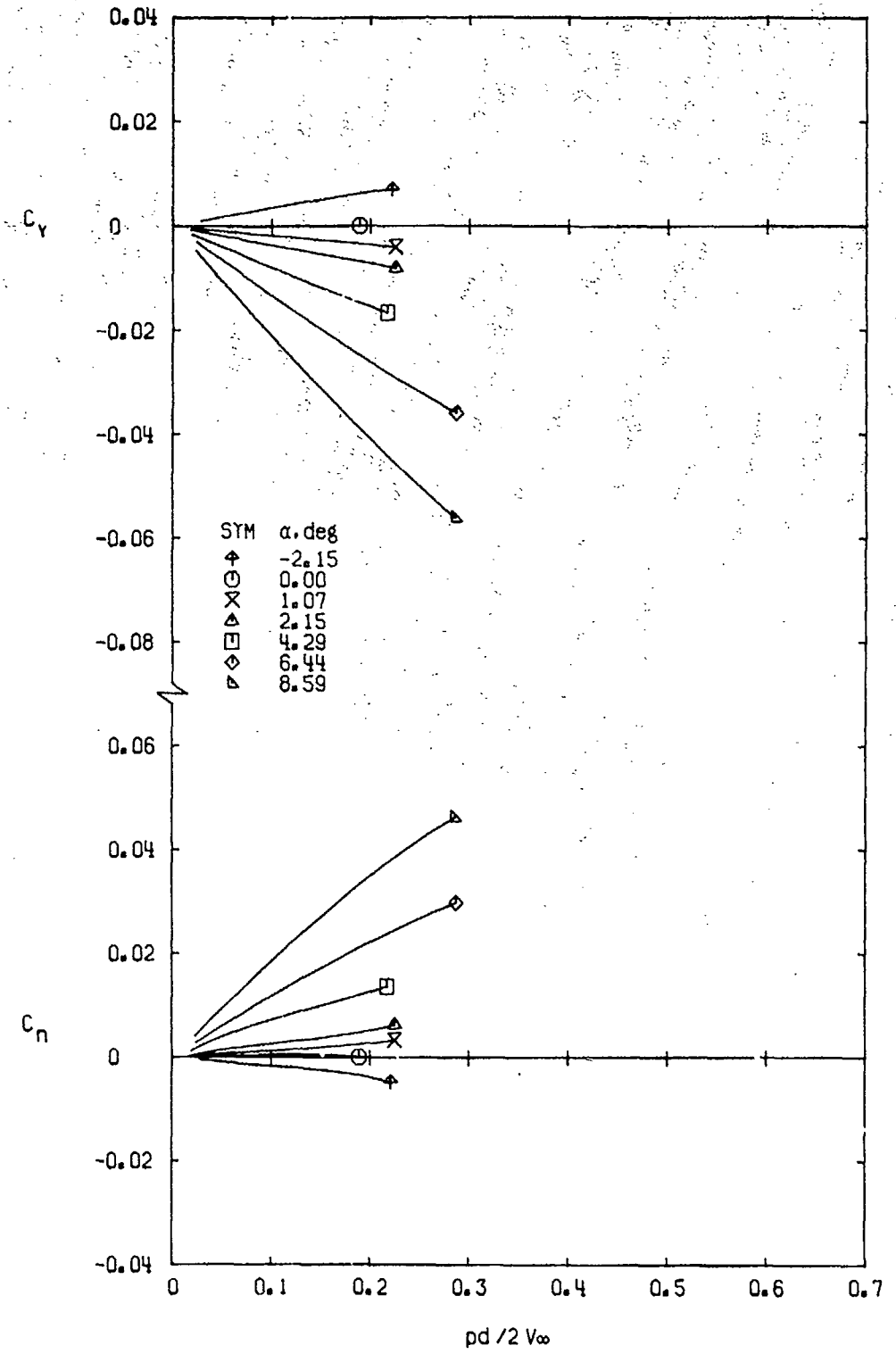

g. $M_\infty = 1.30$

Figure 11. Concluded.

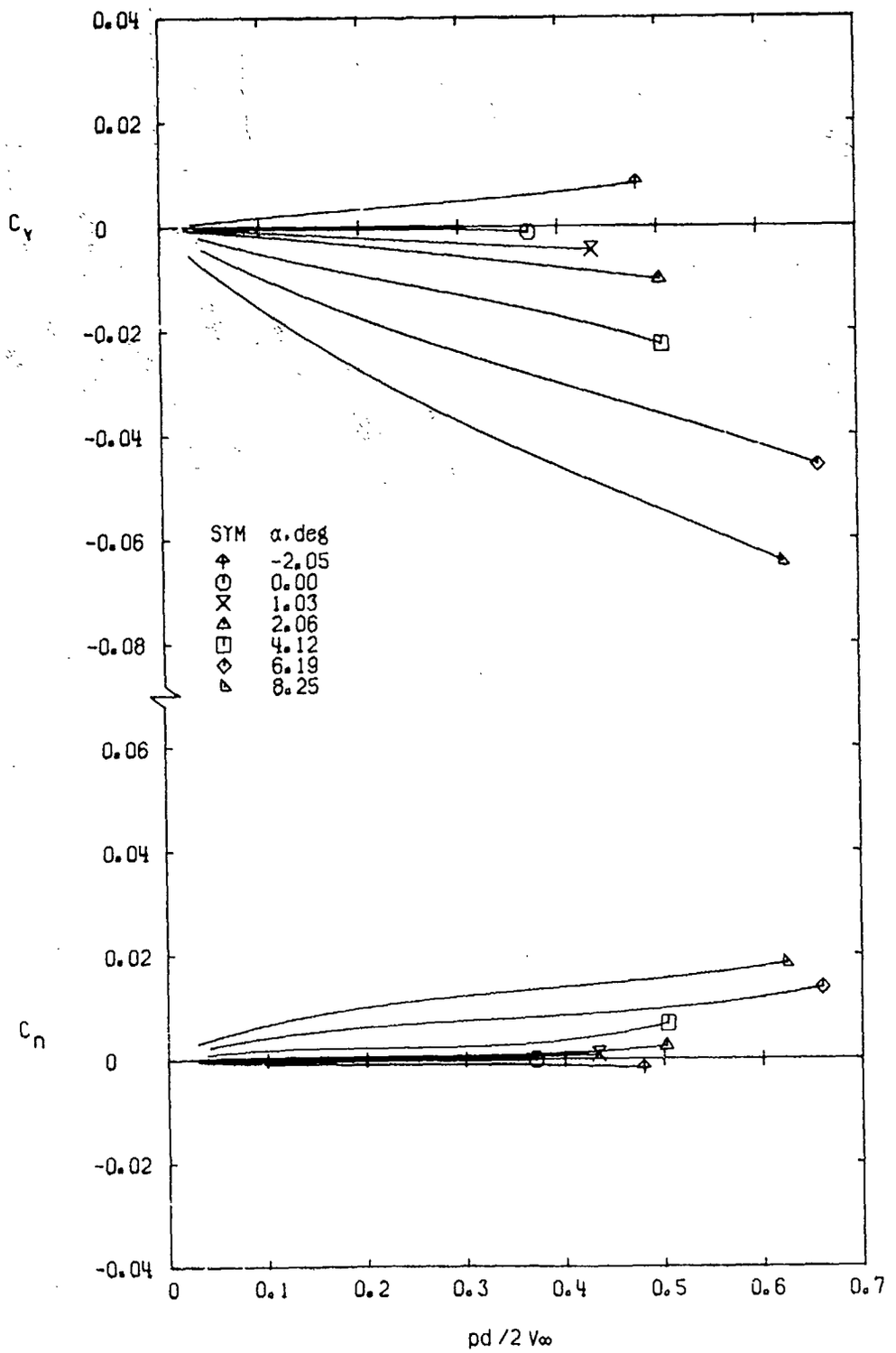

a. $M_\infty = 0.50$

Figure 12. Variation of C_Y and C_n with $pd/2V_\infty$ for Configuration 4.

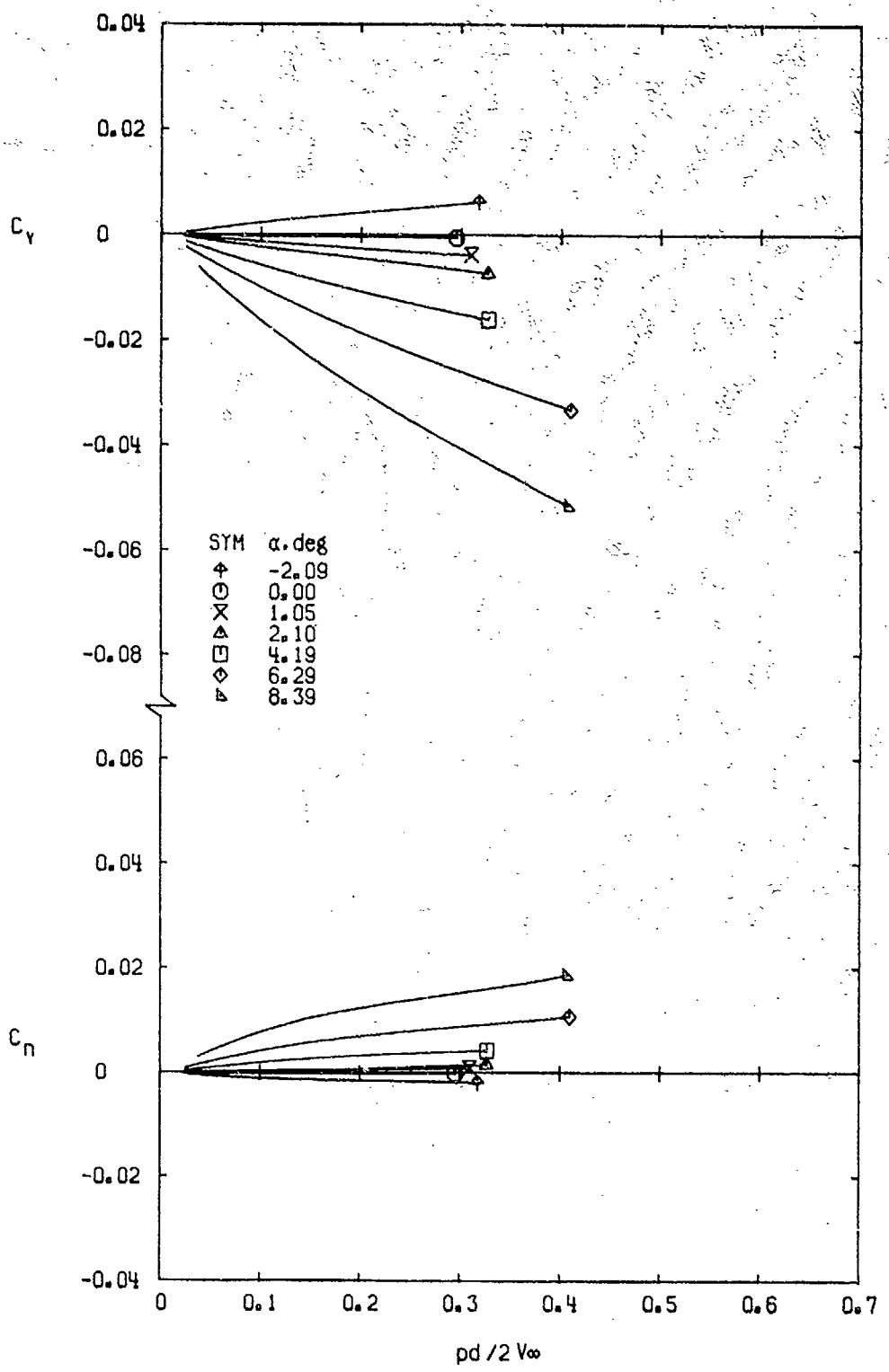

b. $M_\infty = 0.80$

Figure 12. Continued.

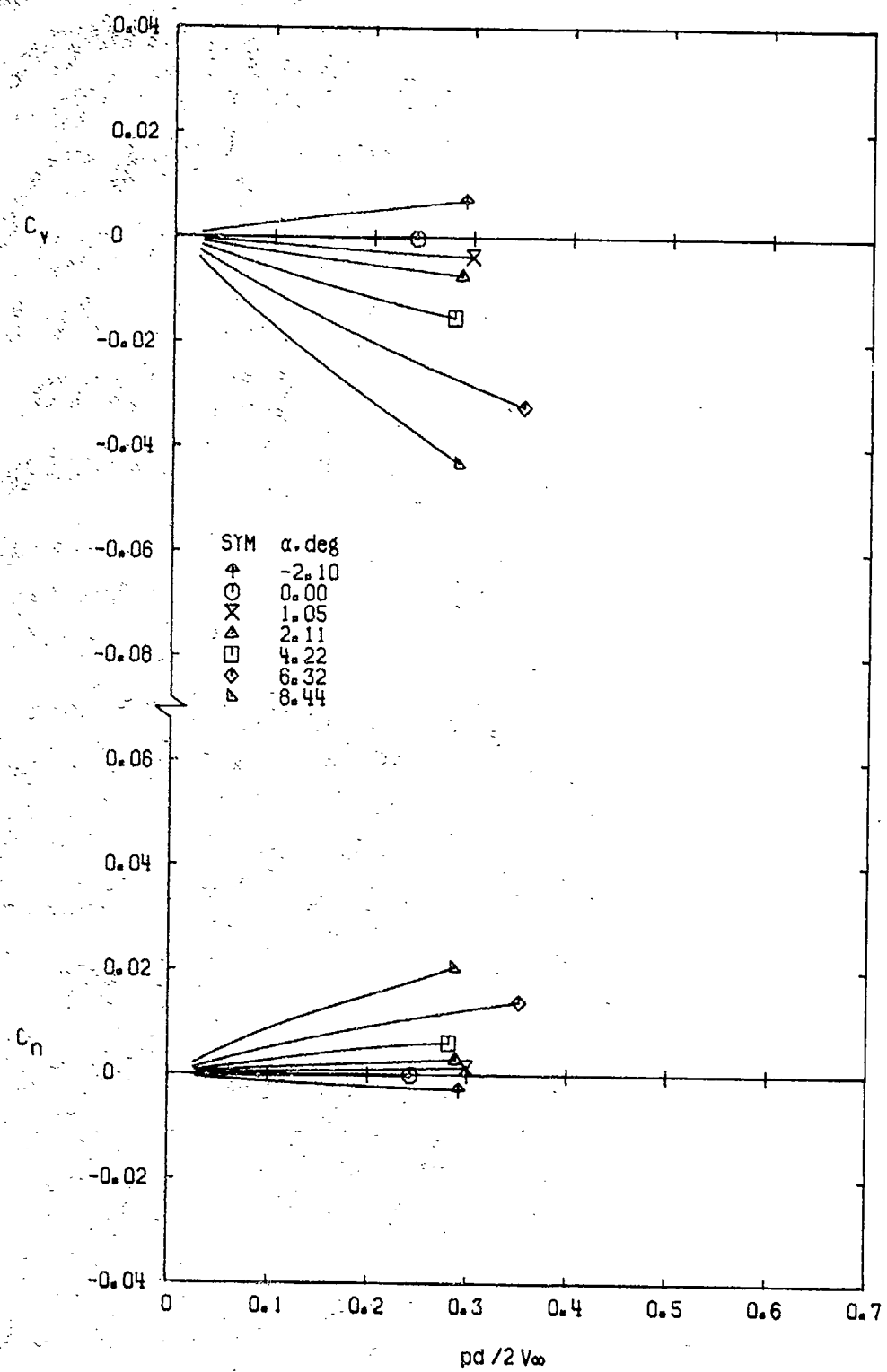

c. $M_\infty = 0.90$

Figure 12. Continued.

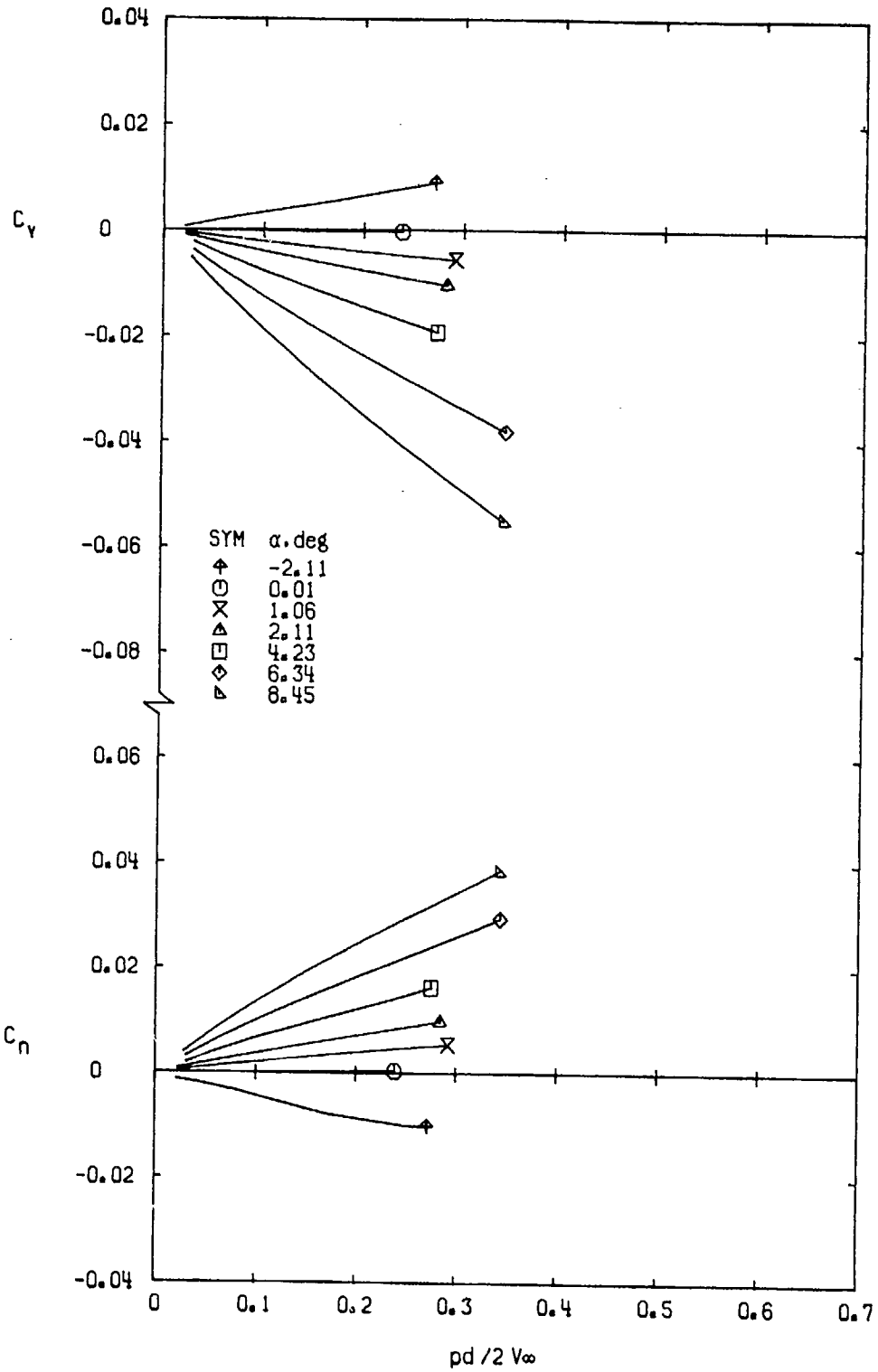

d. $M_\infty = 0.95$

Figure 12. Continued.

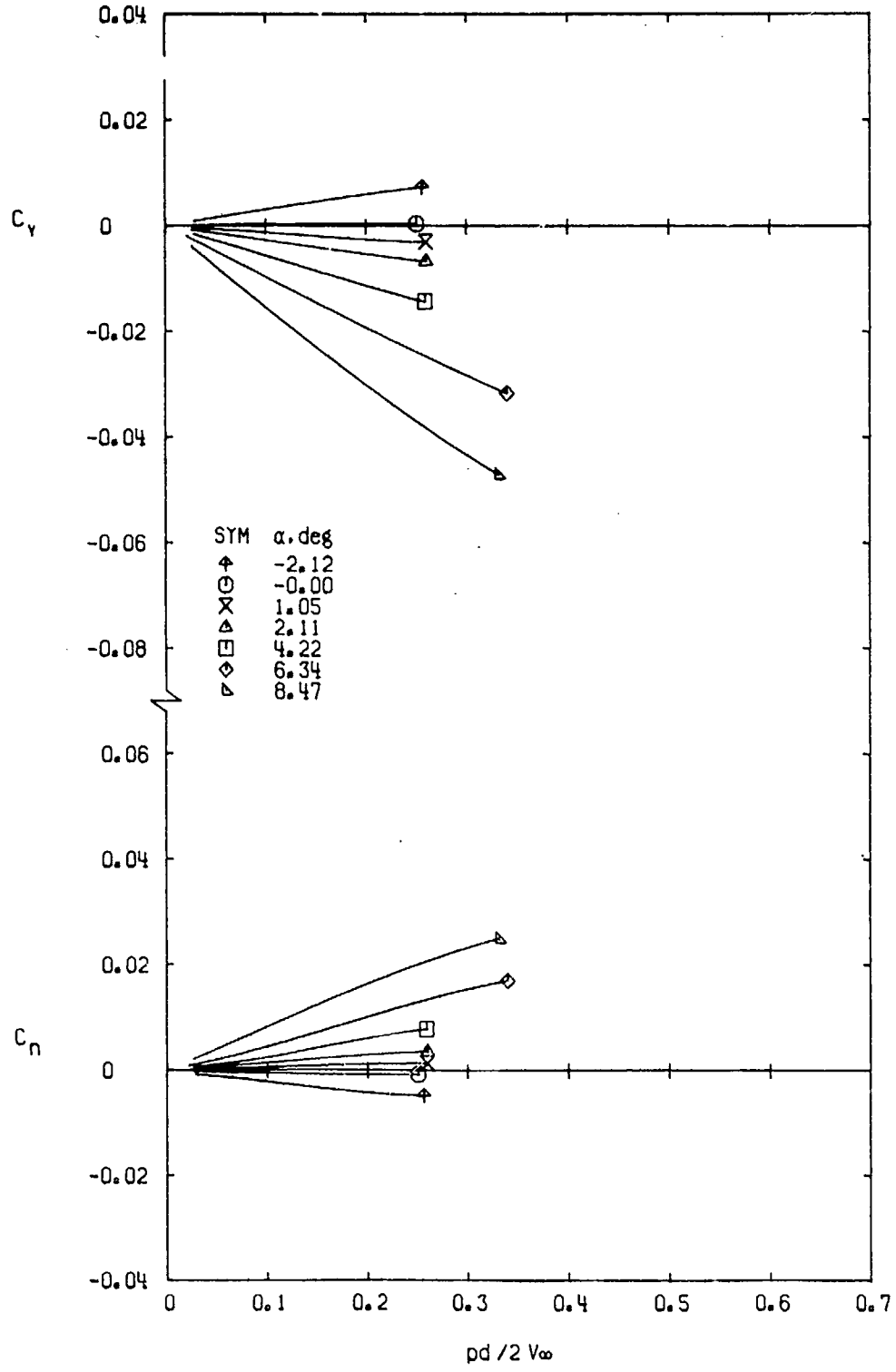

e. M_∞ = 1.00

Figure 12. Continued.

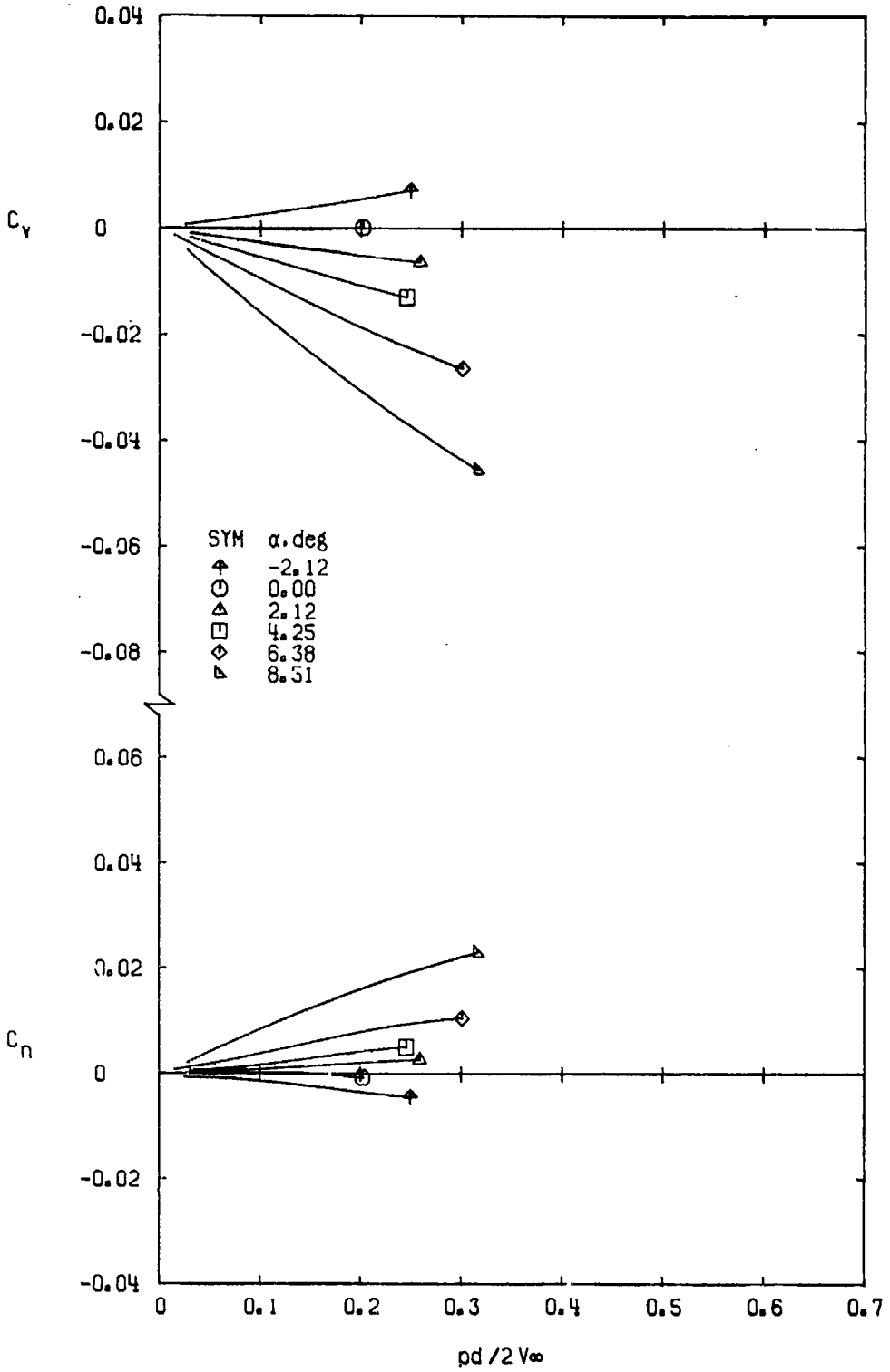

f. $M_\infty = 1.10$

Figure 12. Continued.

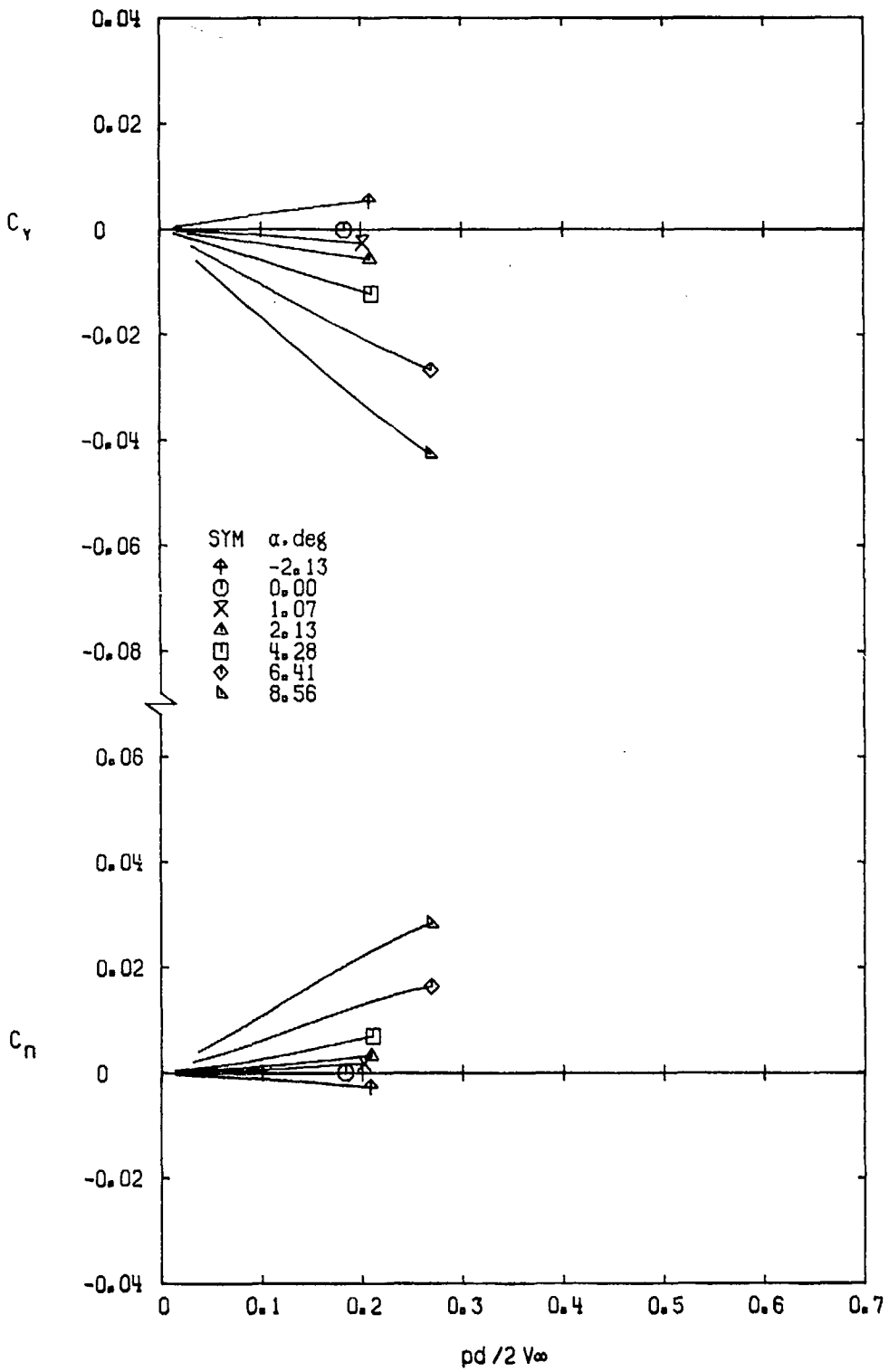

g. M_∞ = 1.30
Figure 12. Concluded.

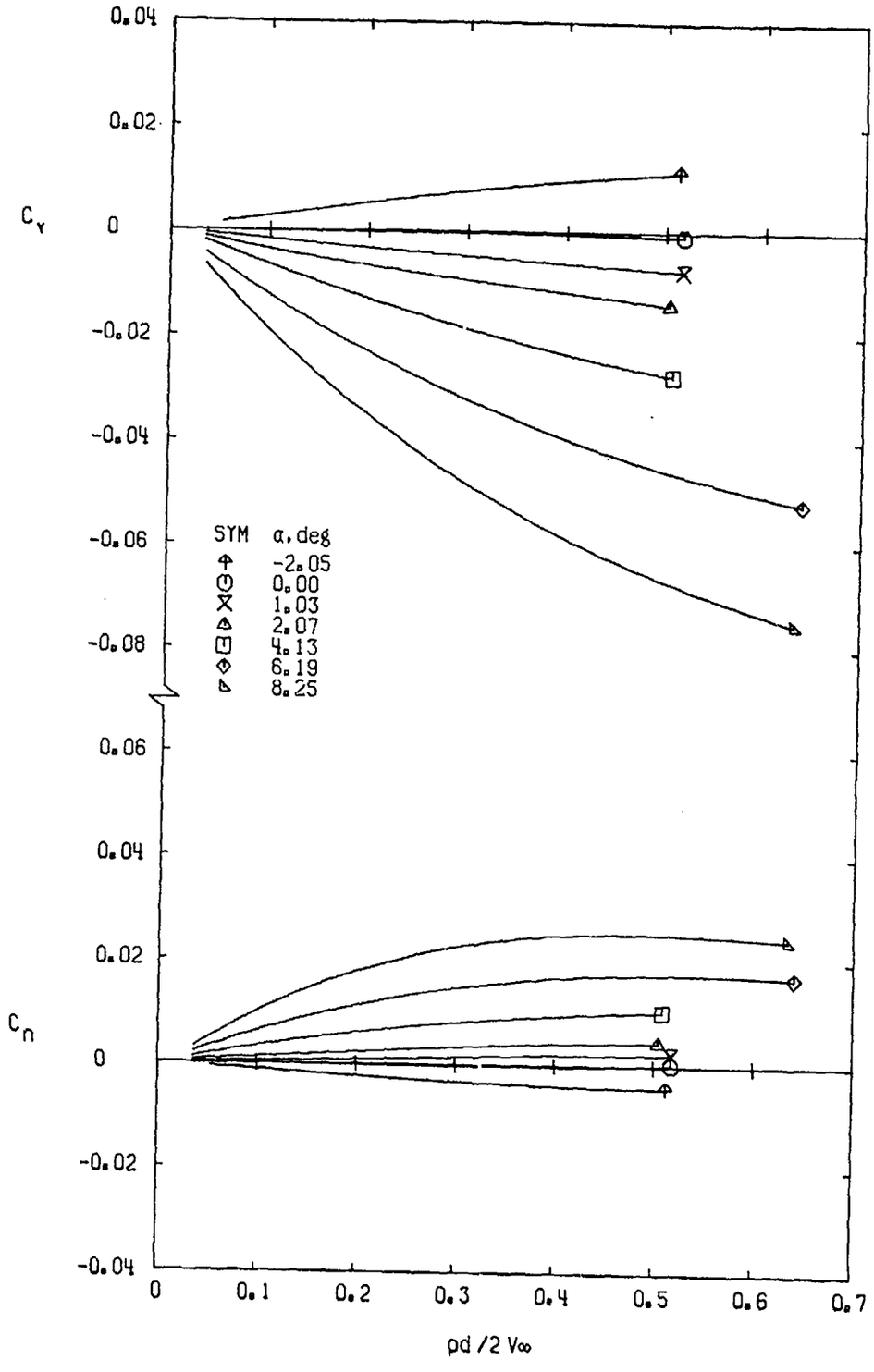

a. $M_\infty = 0.50$

Figure 13. Variation of C_Y and C_n with $pd/2V_\infty$ for Configuration 5.

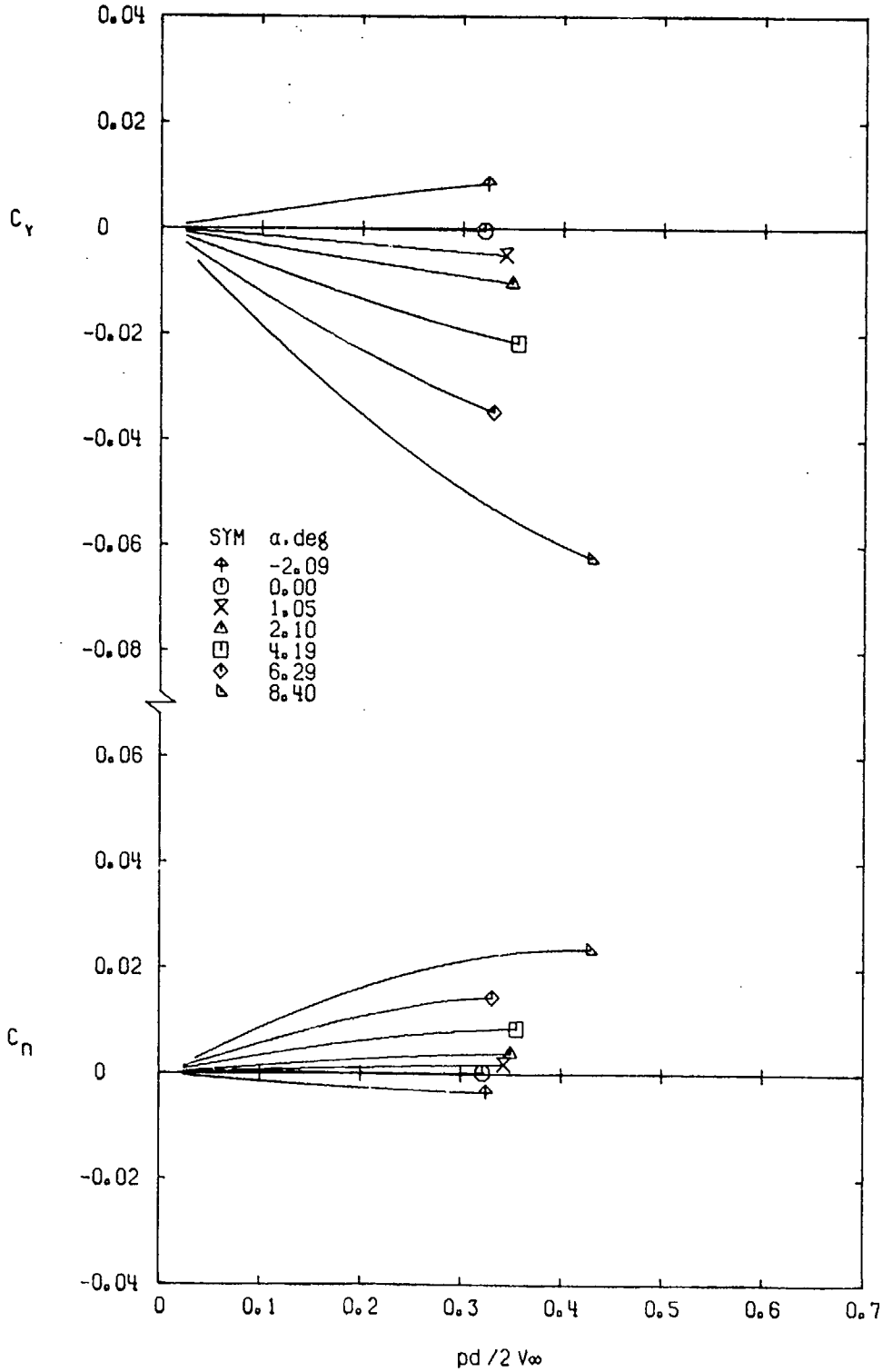

b. $M_\infty = 0.30$

Figure 13. Continued.

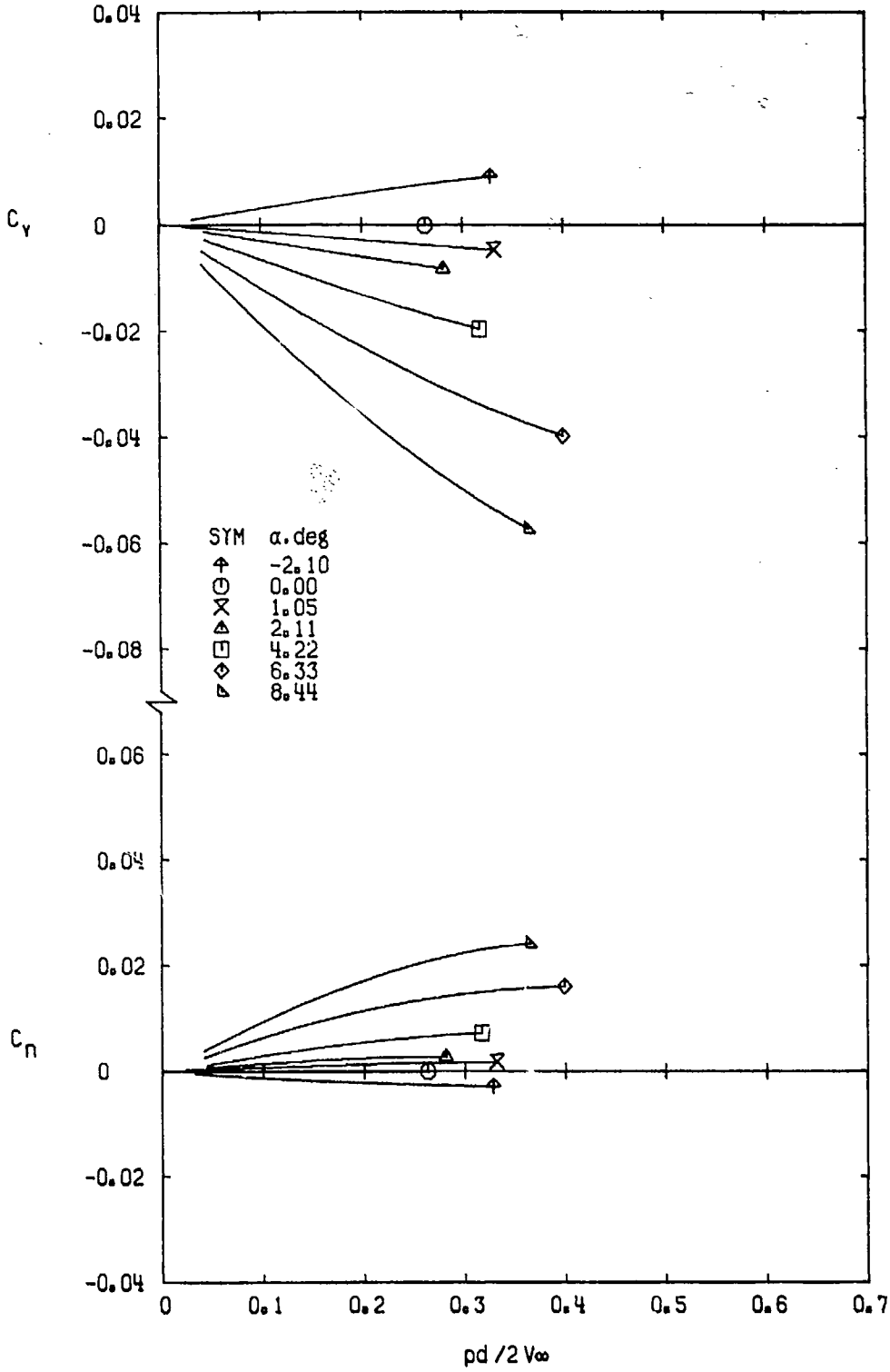

c. $M_\infty = 0.90$

Figure 13. Continued.

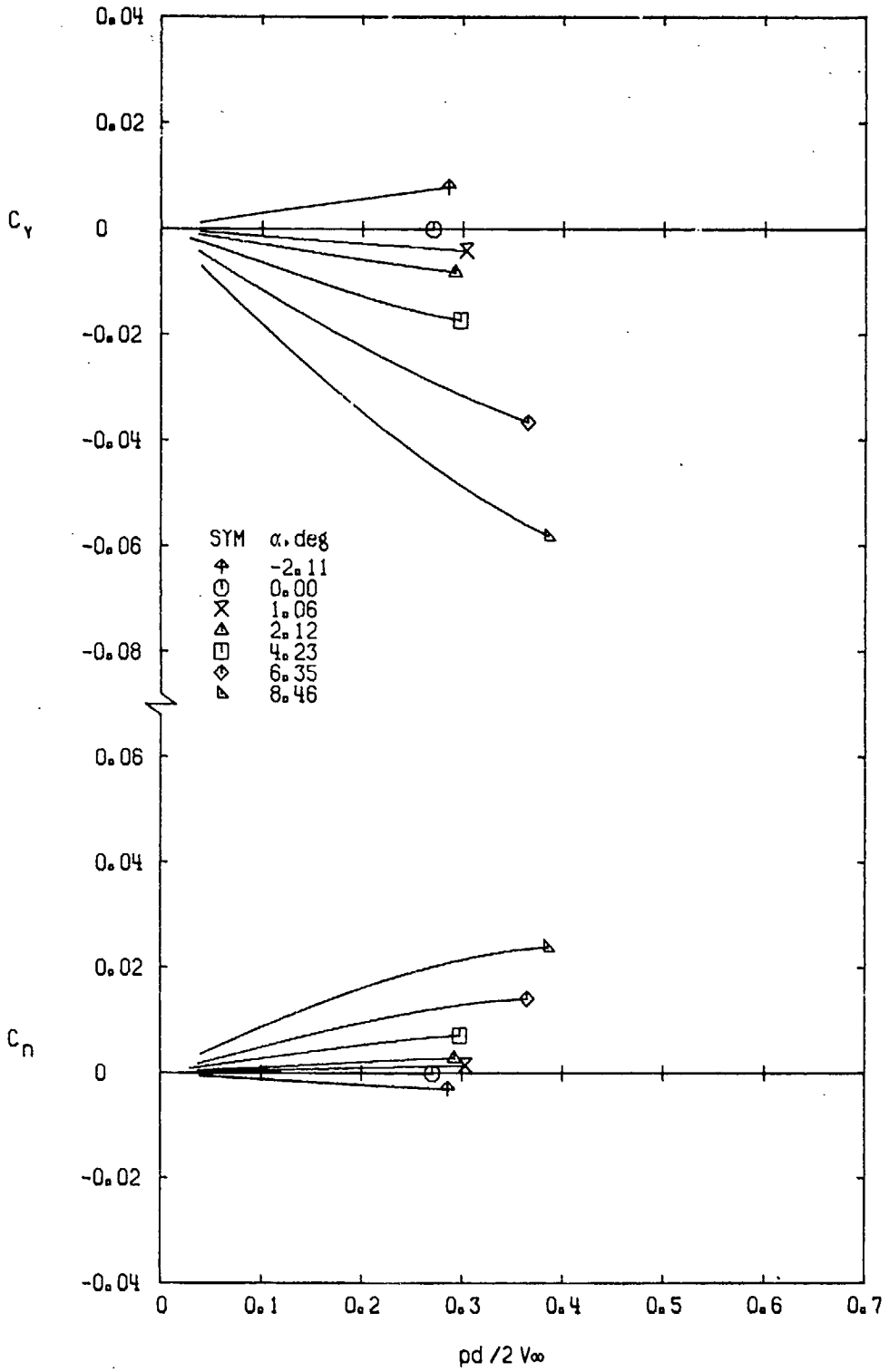

d. $M_\infty = 0.95$

Figure 13. Continued.

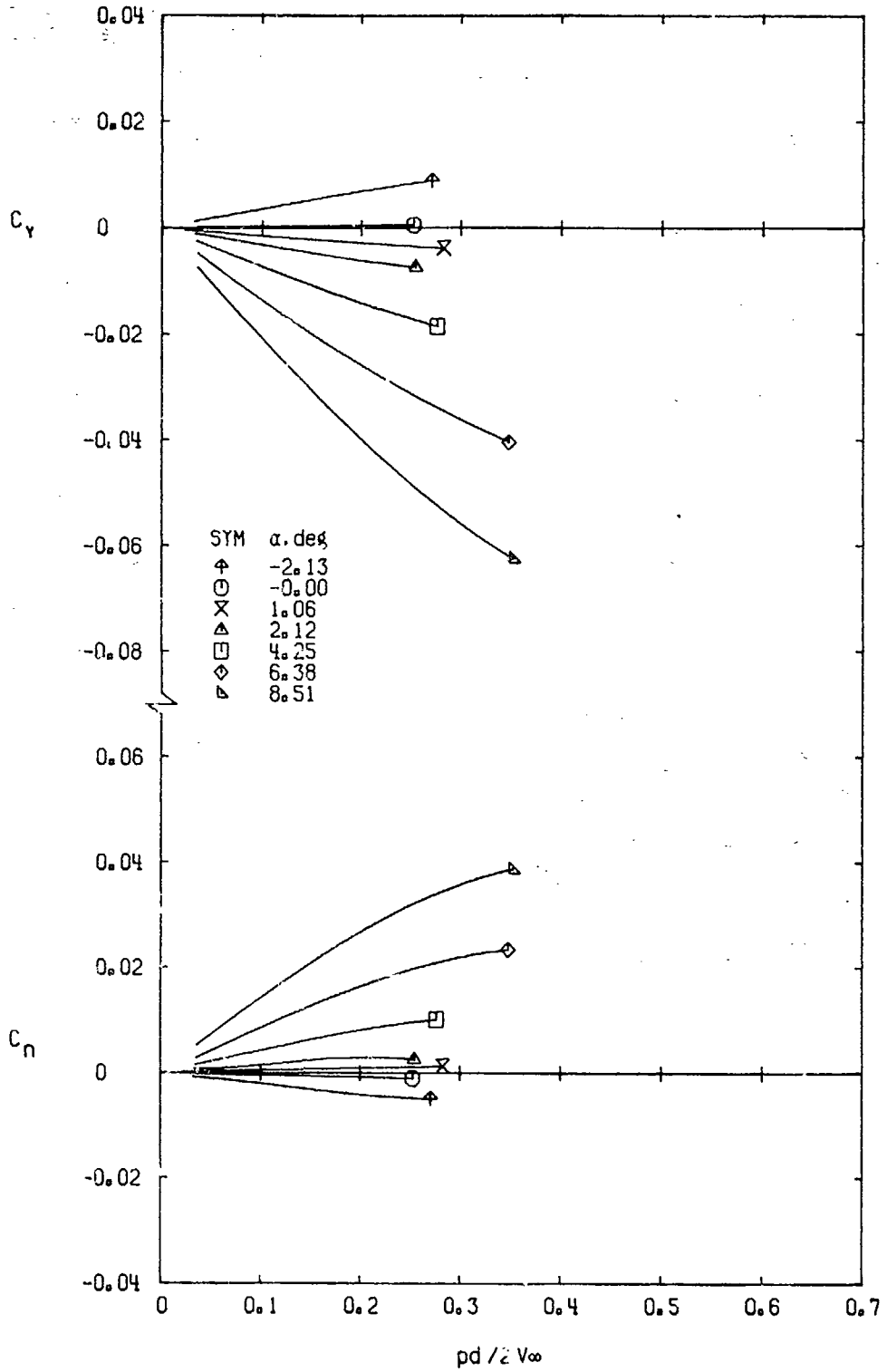

e. M_∞ = 1.00

Figure 13. Continued.

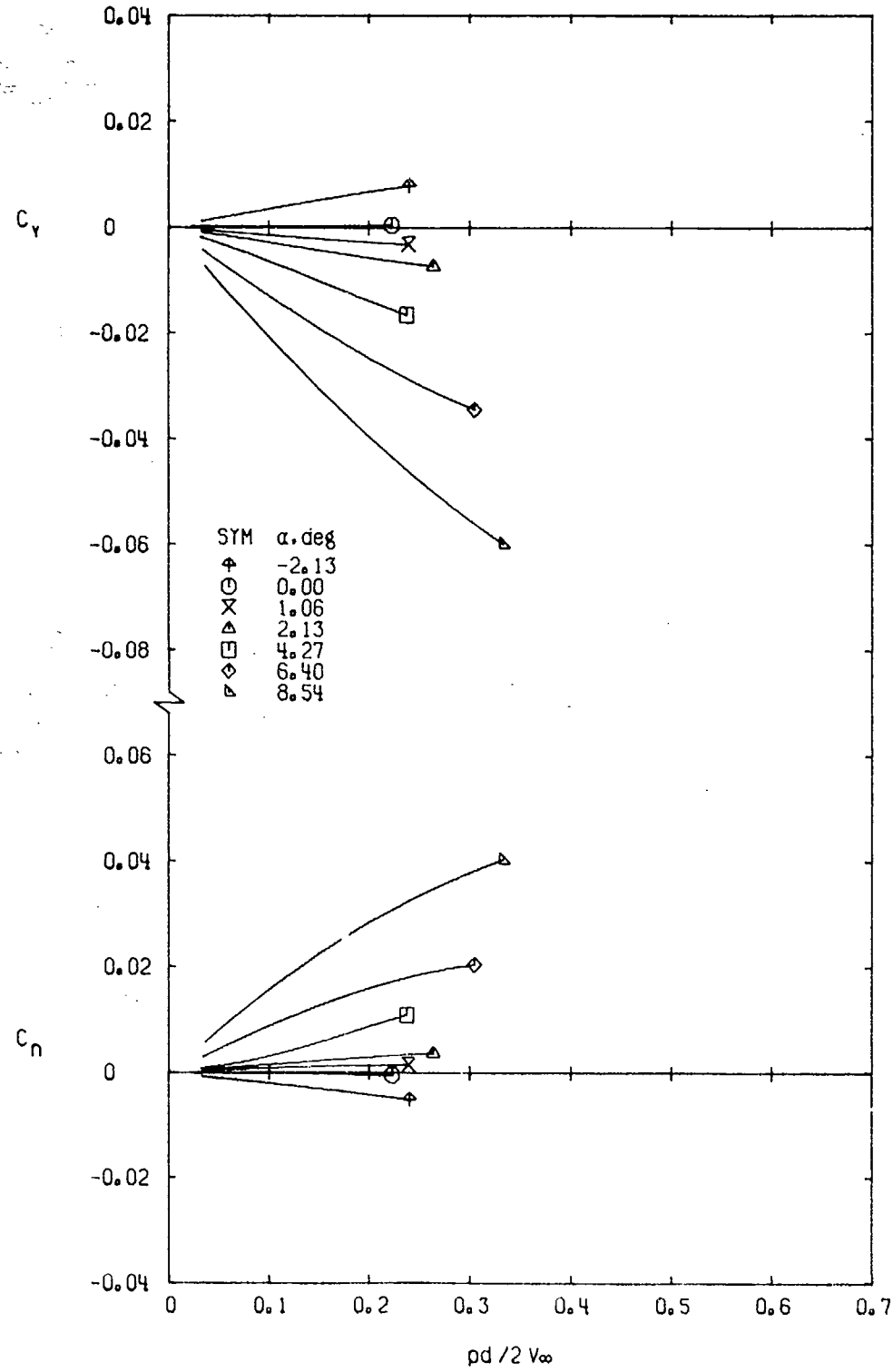

f. M_∞ = 1.10

Figure 13. Continued.

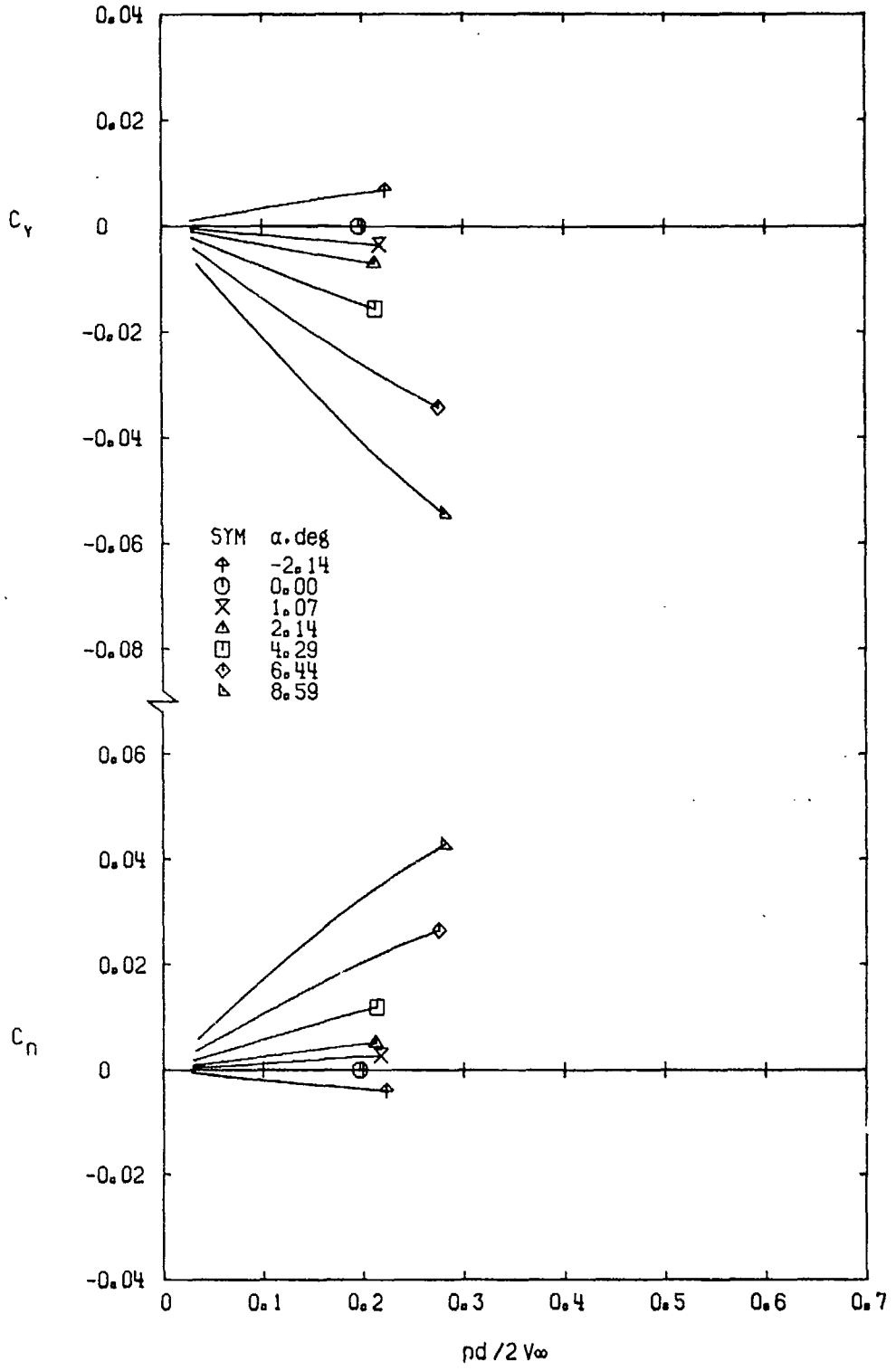

g. M_∞ = 1.30

Figure 13. Concluded.

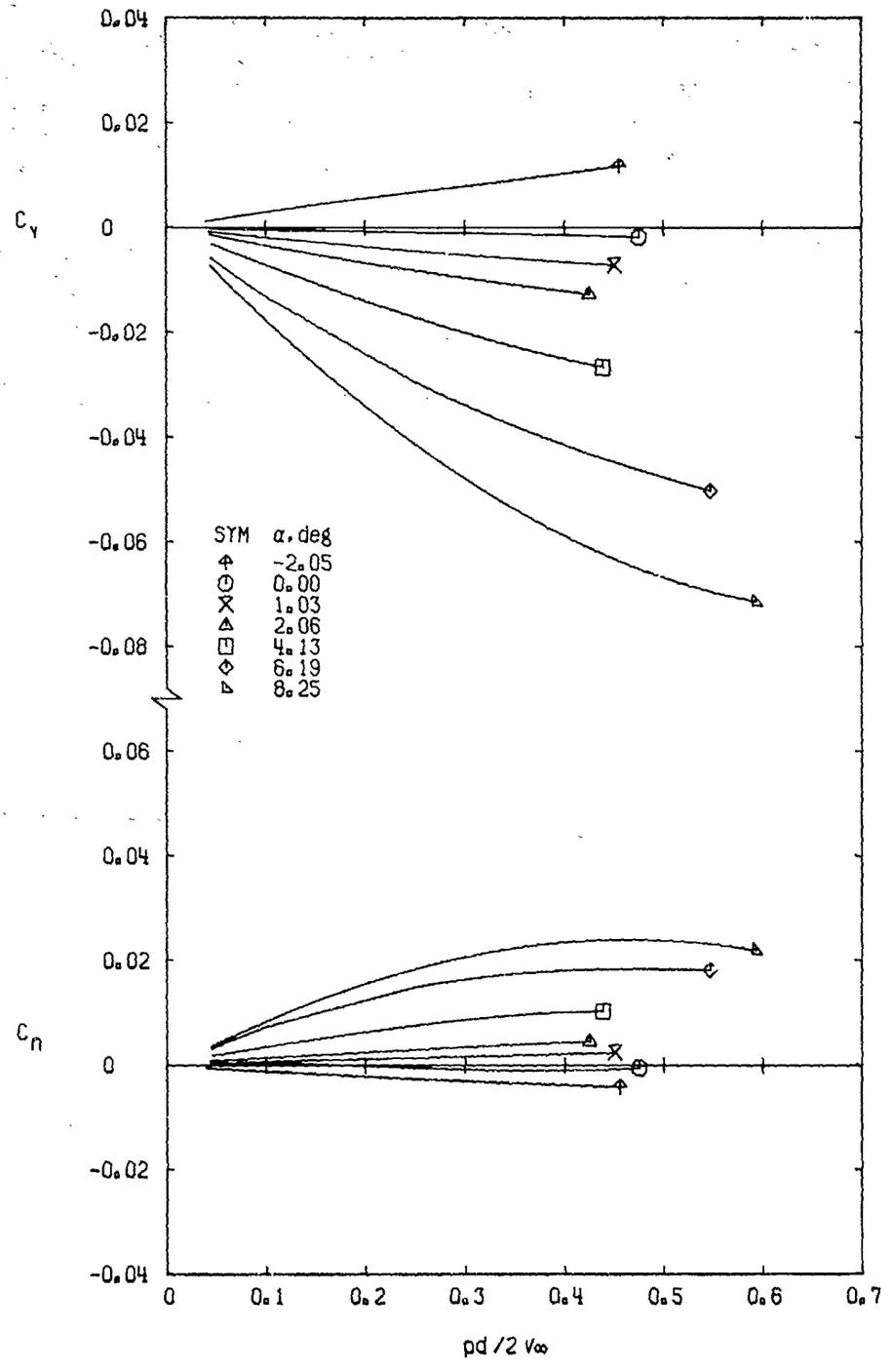

a. $M_\infty = 0.50$

Figure 14. Variation of C_Y and C_n with $pd/2V_\infty$ for Configuration 6.

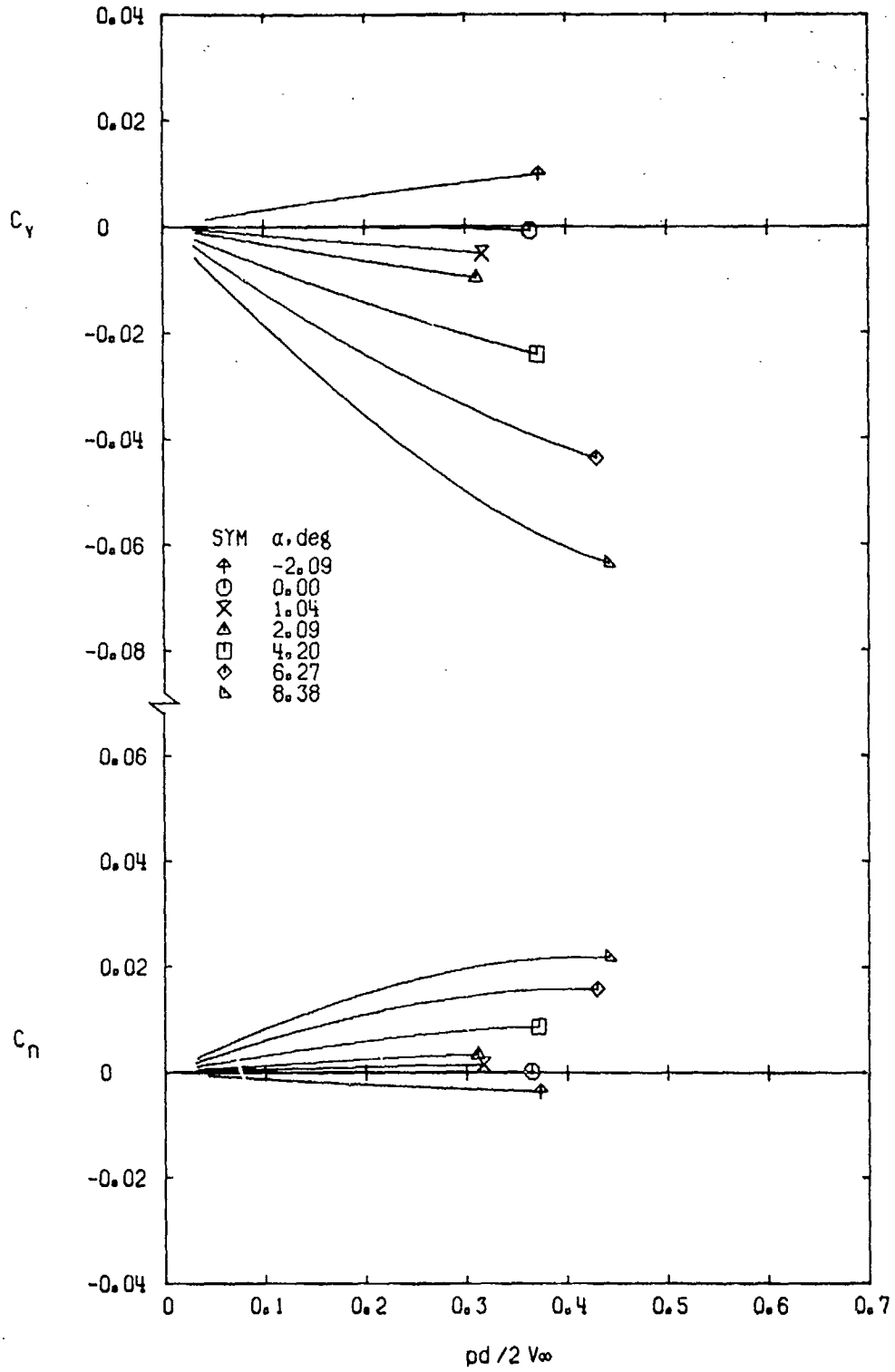

b. $M_\infty = 0.80$

Figure 14. Continued.

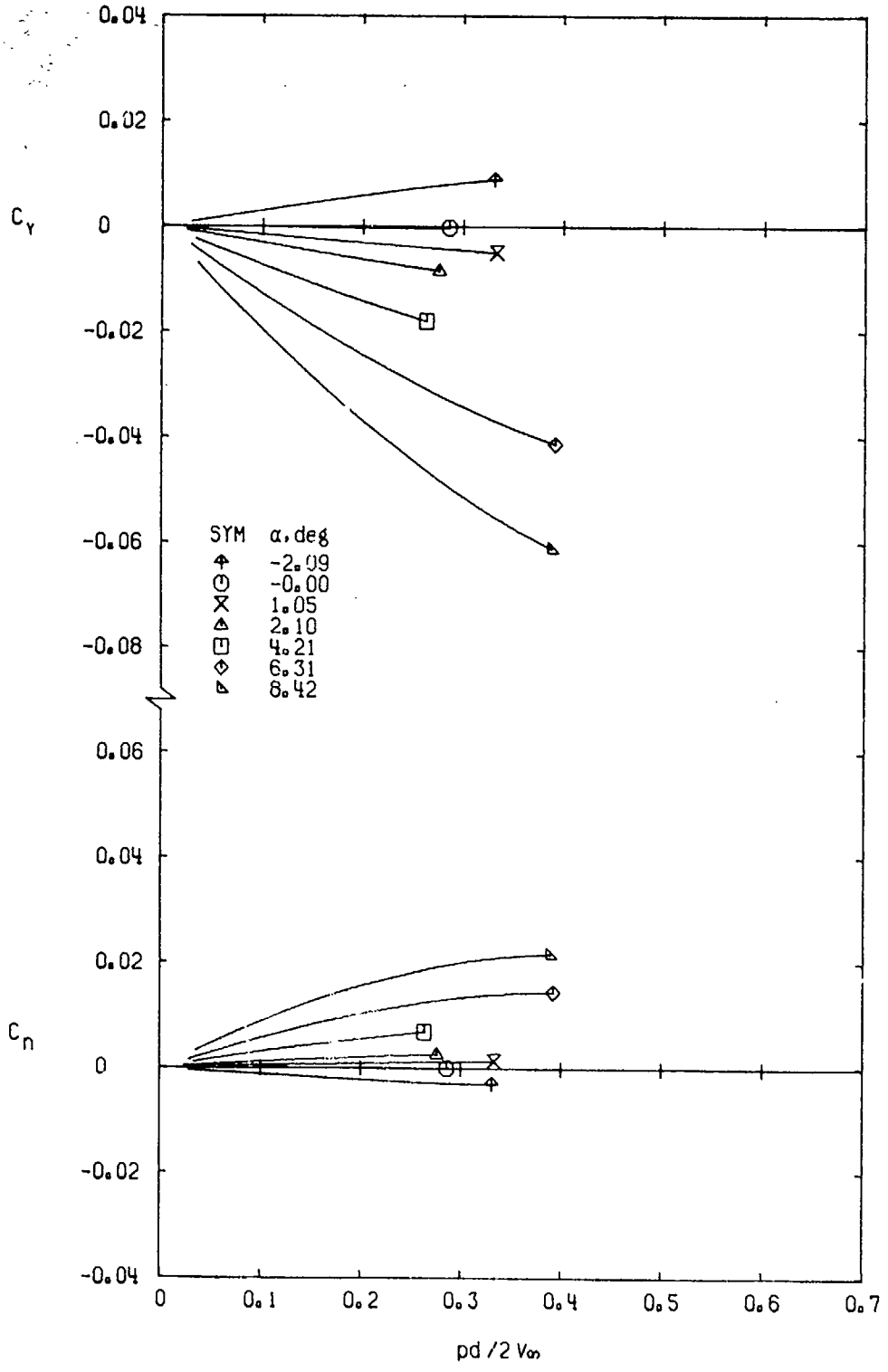

c. $M_\infty = 0.90$

Figure 14. Continued.

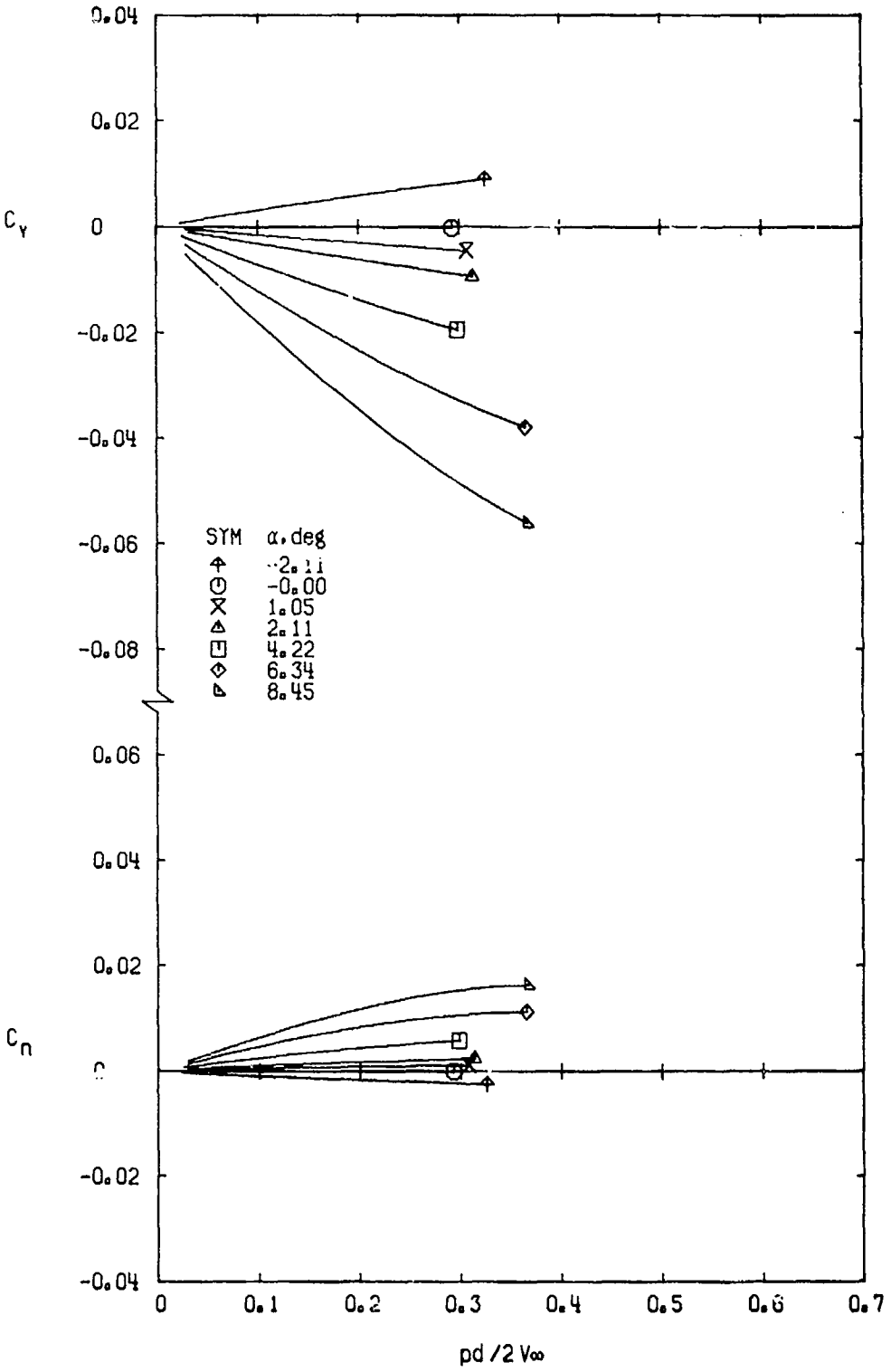

d. $M_\infty = 0.95$

Figure 14. Continued.

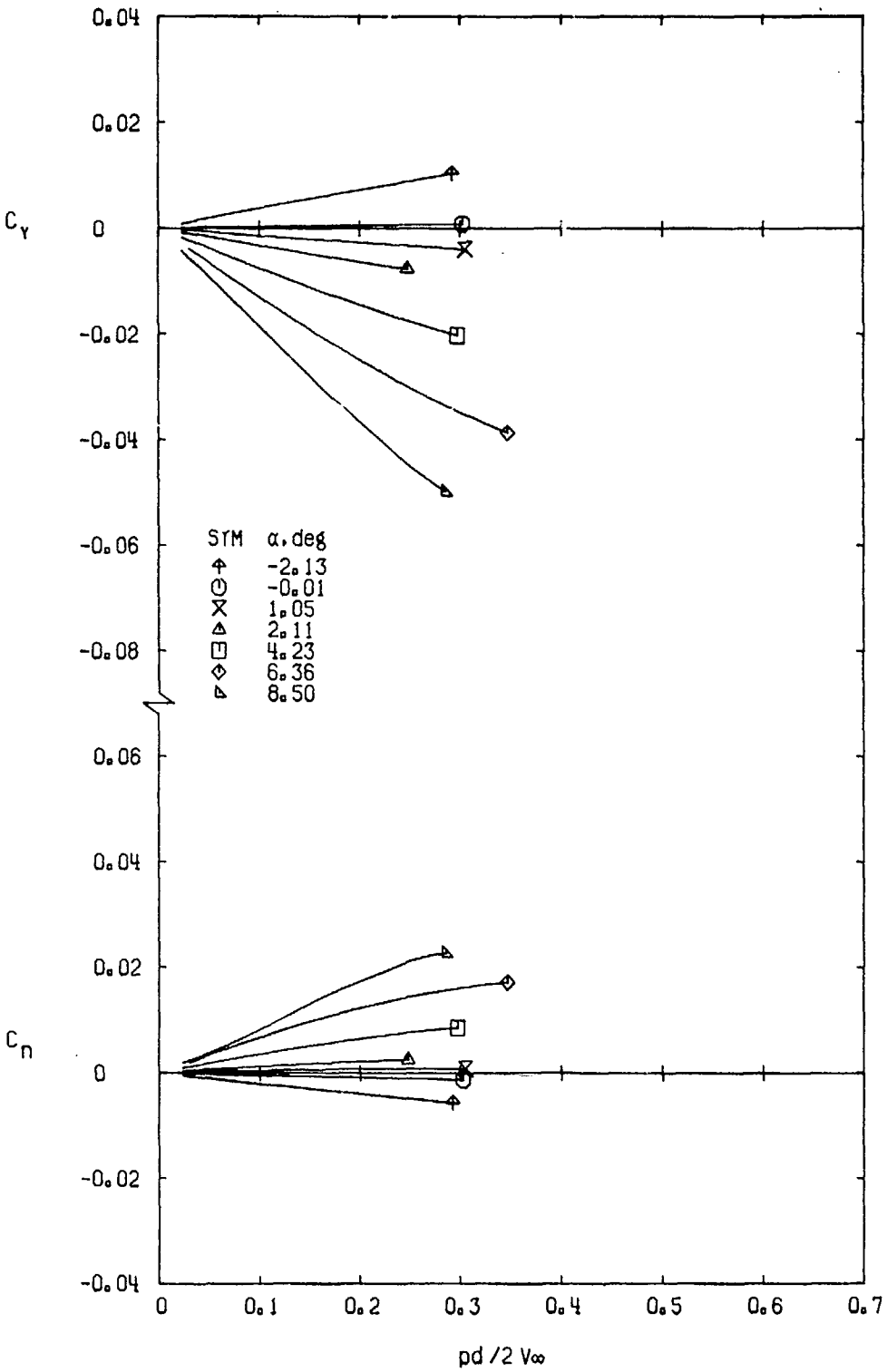

e. M_∞ = 1.00

Figure 14. Continued.

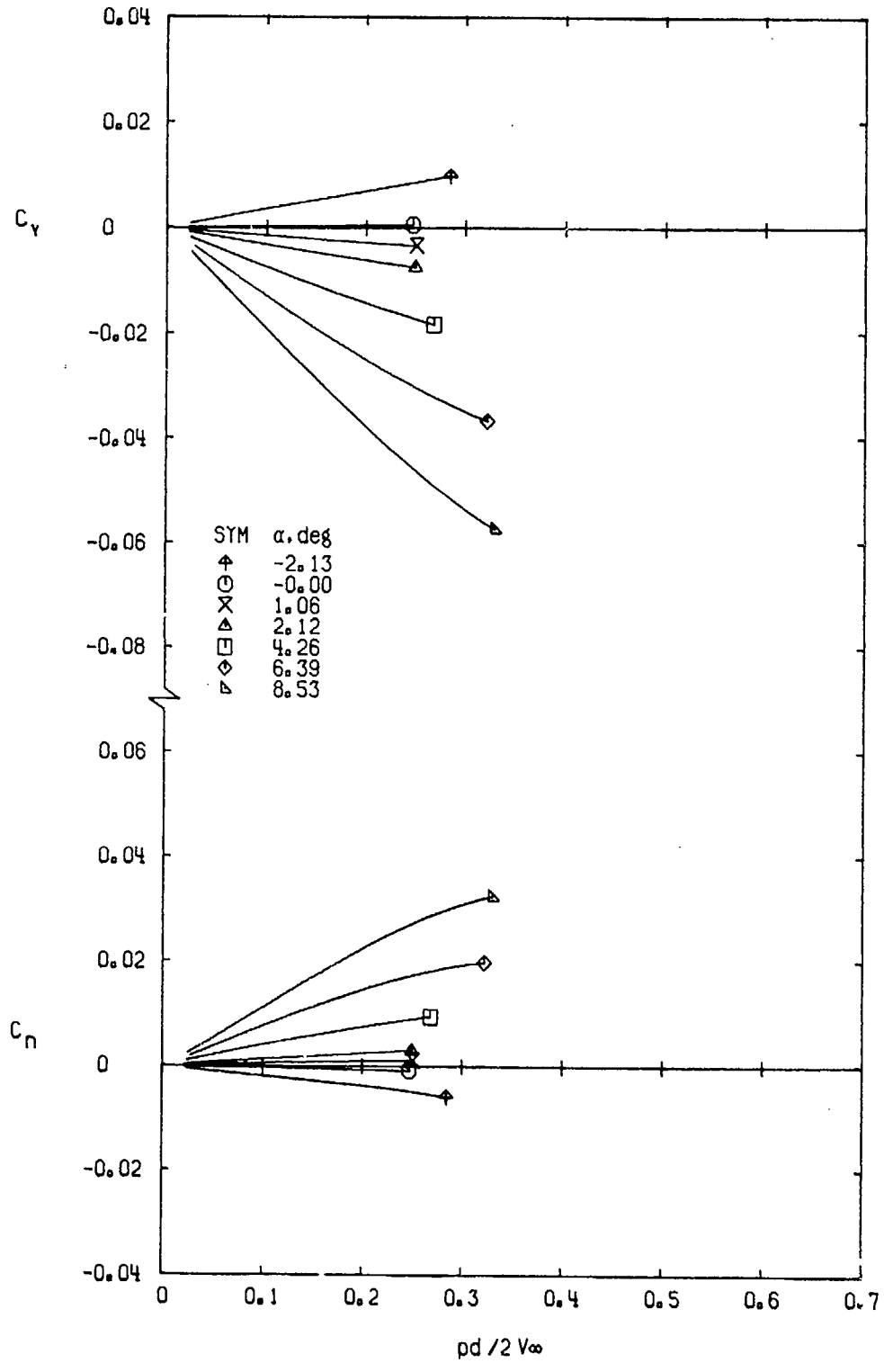

f. M_∞ = 1.10
Figure 14. Continued.

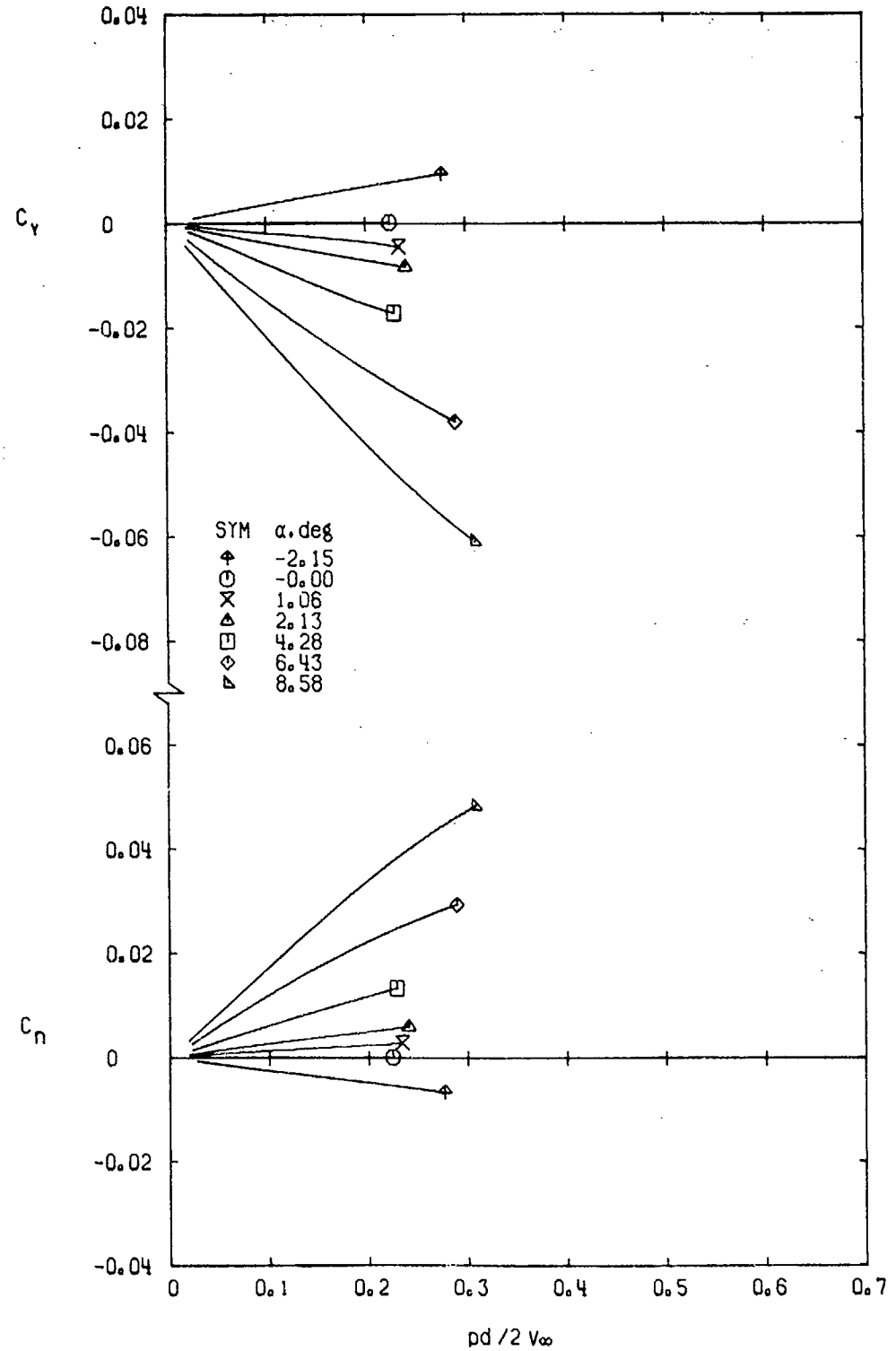

g. M_∞ = 1.30

Figure 14. Concluded.

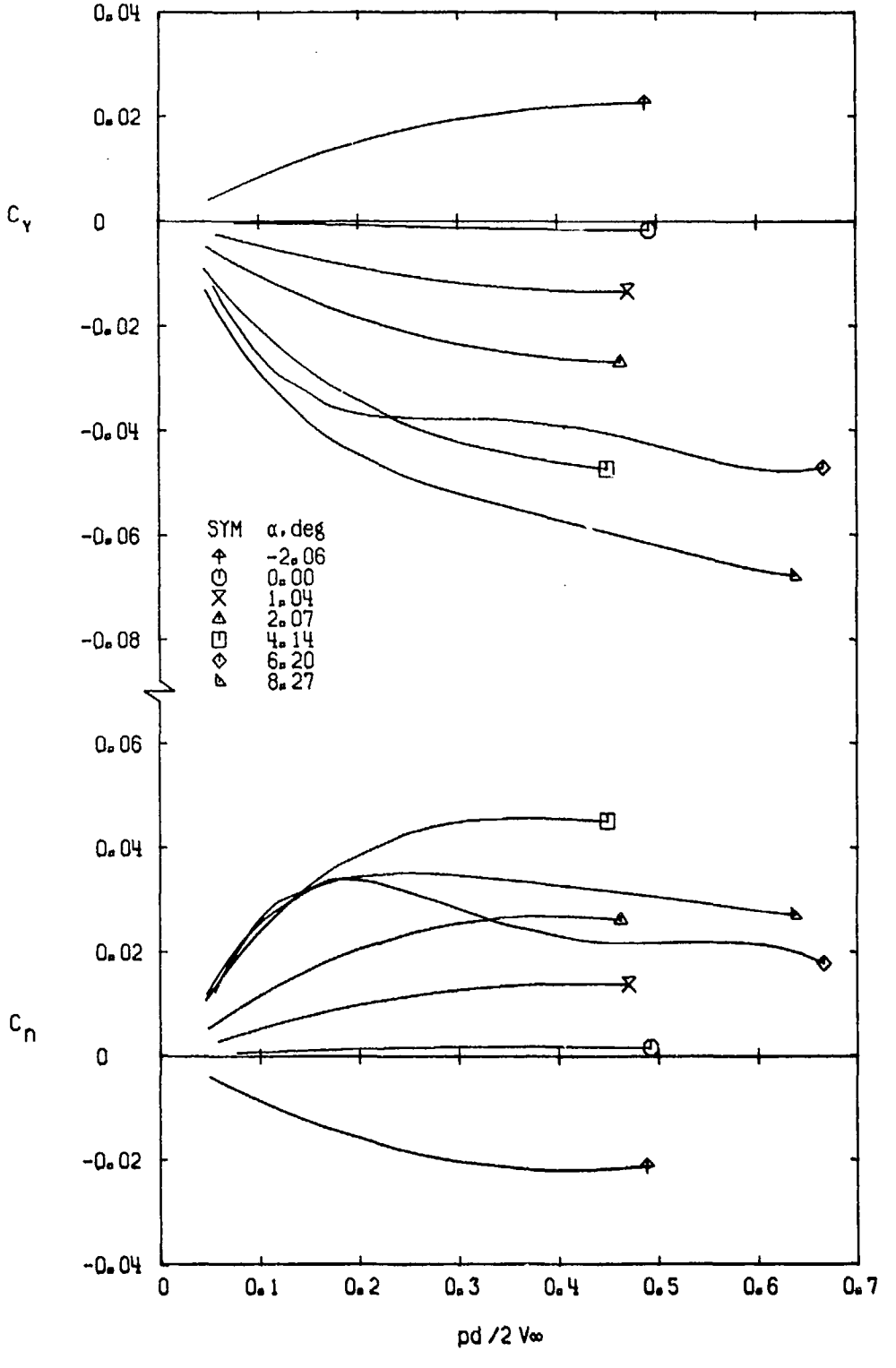

a. $M_\infty = 0.50$

Figure 15. Variation of C_Y and C_n with $pd/2V_\infty$ for Configuration 7.

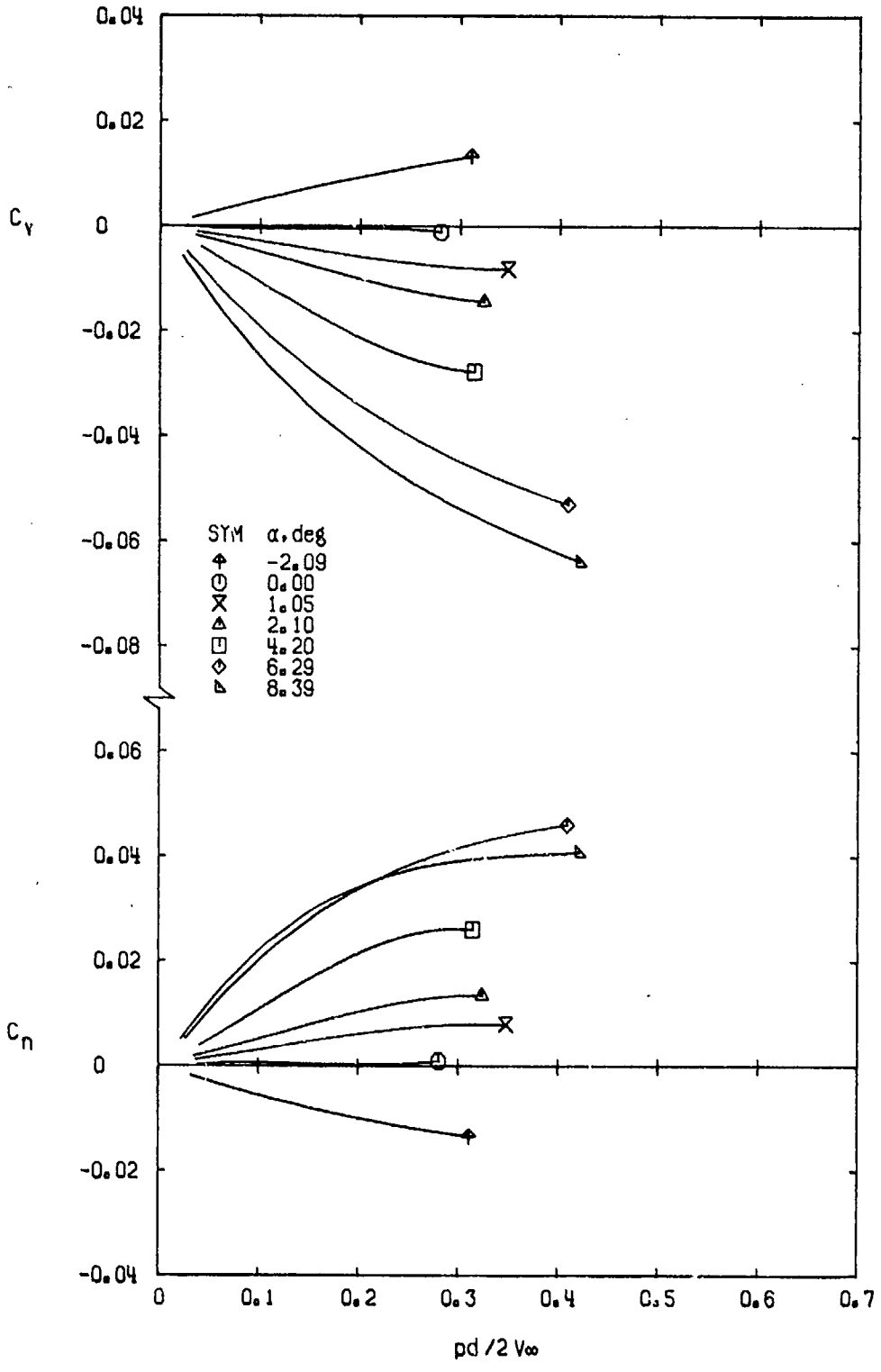

b. $M_\infty = 0.80$

Figure 15. Continued.

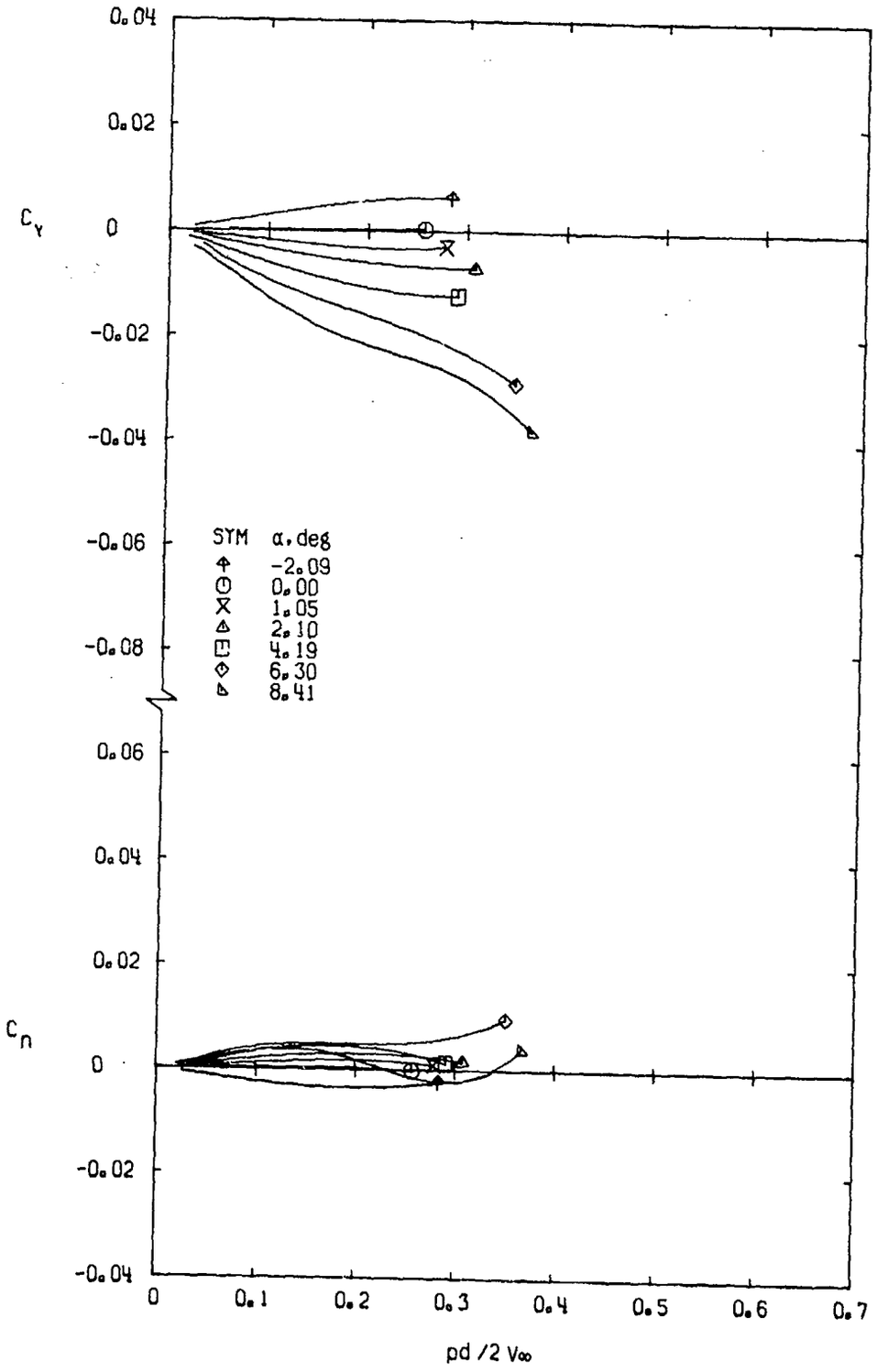

c. $M_\infty = 0.90$

Figure 15. Continued.

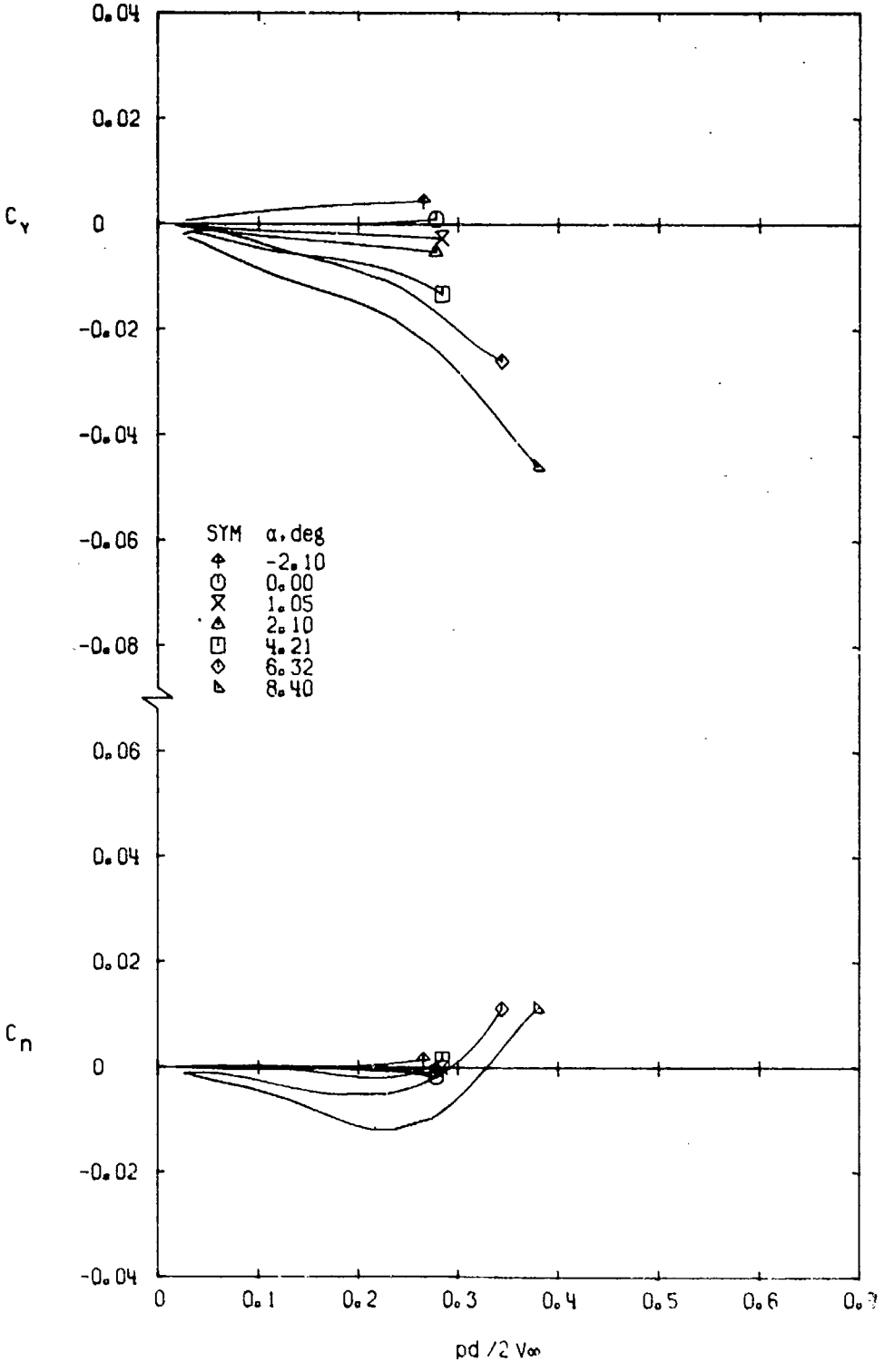

d. M_∞ = 0.95

Figure 15. Continued.

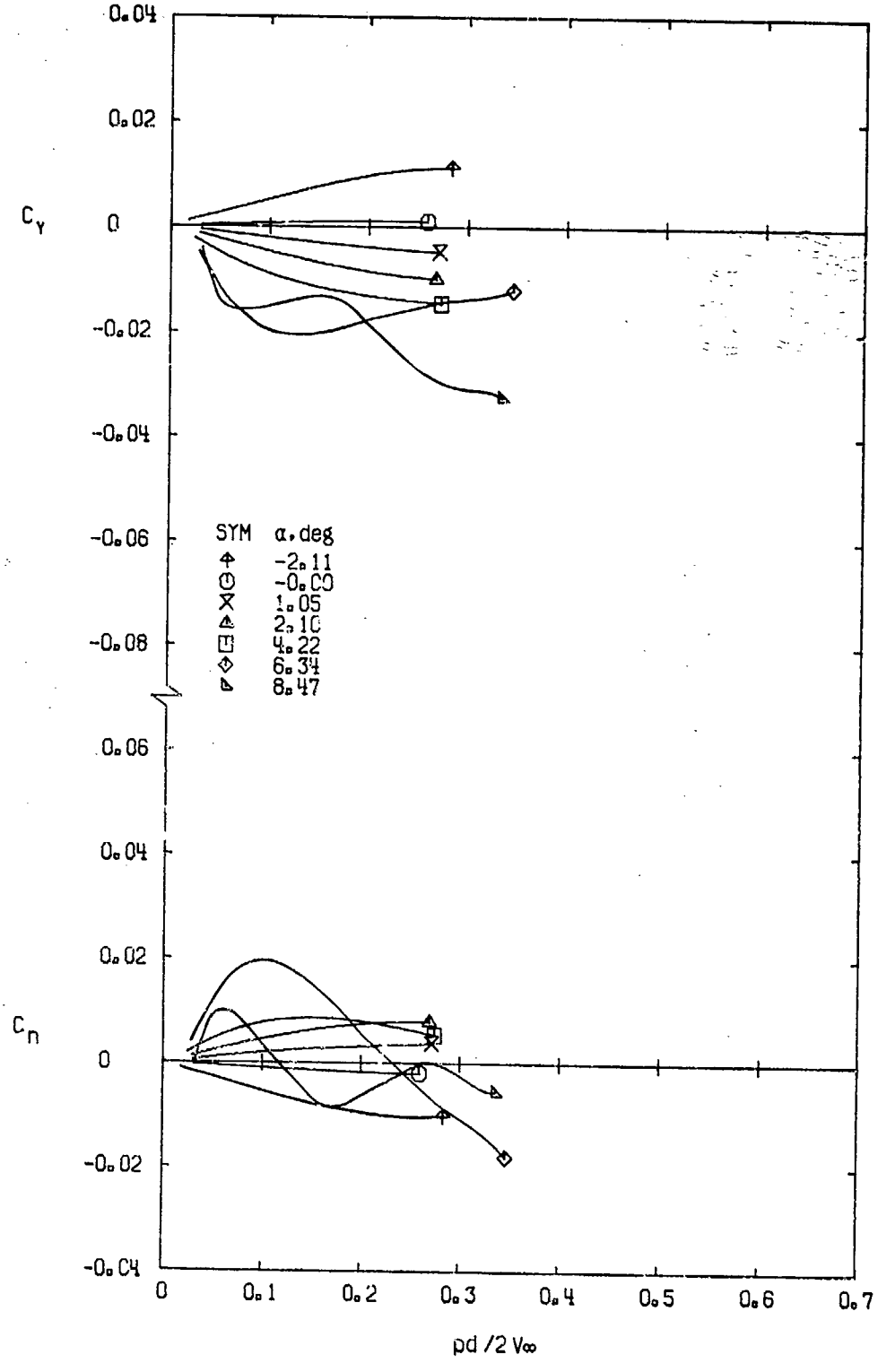

e. M_∞ = 1.00

Figure 15. Continued.

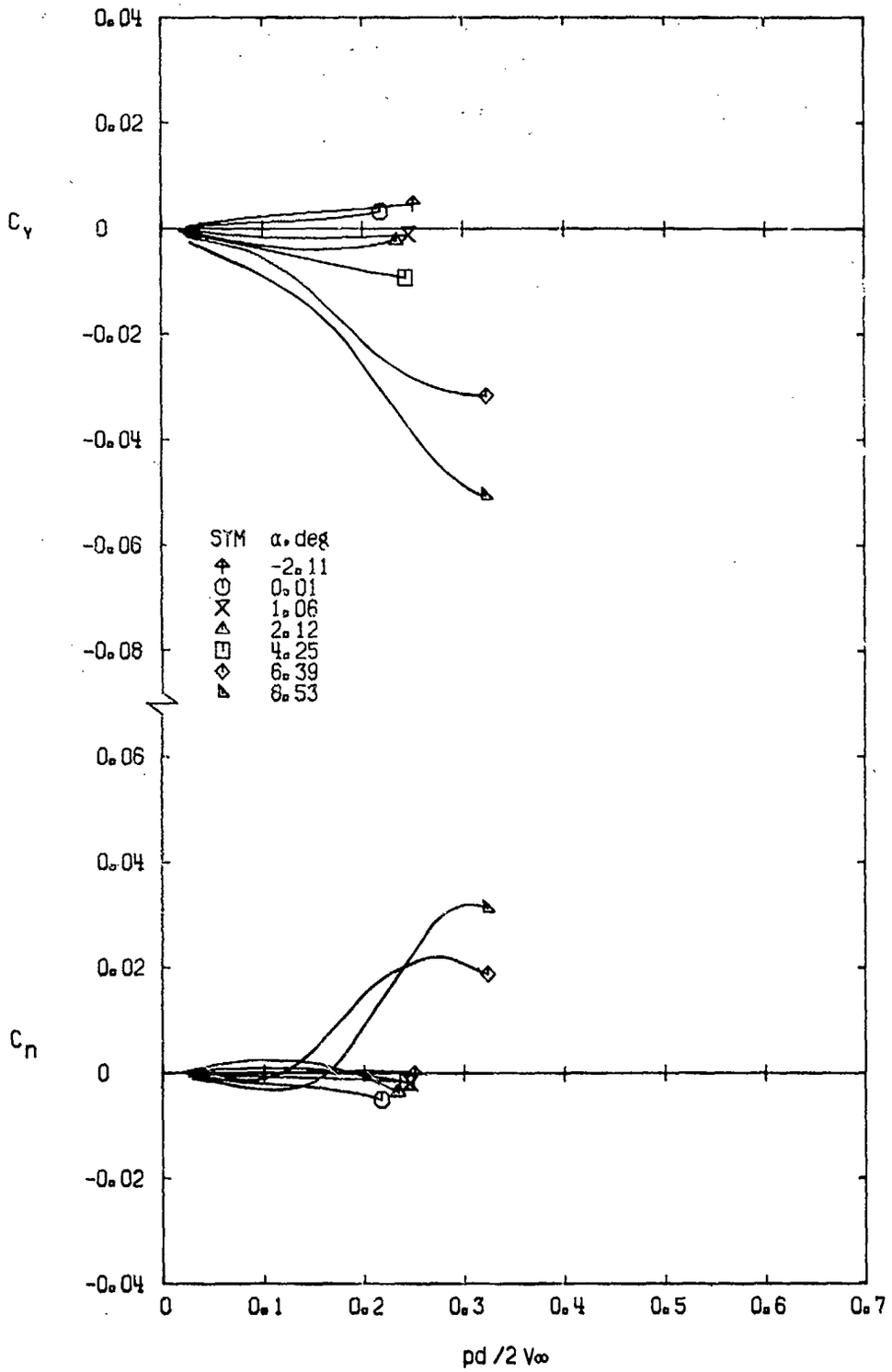

f. M_∞ = 1.10
Figure 15. Continued.

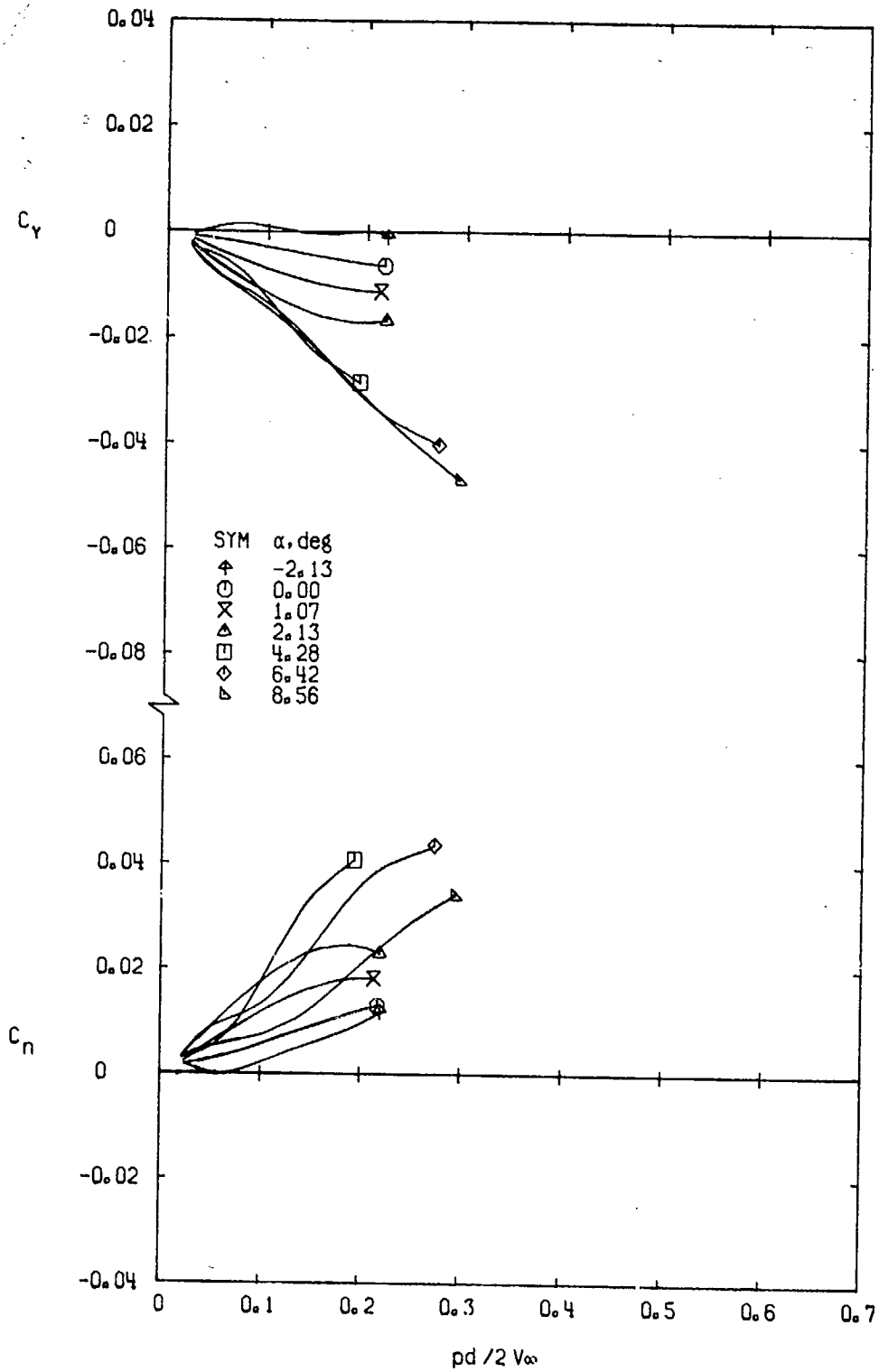

g. M_∞ = 1.30

Figure 15. Concluded.

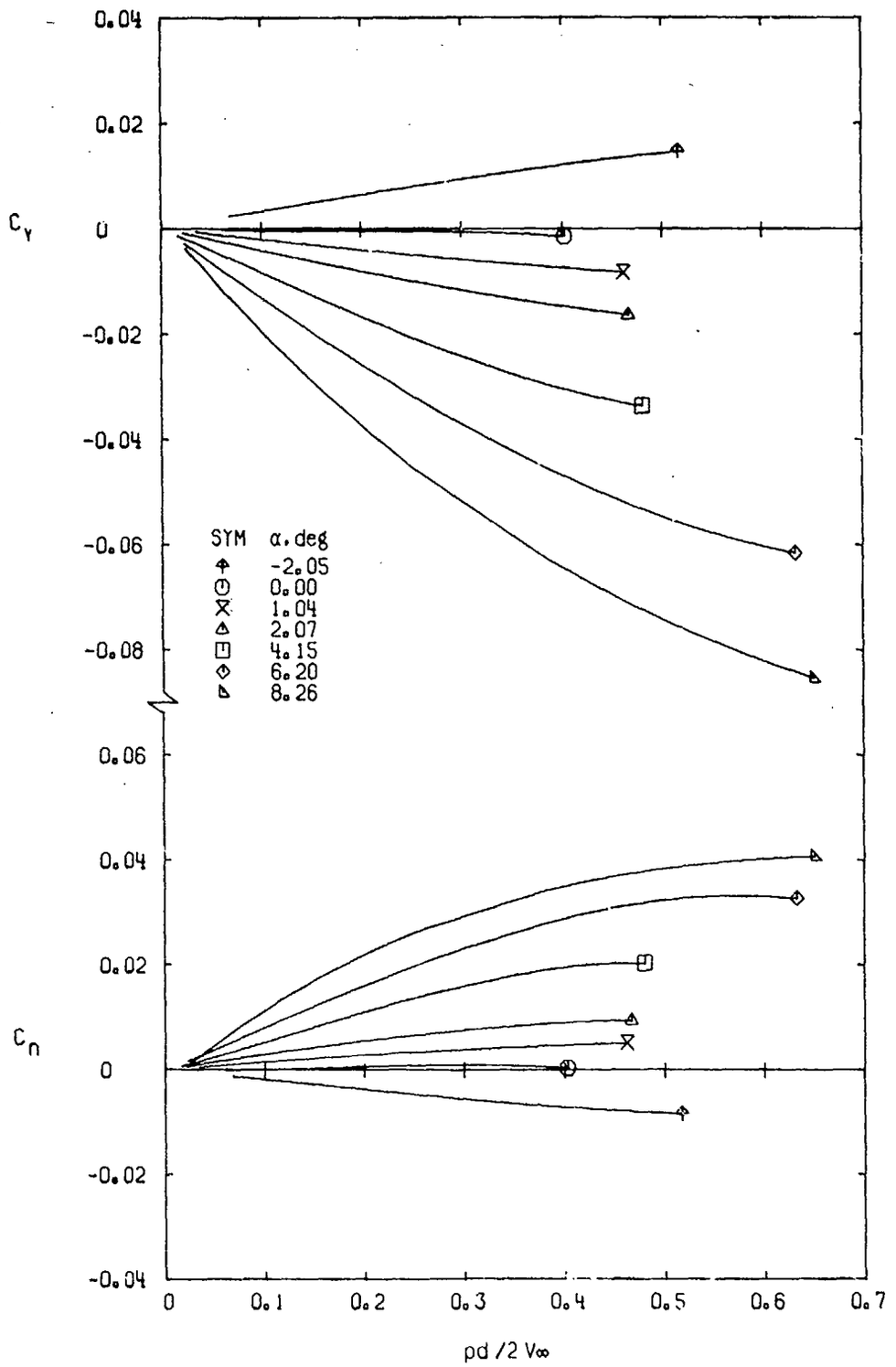

a. $M_\infty = 0.50$

Figure 16. Variation of C_Y and C_n with $pd/2V_\infty$ for Configuration 8.

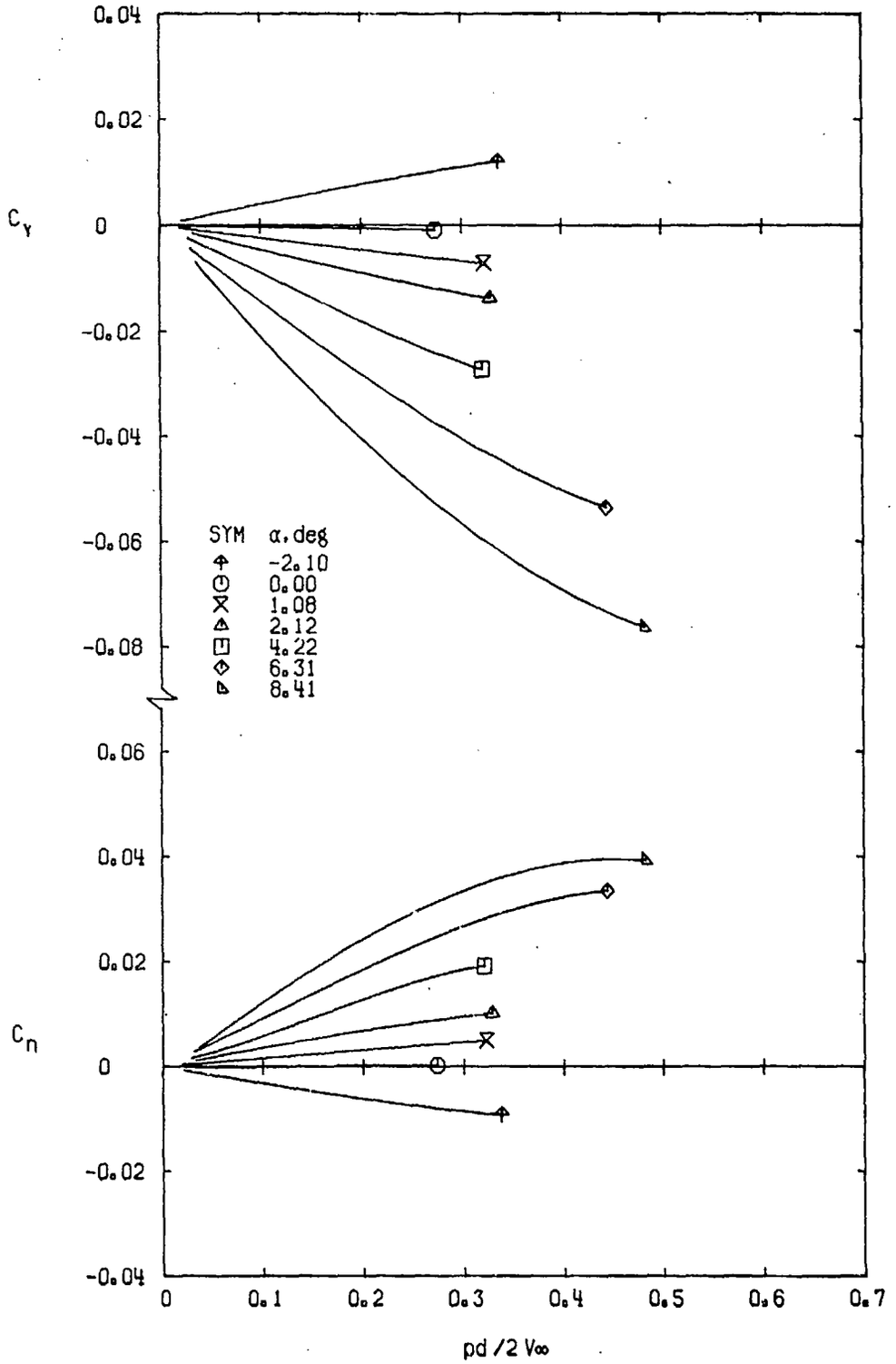

b. $M_\infty = 0.80$

Figure 16. Continued.

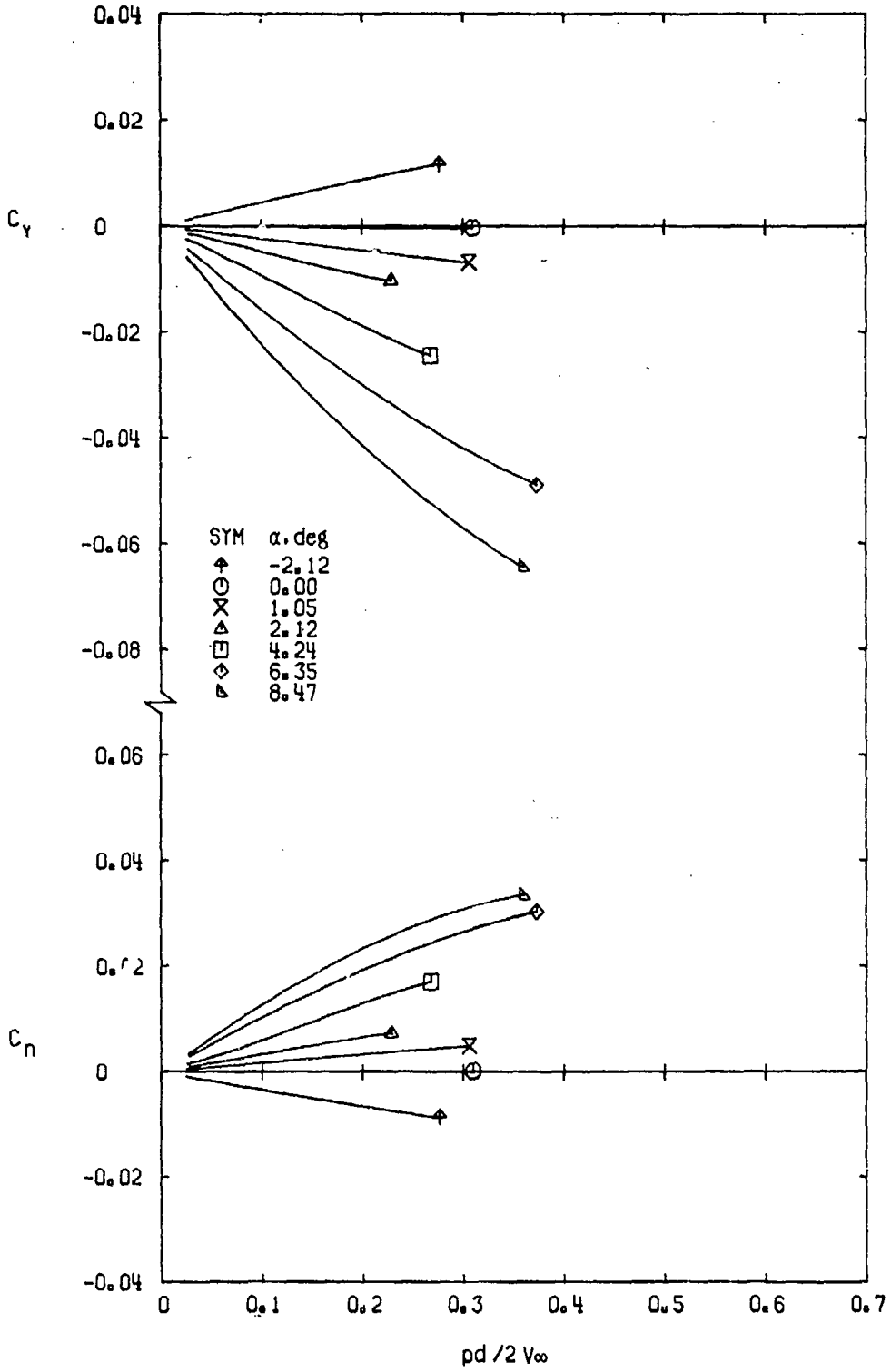

c. $M_\infty = 0.90$

Figure 16. Continued.

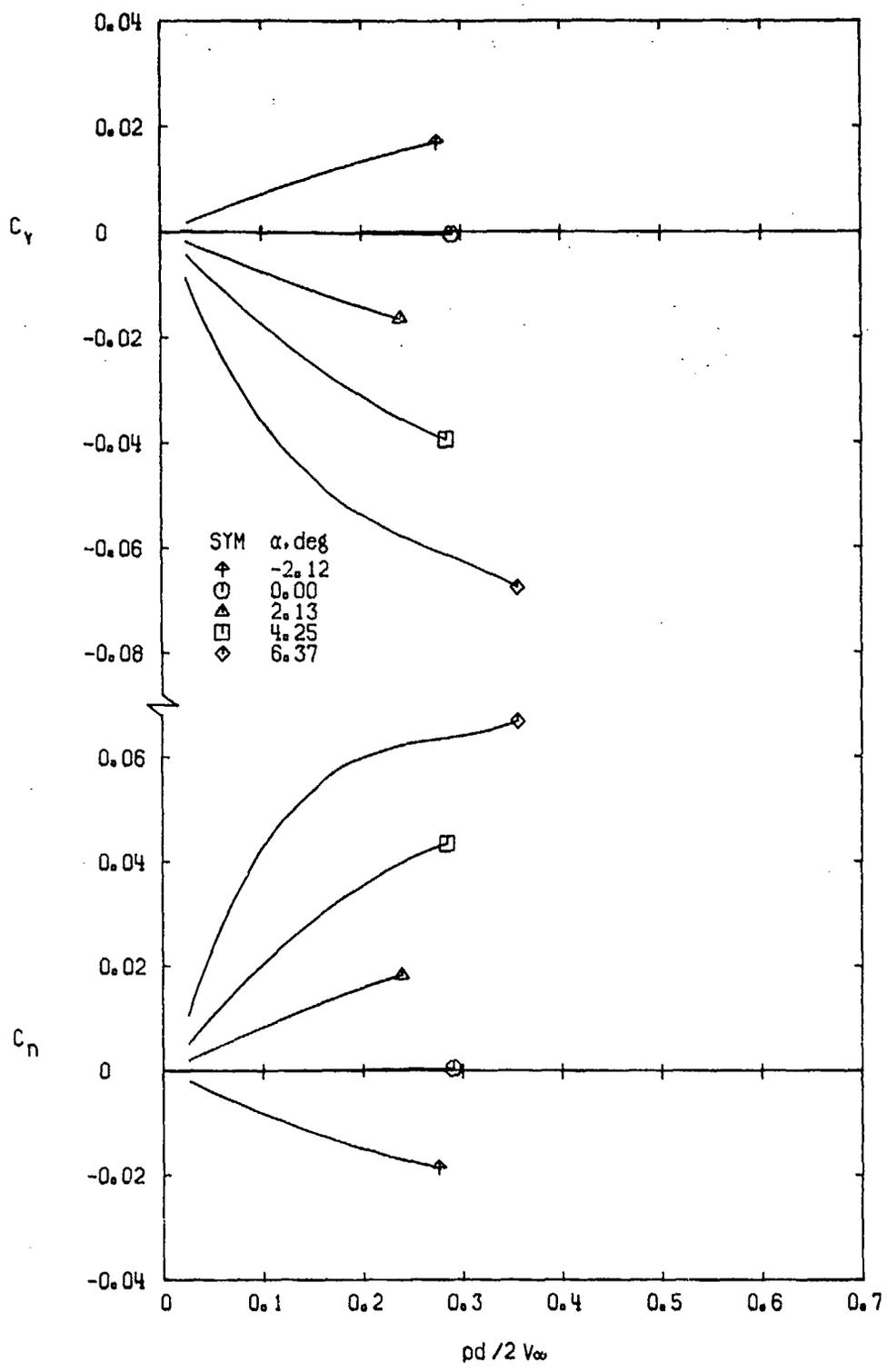

d. $M_\infty = 0.95$

Figure 16. Continued.

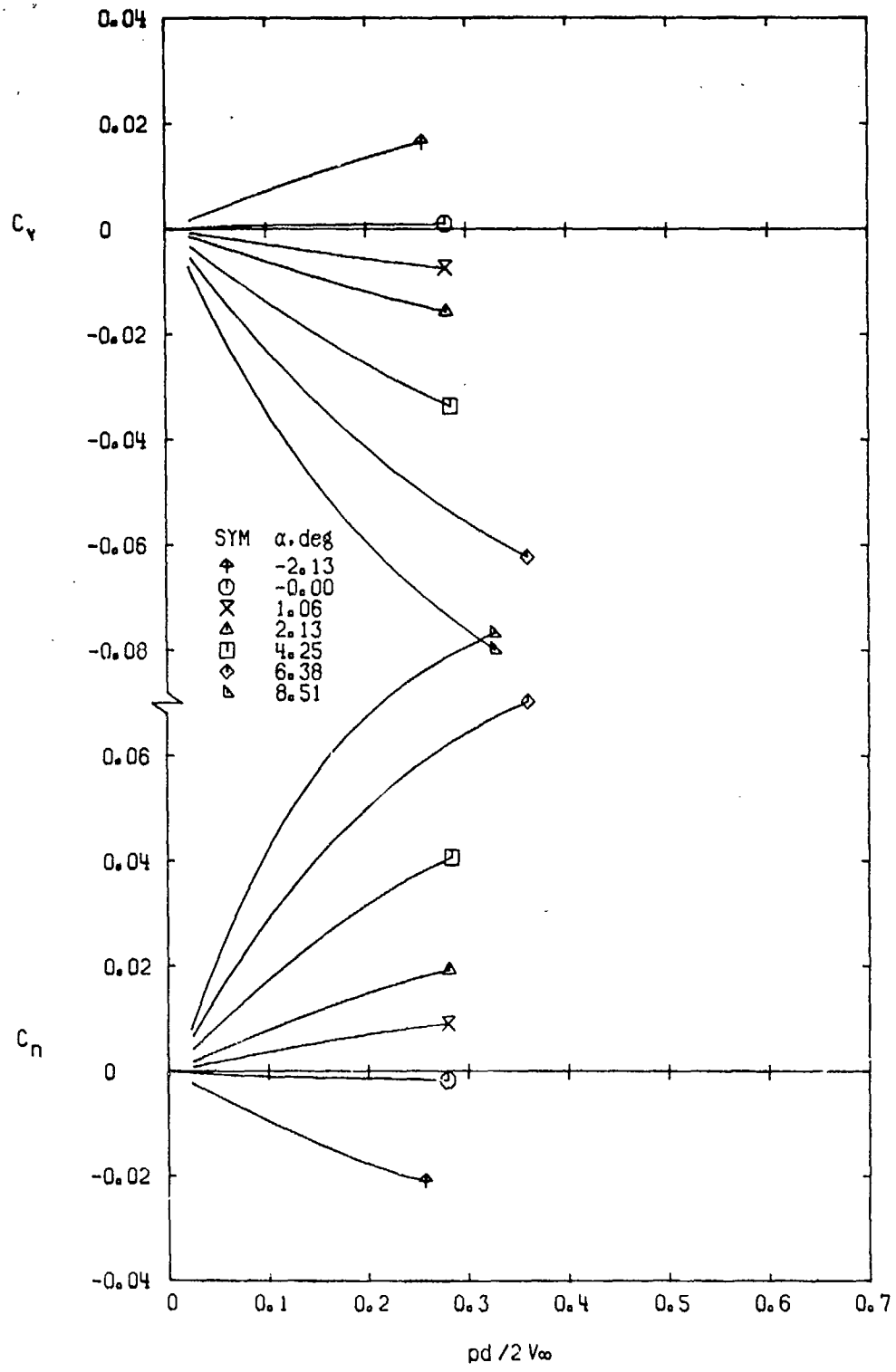

e. $M_\infty = 1.00$

Figure 16. Continued.

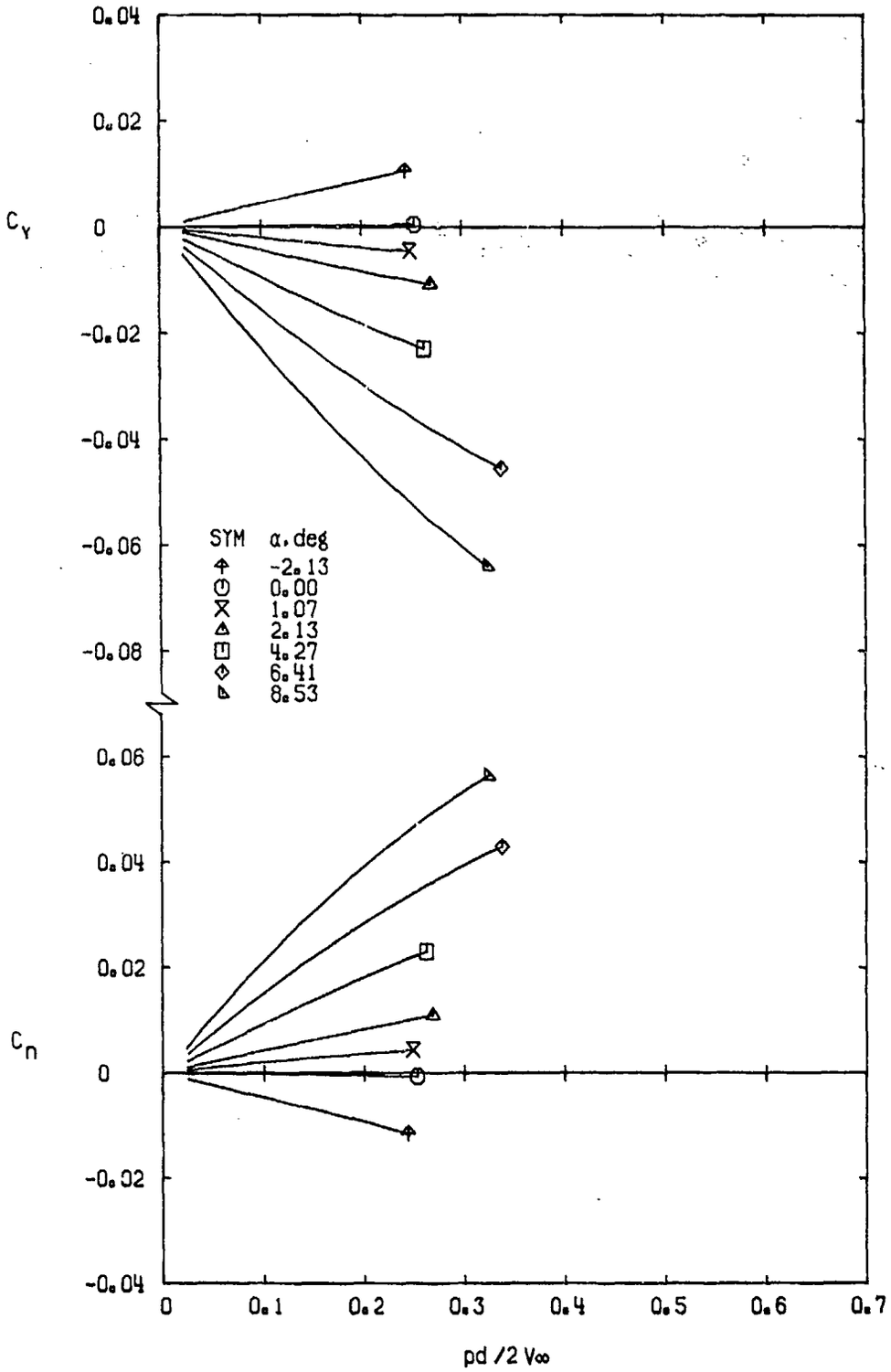

f. $M_\infty = 1.10$

Figure 16. Continued.

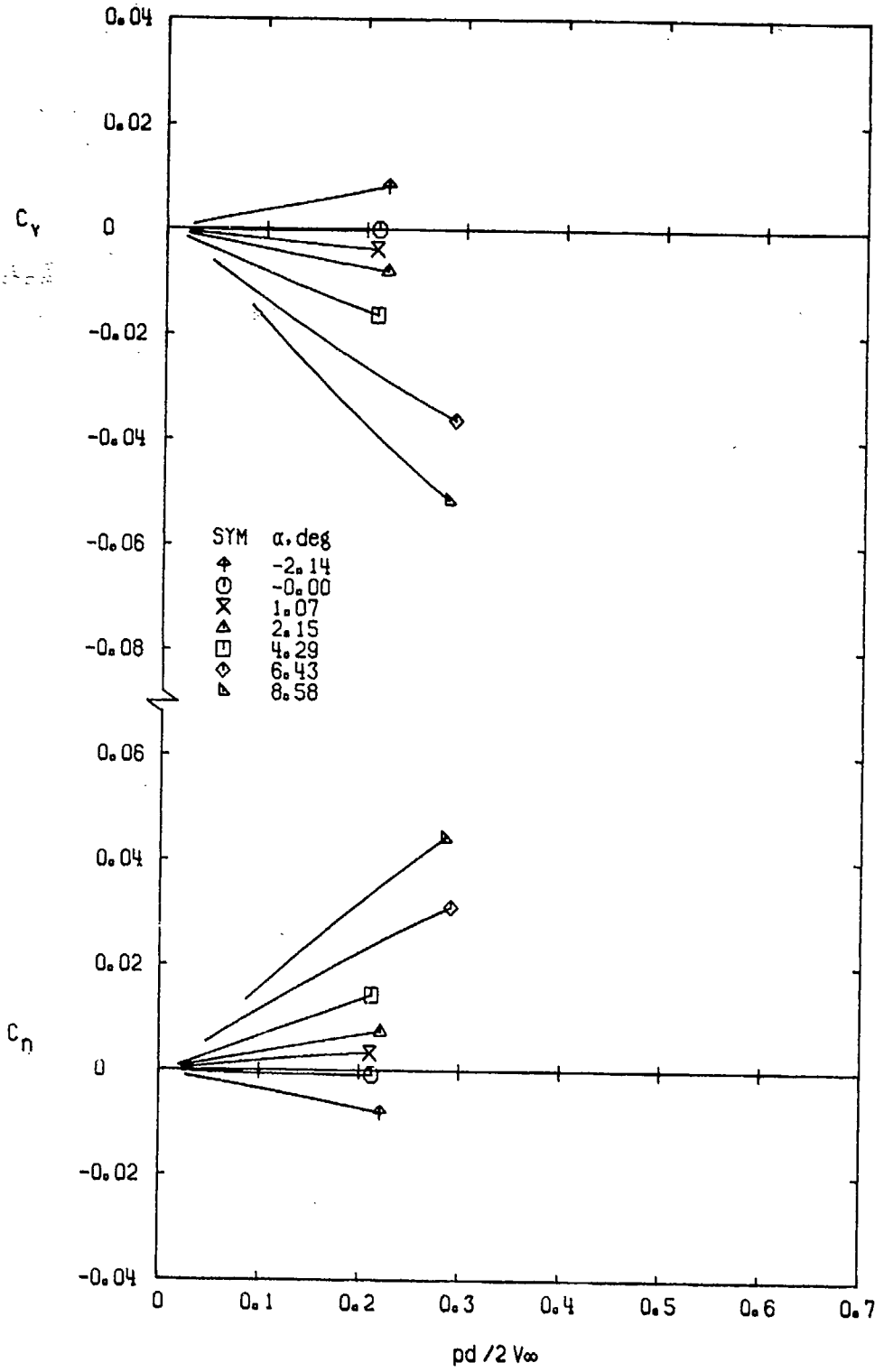

g. M_∞ = 1.30

Figure 16. Concluded.

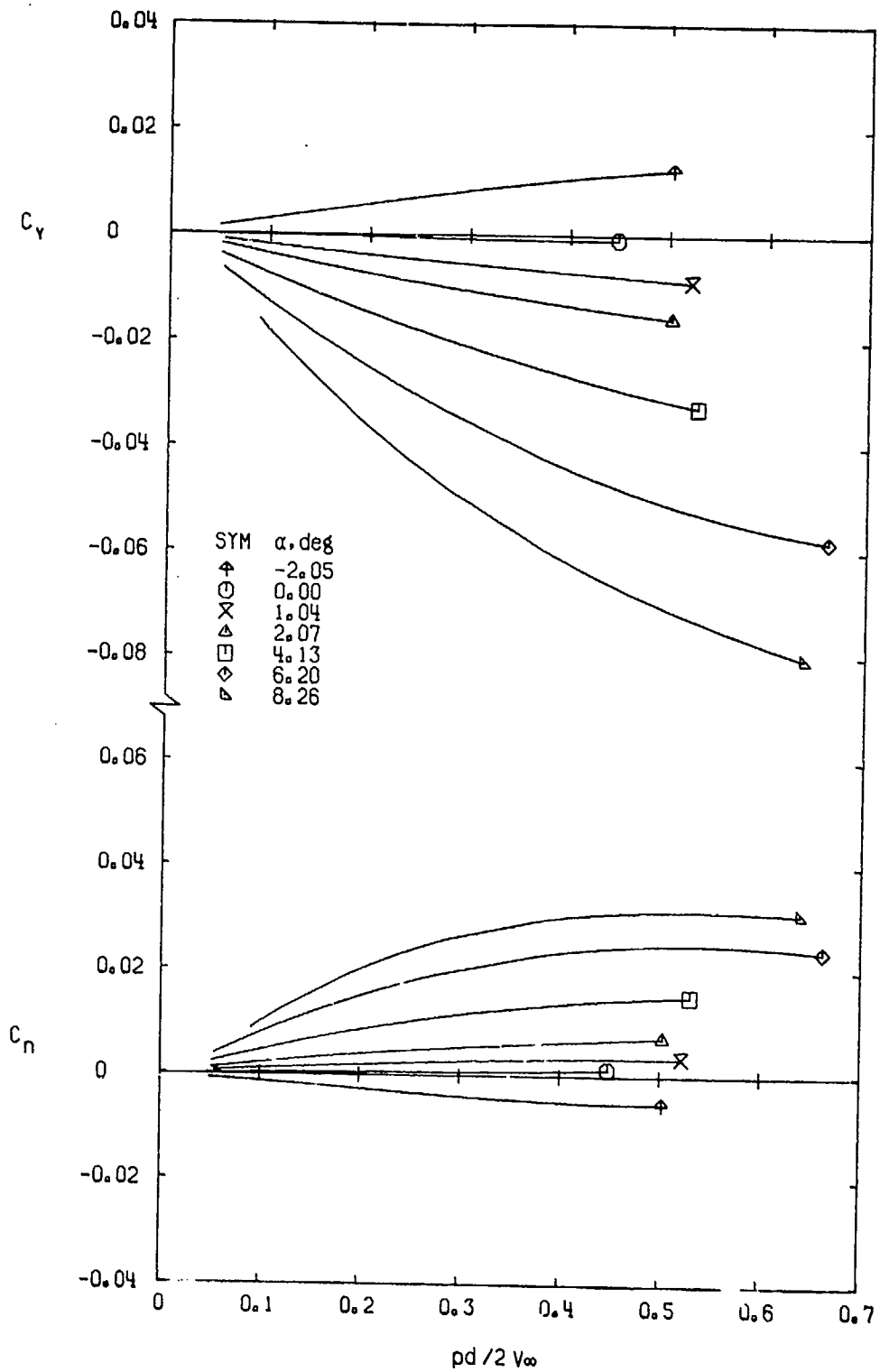

a. $M_\infty = 0.50$

Figure 17. Variation of C_Y and C_n with $pd/2V_\infty$ for Configuration 9.

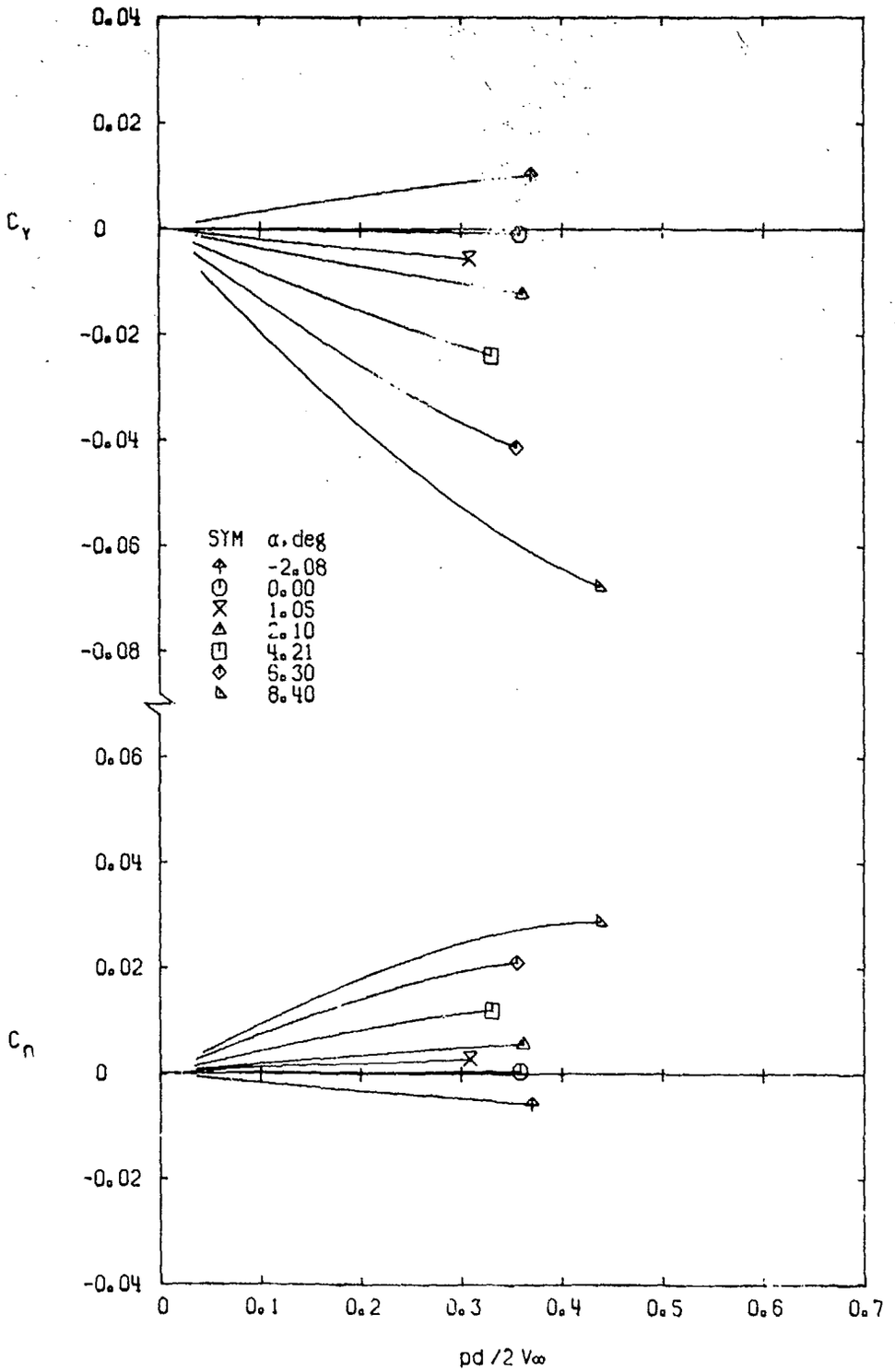

b. $M_\infty = 0.80$

Figure 17. Continued.

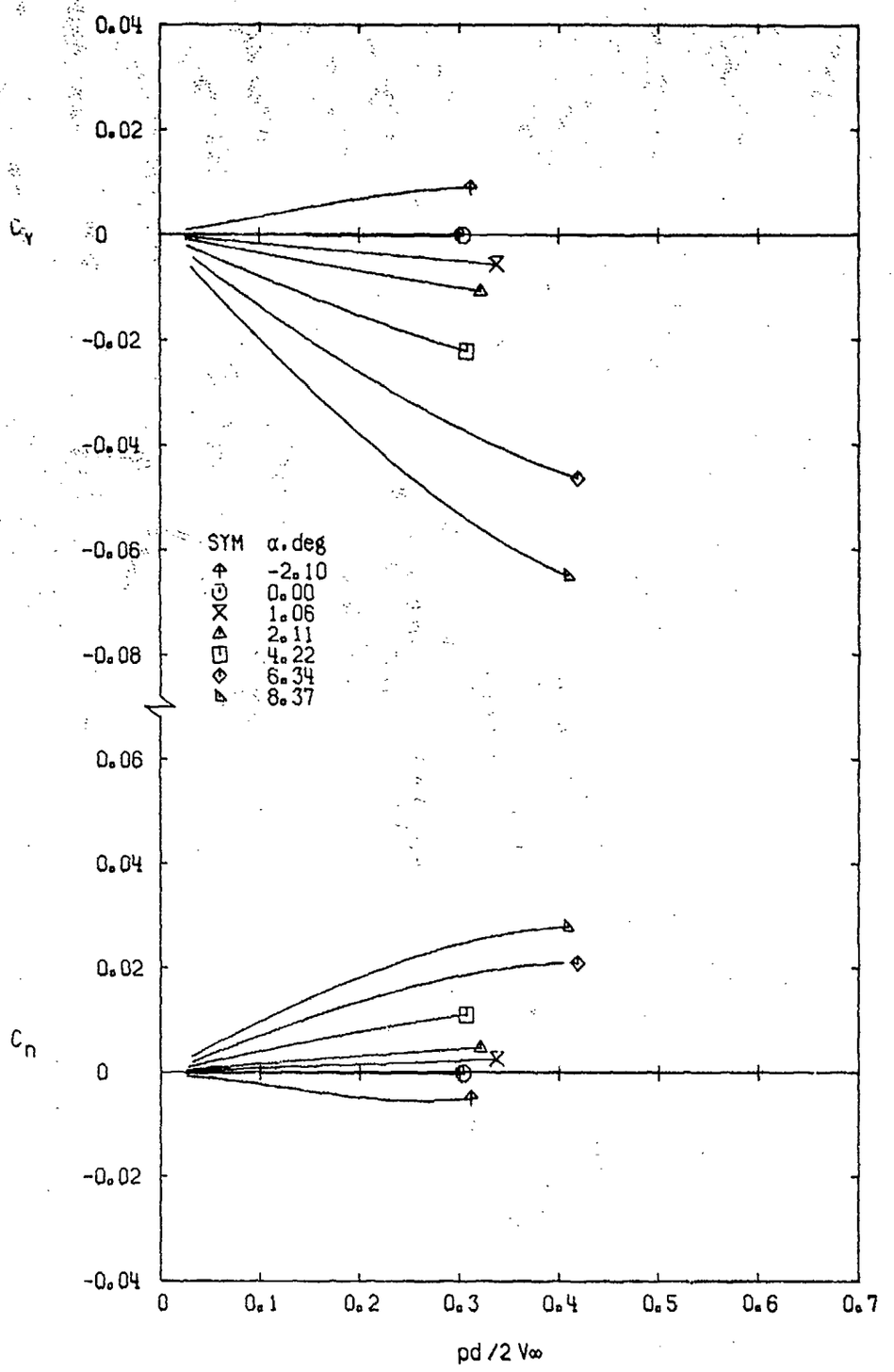

c. $M_\infty = 0.90$

Figure 17. Continued.

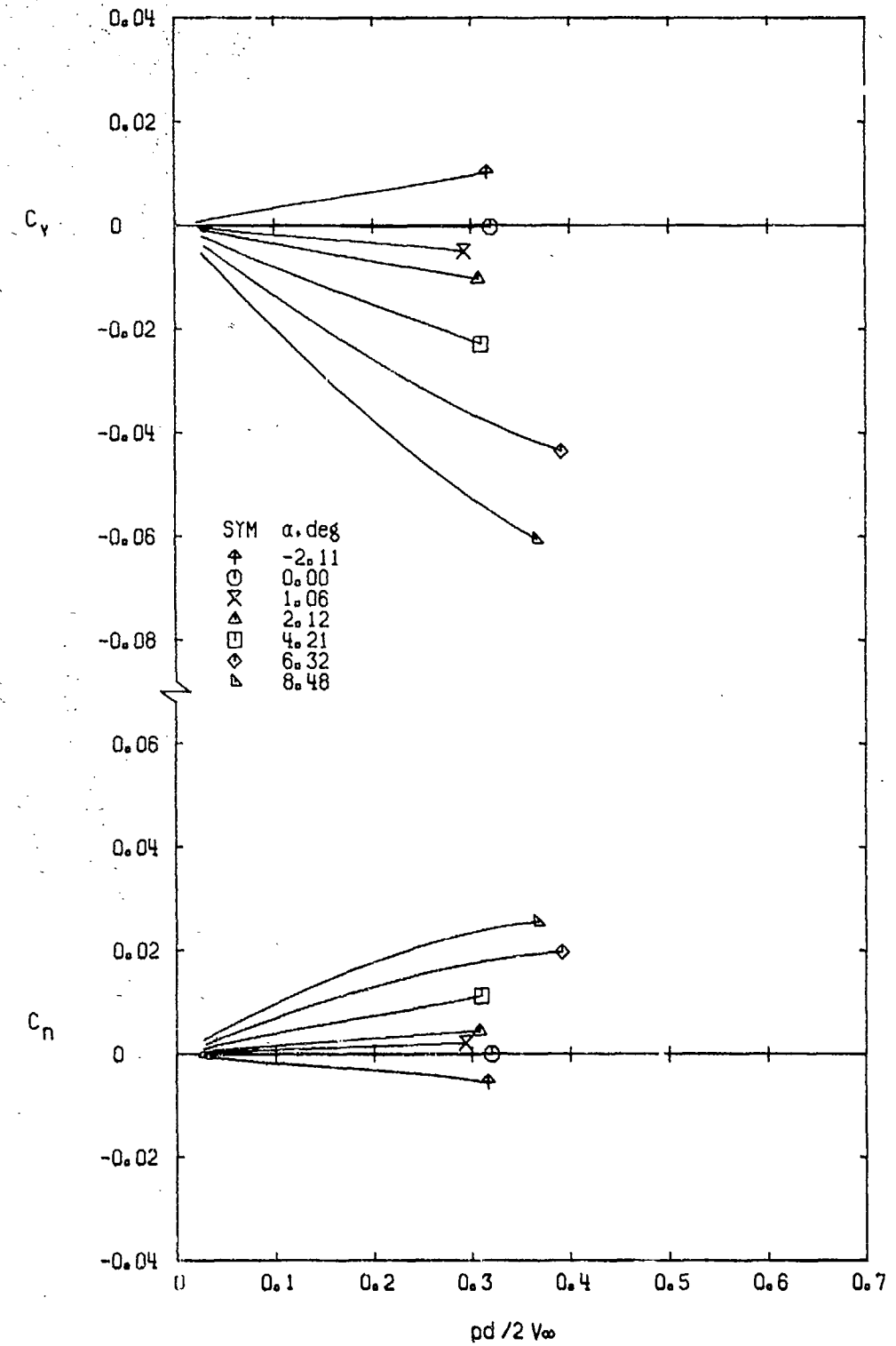

d. M_∞ = 0.95

Figure 17. Continued.

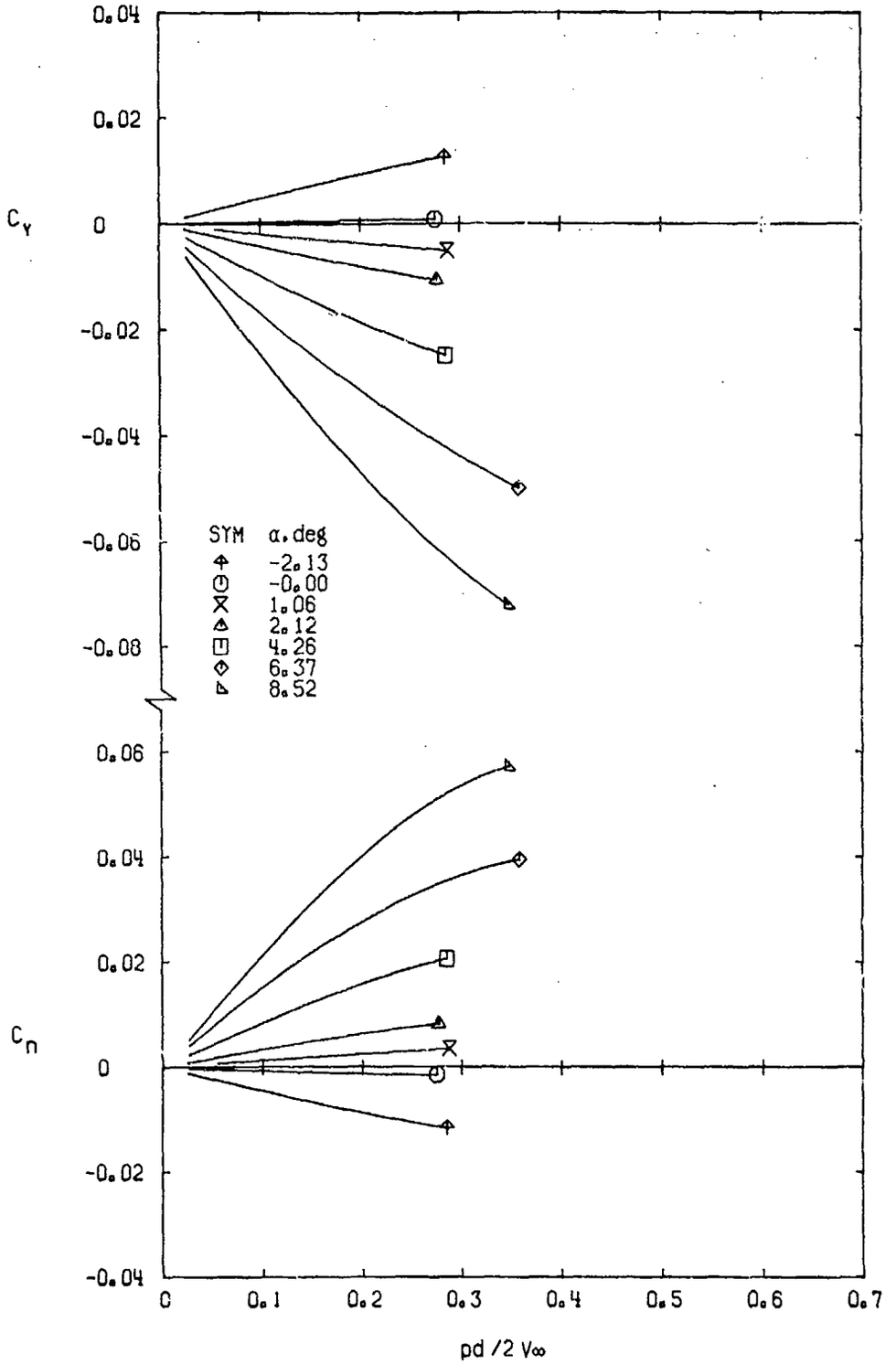

e. M_∞ = 1.00

Figure 17. Continued.

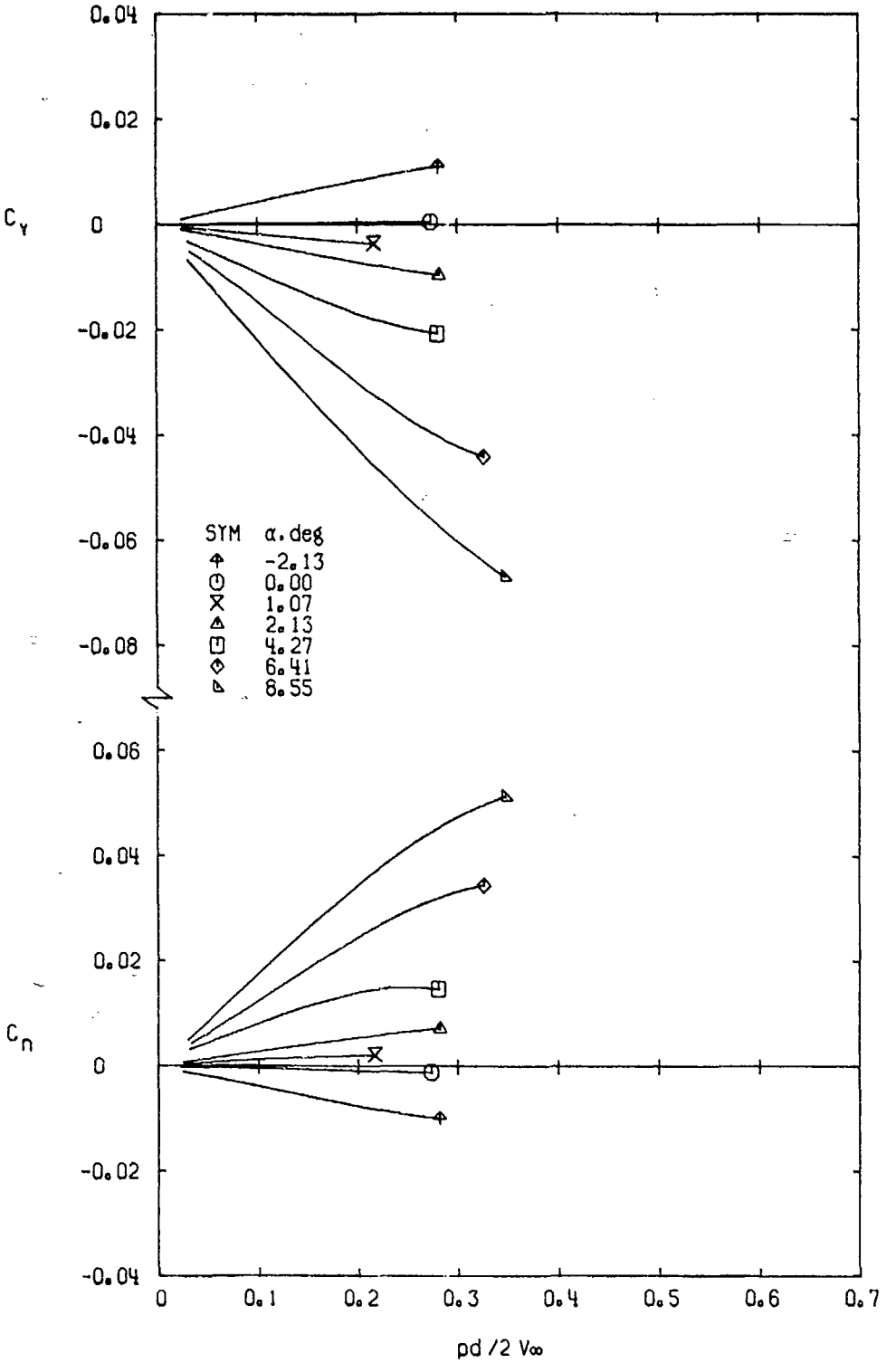

f. M_∞ = 1.10
Figure 17. Continued.

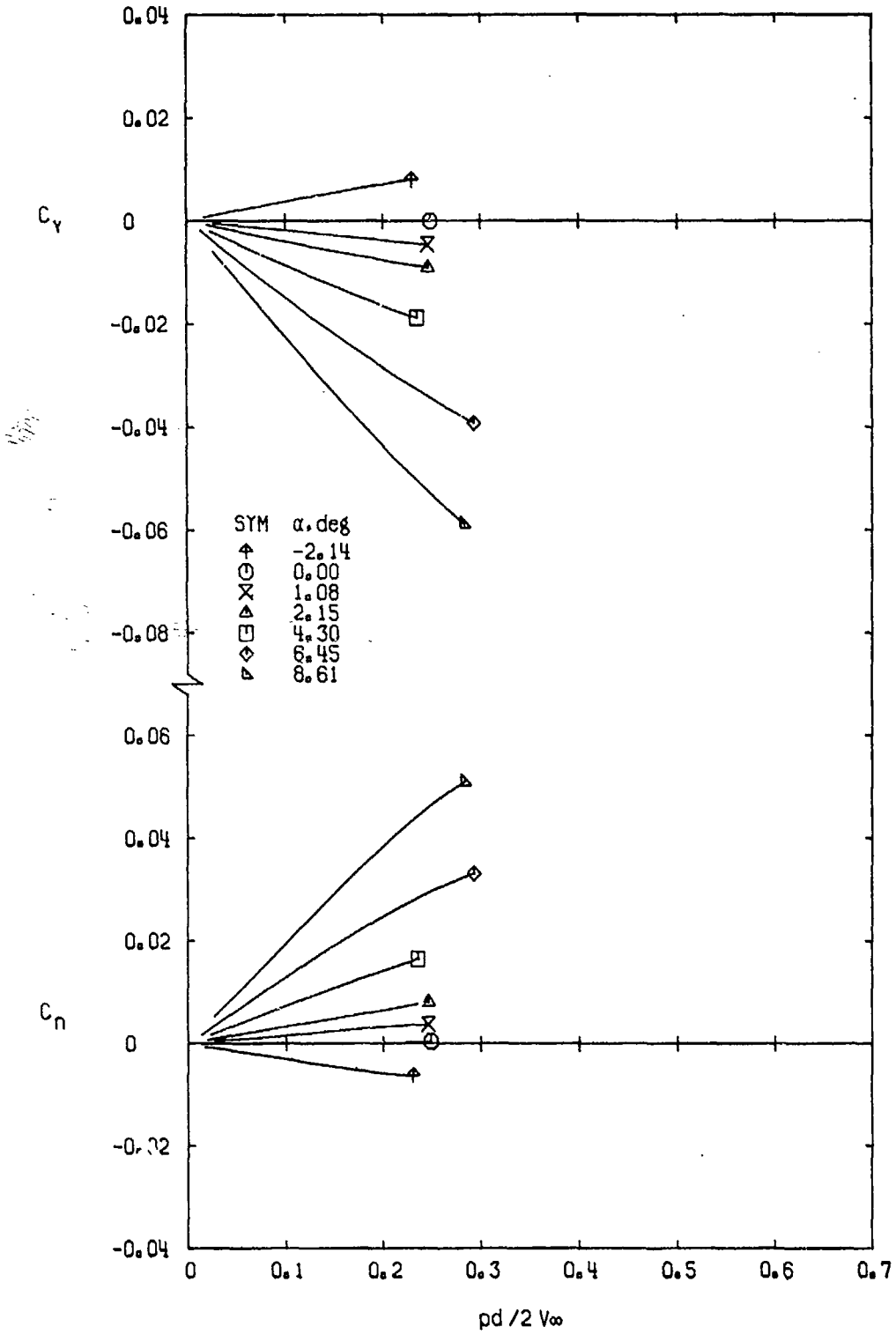

g. $M_\infty = 1.30$

Figure 17. Concluded.

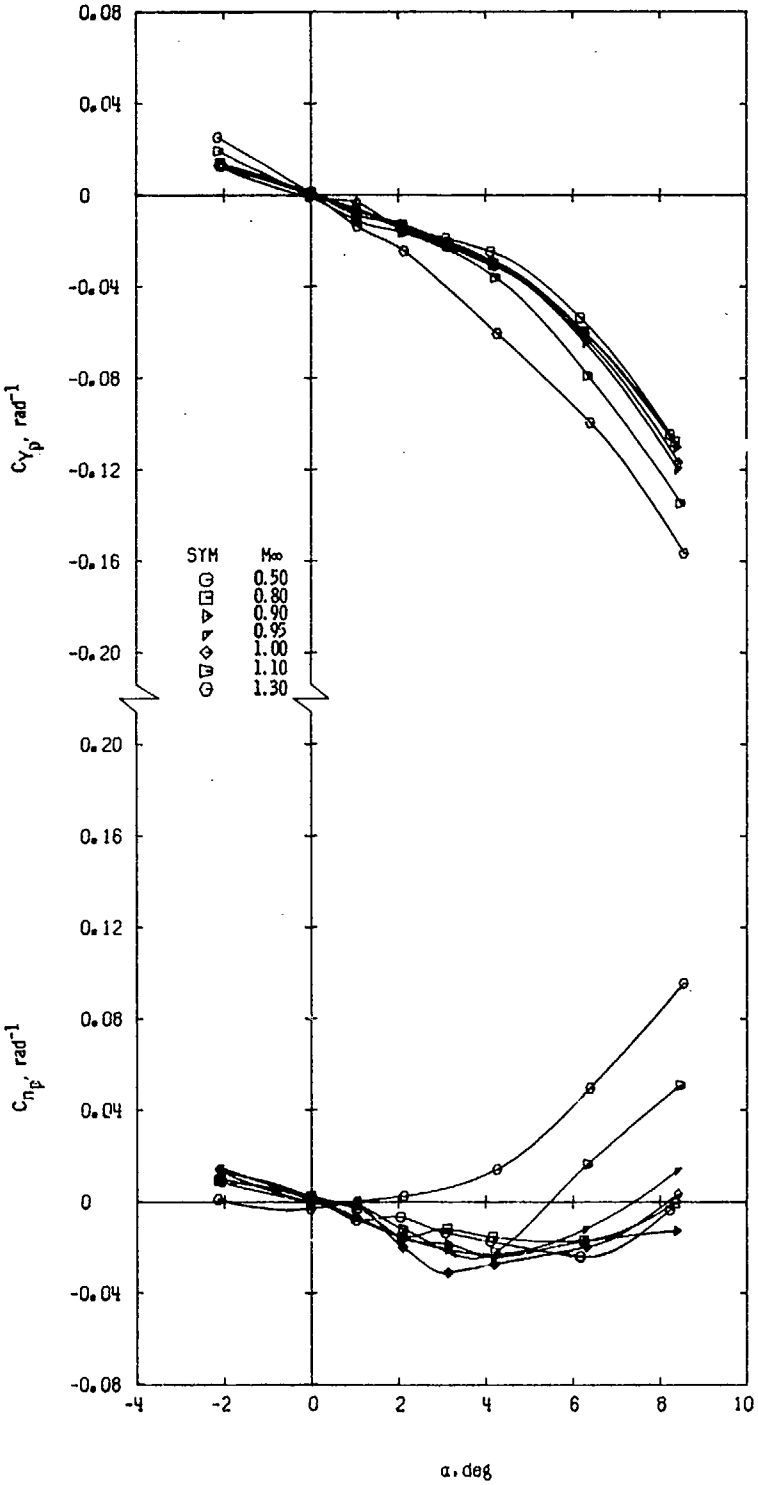

a. Configuration 0

Figure 18. Variation of C_{Y_p} and C_{n_p} with angle of attack, $Re_\ell = 9.6 \times 10^6$.

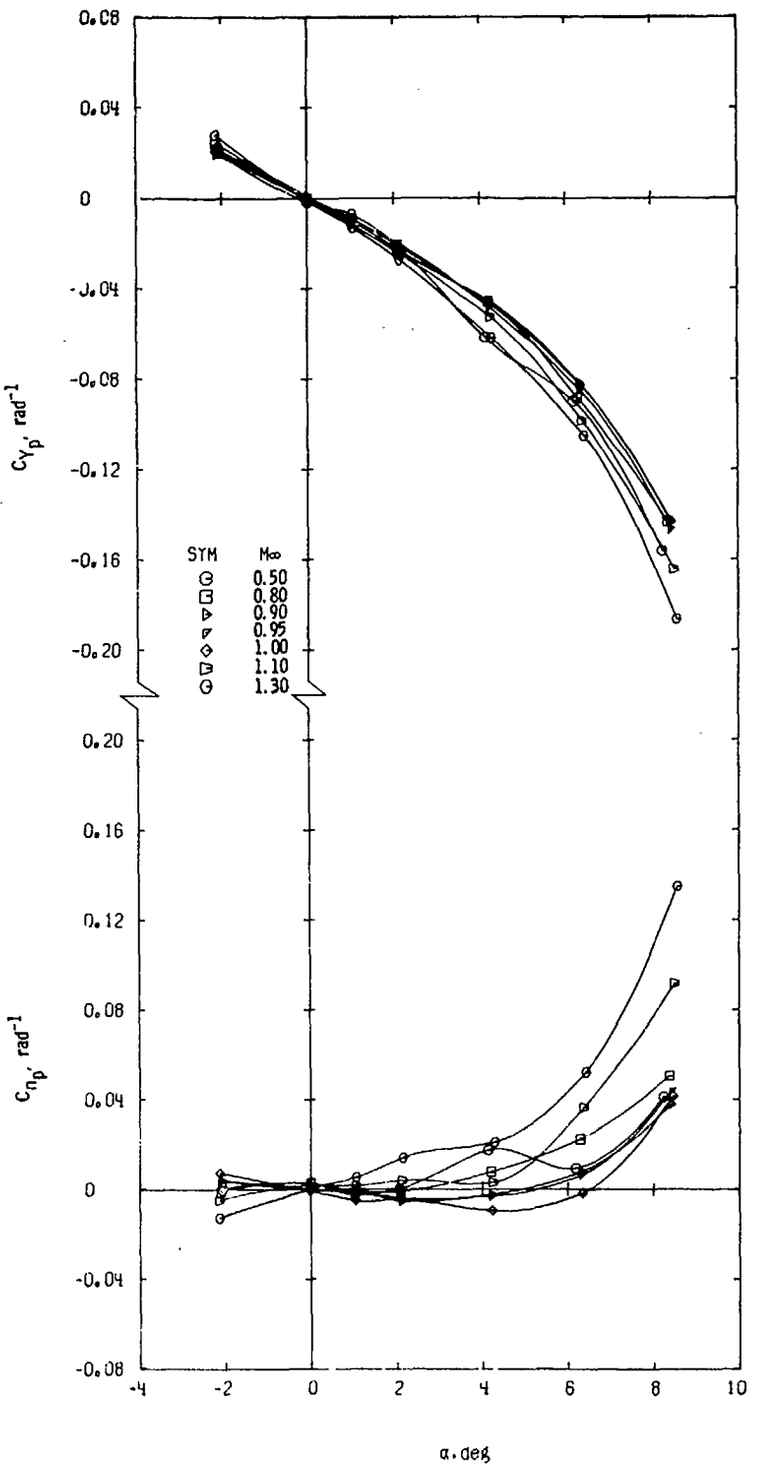

b. Configuration 1
Figure 18. Continued.

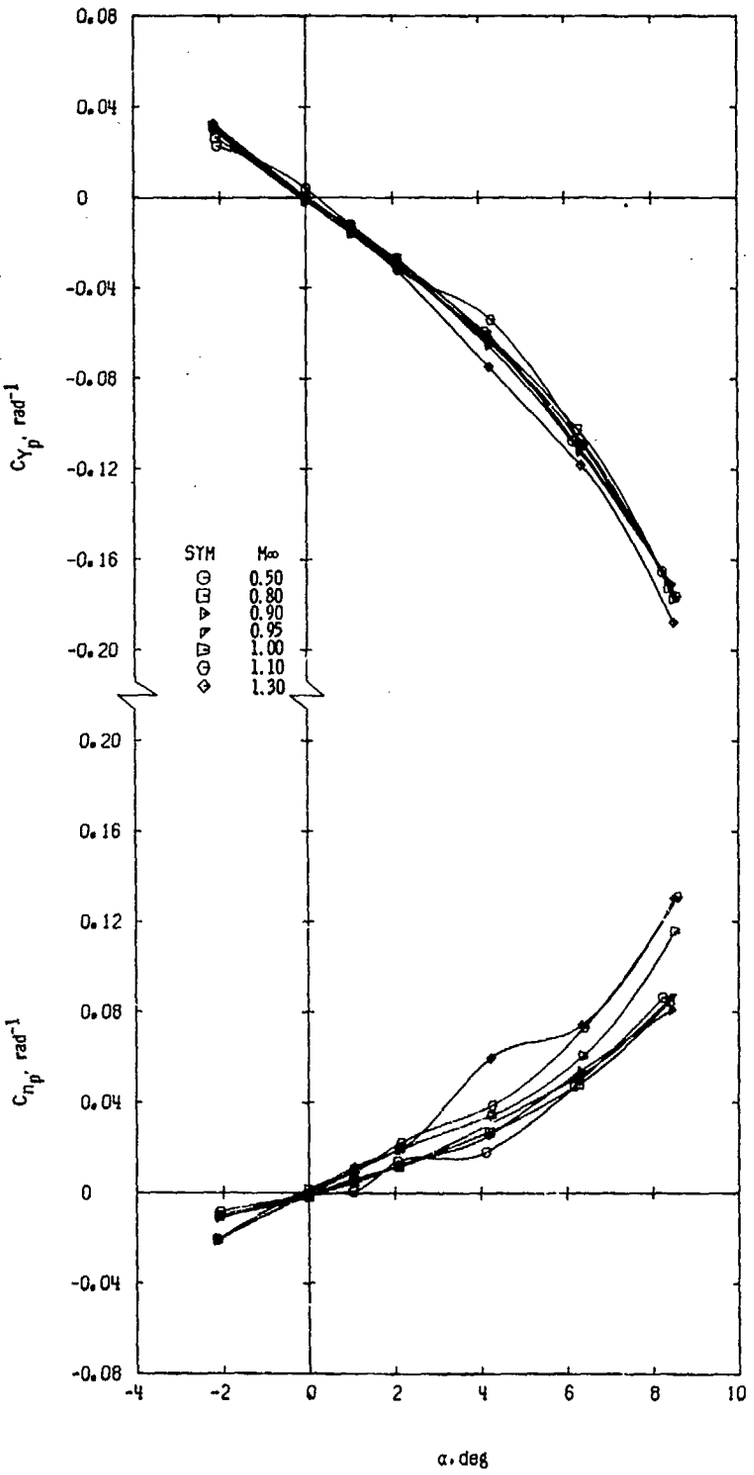

c. Configuration 2
Figure 18. Continued.

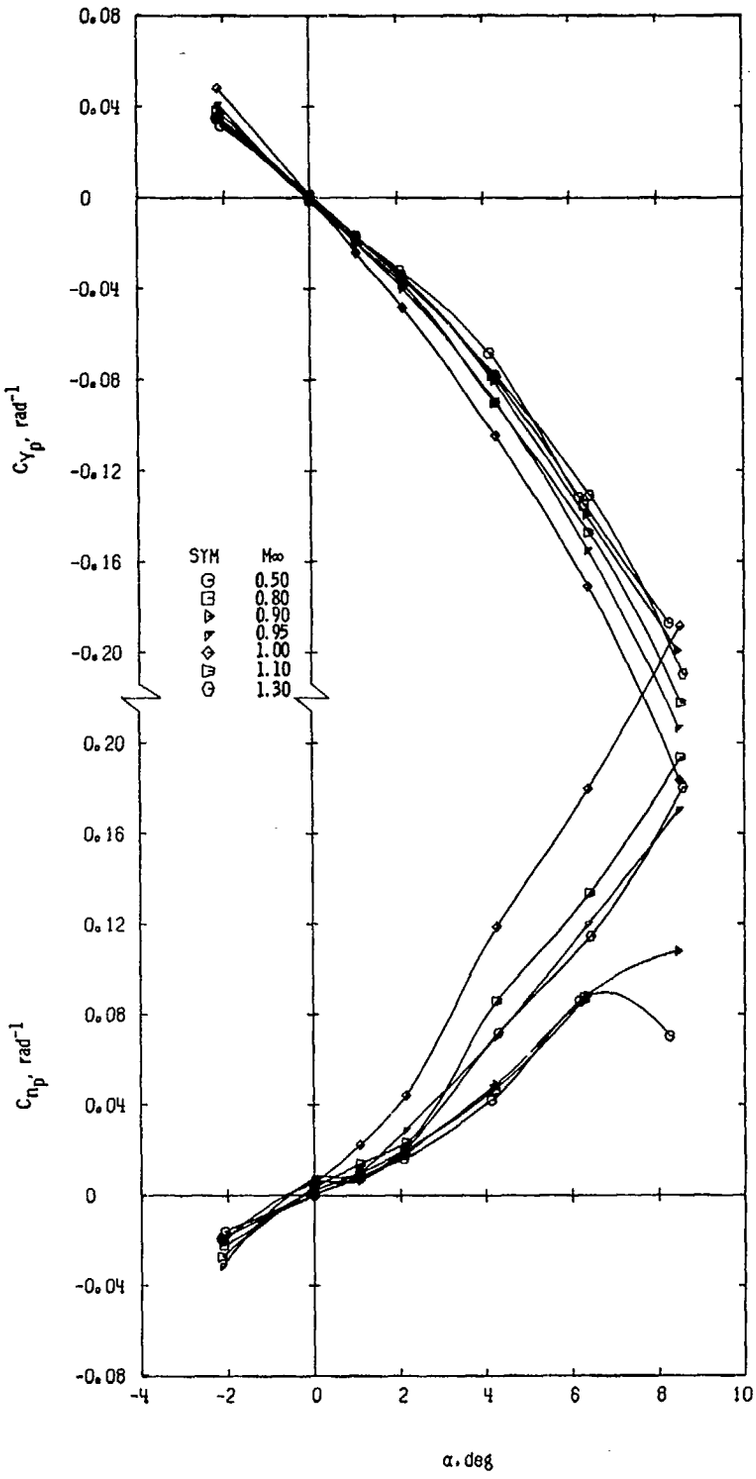

d. Configuration 3
Figure 18. Continued.

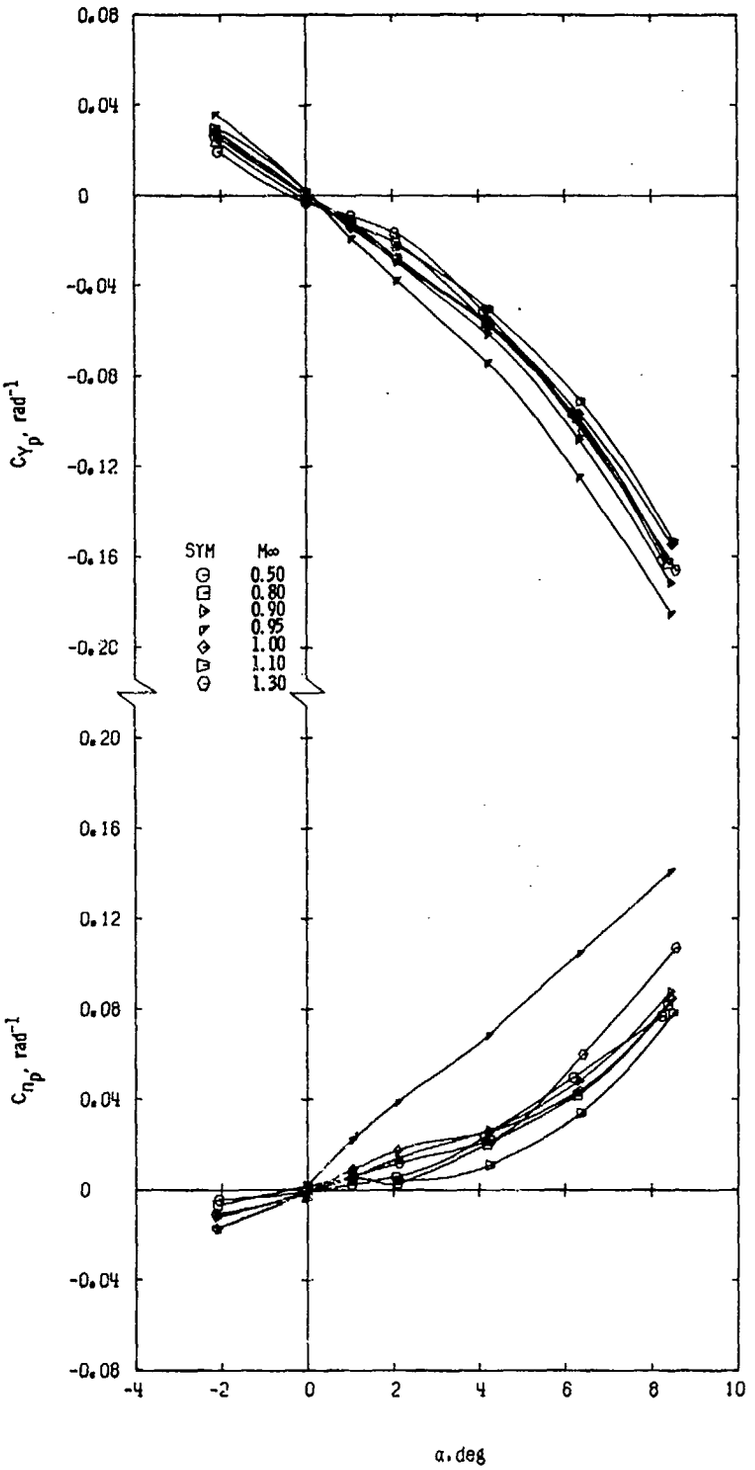

e. Configuration 4
Figure 18. Continued.

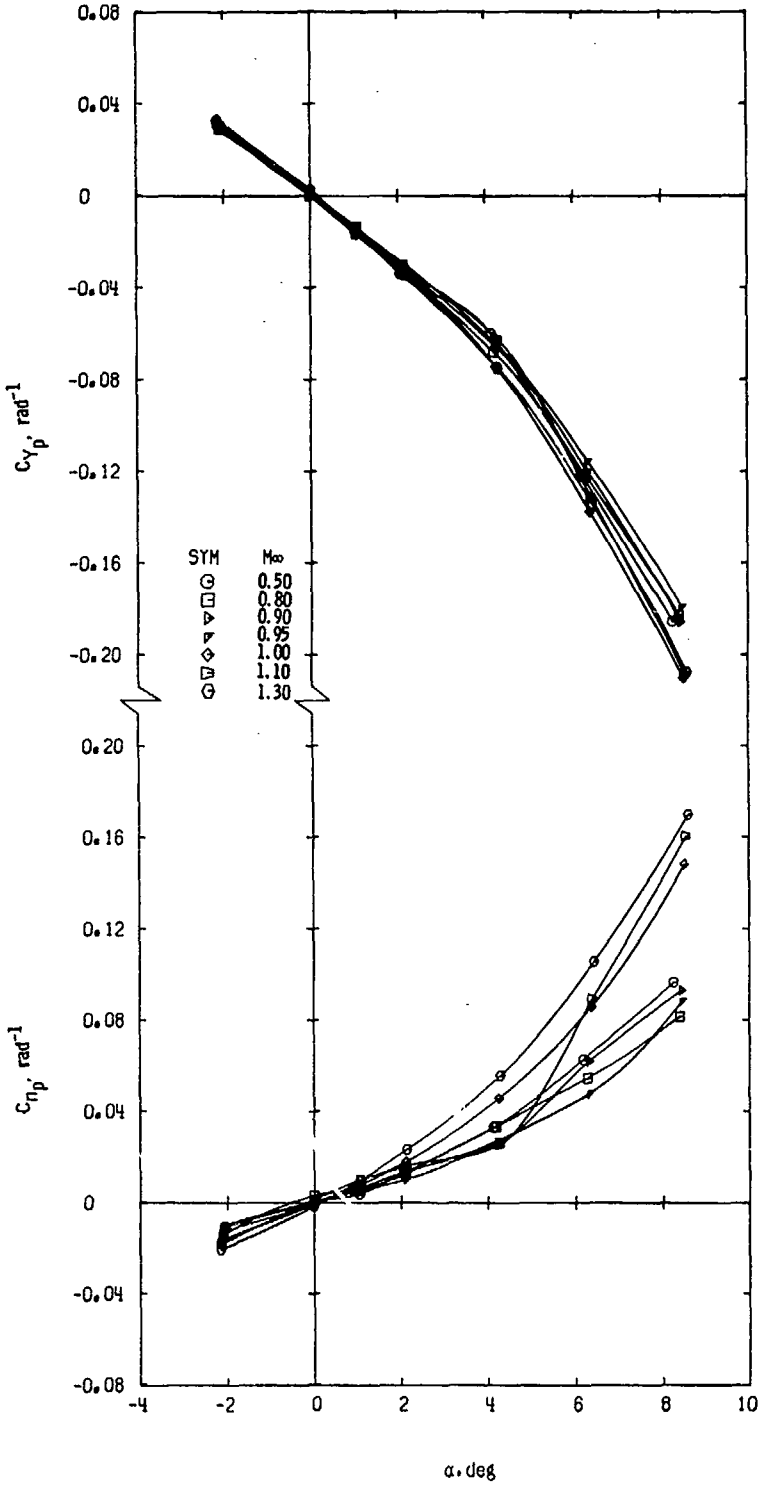

f. Configuration 5
Figure 18. Continued.

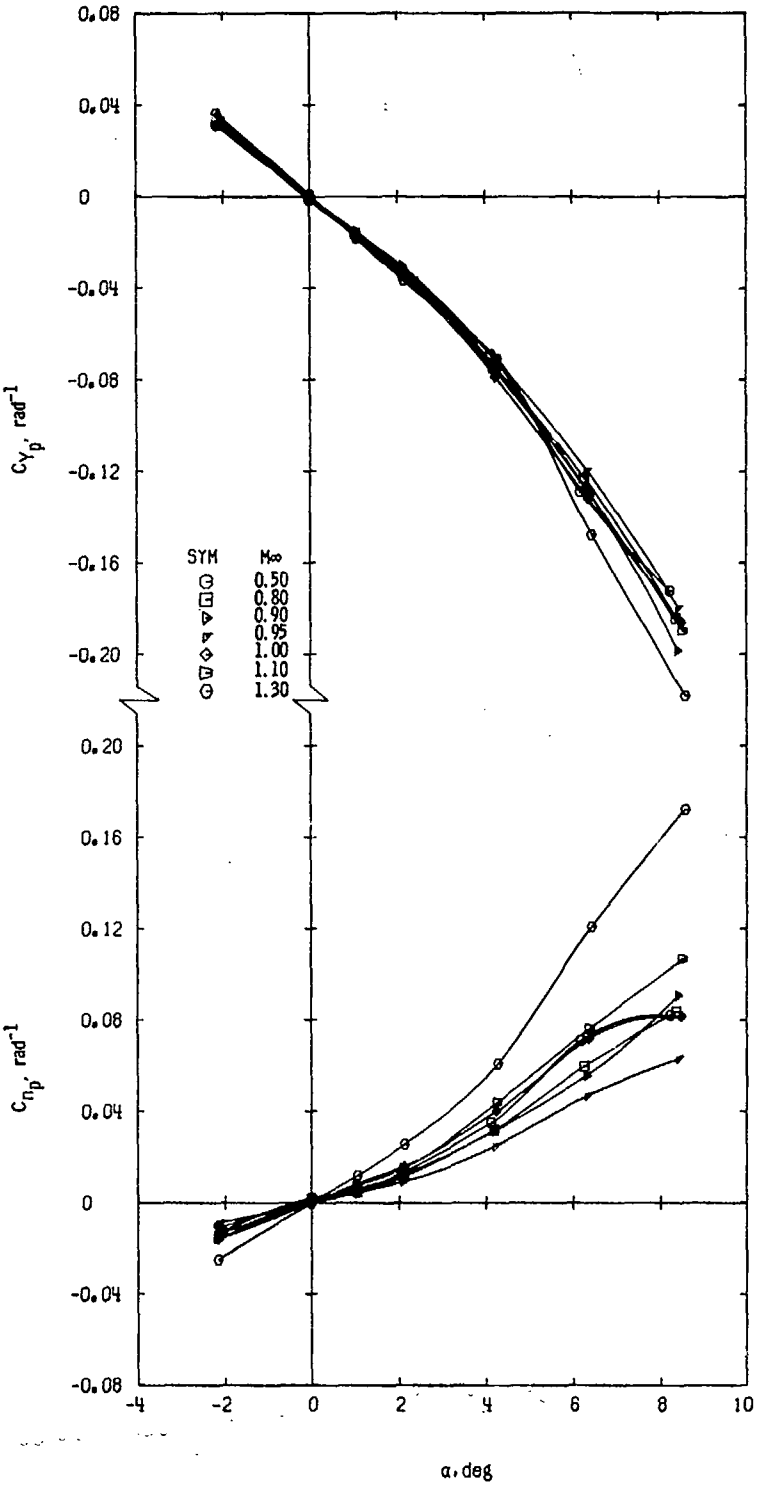

g. Configuration 6
Figure 18. Continued.

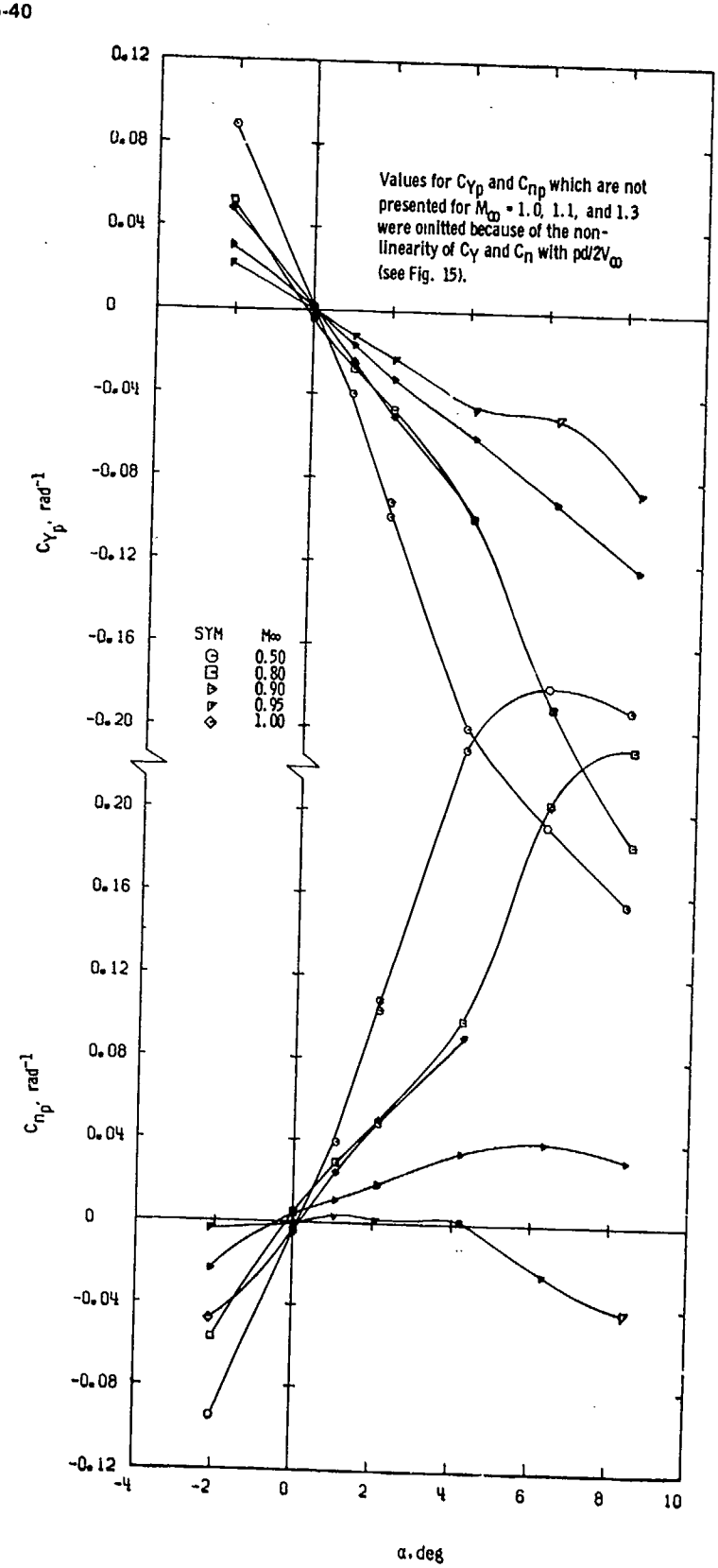

h. Configuration 7
Figure 18. Continued.

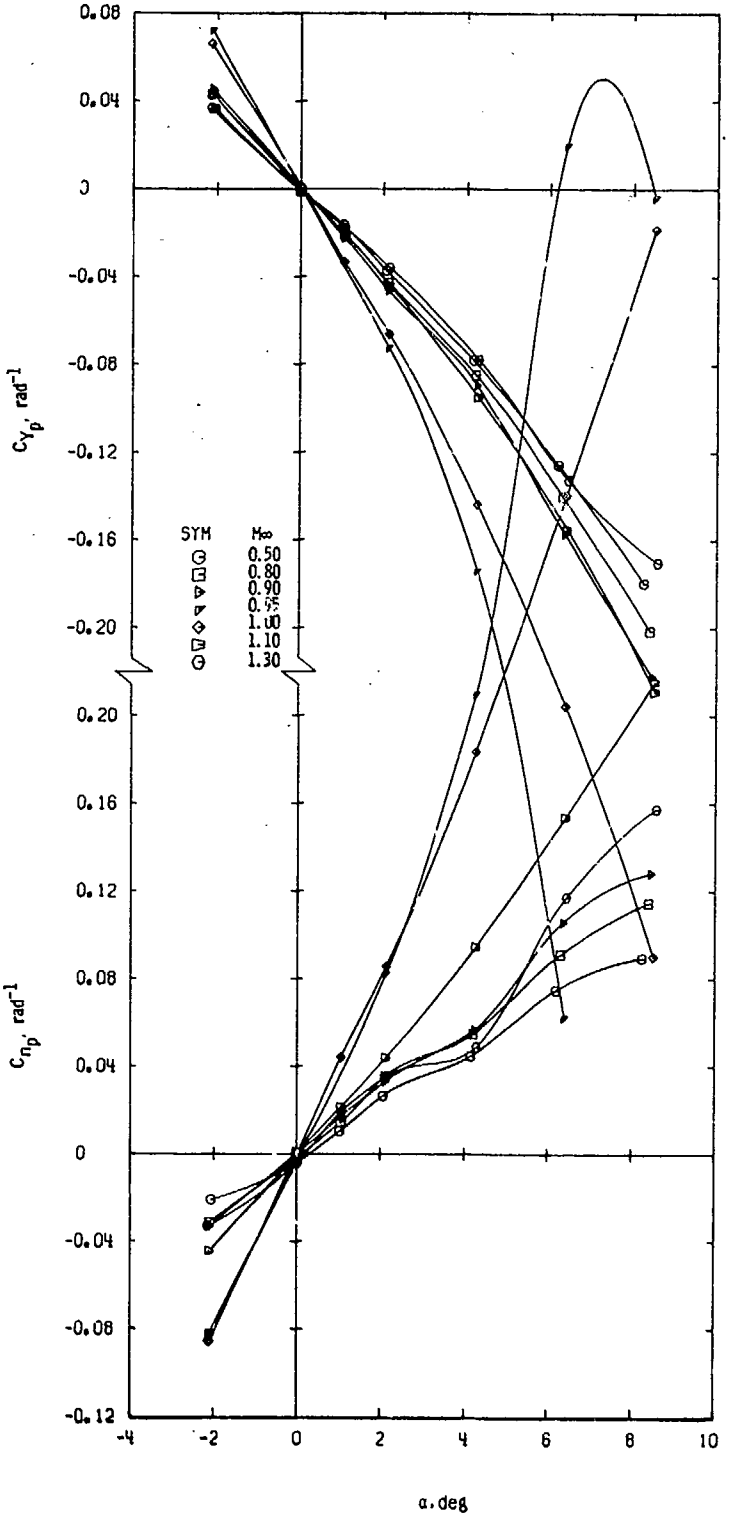

i. Configuration 8

Figure 18. Continued.

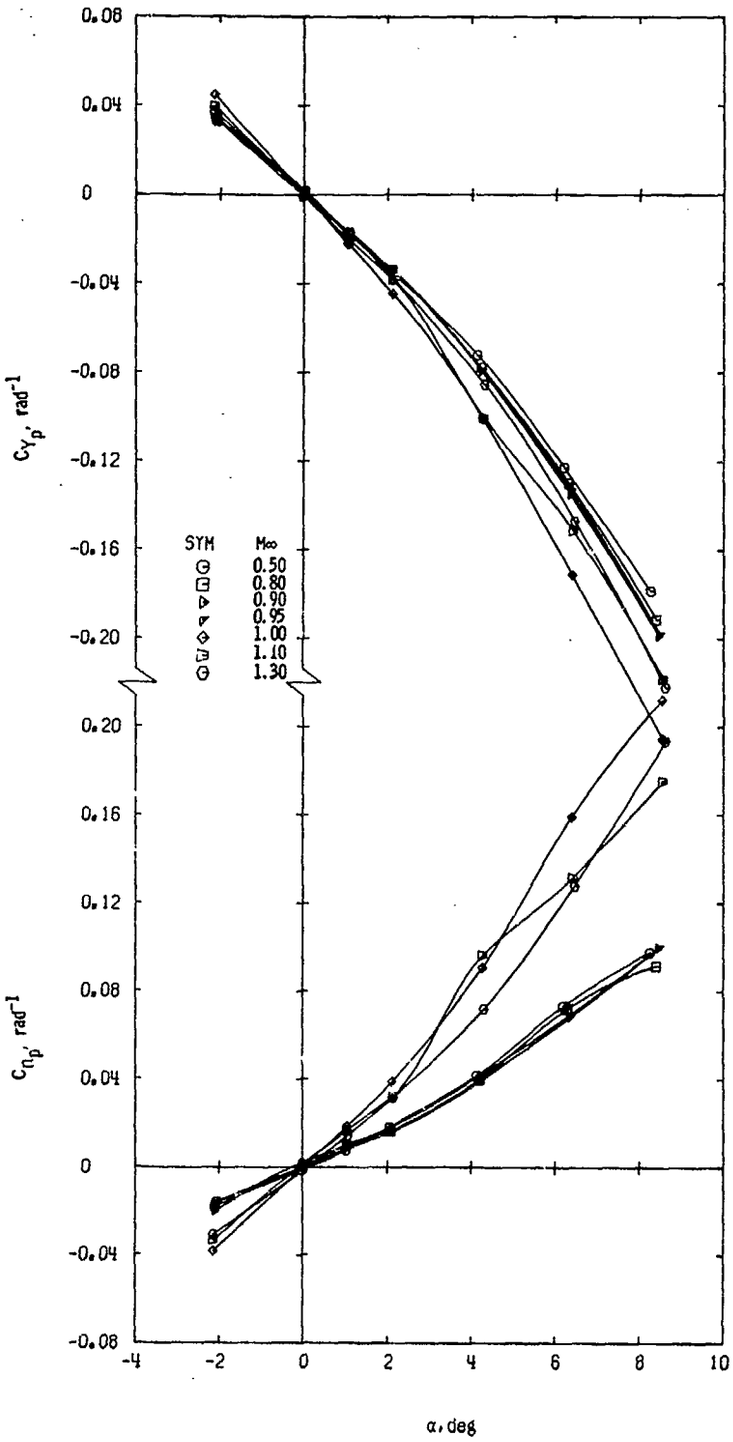

j. Configuration 9

Figure 18. Concluded.

Sym	Config	δ_{BT}, deg	ℓ_{BT}, caliber	d_B, caliber
○	0	0	0	1.00
△	1	2.5	1.0	0.91
□	2	5.0	1.0	0.82
◇	3	7.5	1.0	0.74

Solid Symbols - Ref. 3

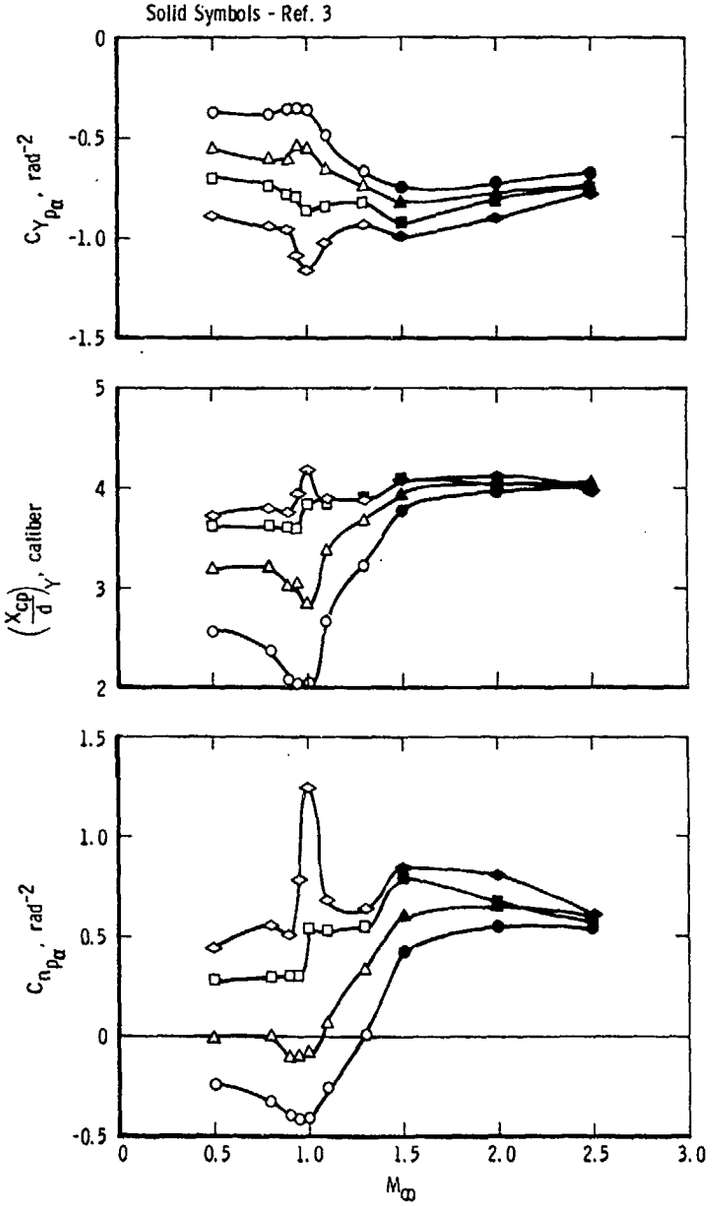

a. Effect of boattail angle with a constant boattail length

Figure 19. Variation of $C_{Y_{p_\alpha}}$, $C_{n_{p_\alpha}}$, and $(X_{cp}/d)_Y$ with Mach number, $Re_\ell = 9.6 \times 10^6$.

Sym	Config	ℓ_{BT}, caliber	δ_{BT}, deg	d_B, caliber
○	0	0	0	1.00
△	4	0.50	5	0.91
□	2	1.00	5	0.82
◇	5	1.35	5	0.76
◊	6	1.70	5	0.70

Solid Symbols - Ref. 3

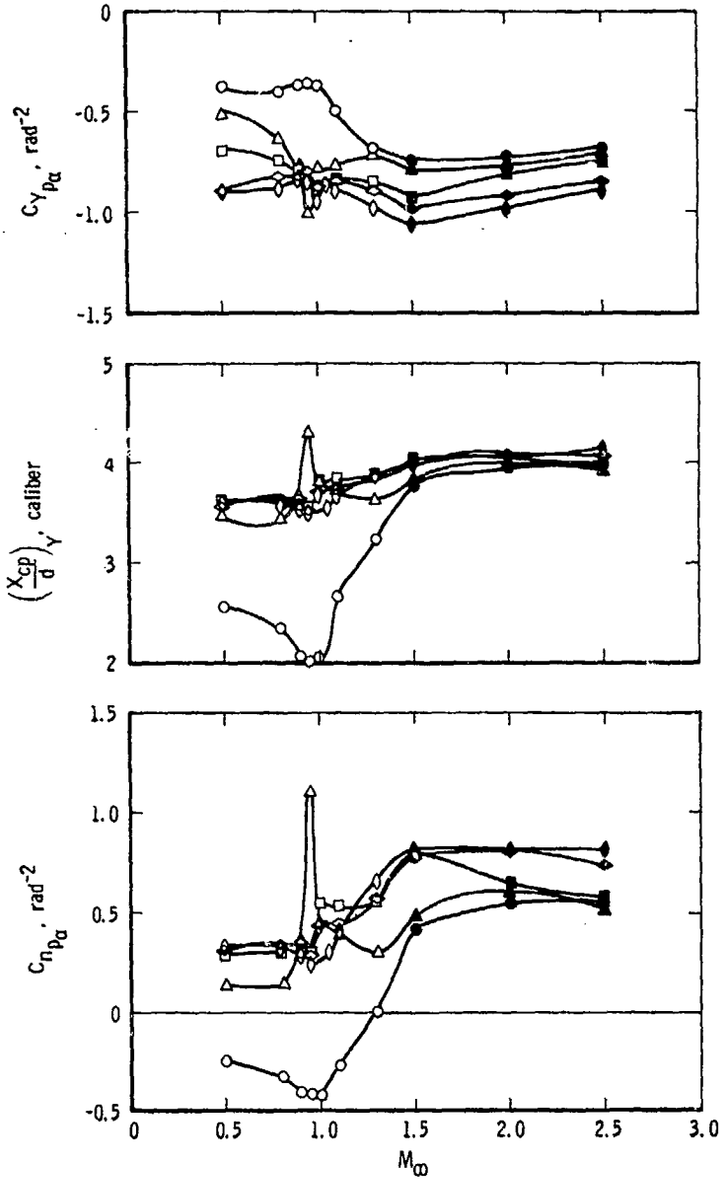

b. Effect of boattail length with a constant boattail angle
Figure 19. Continued.

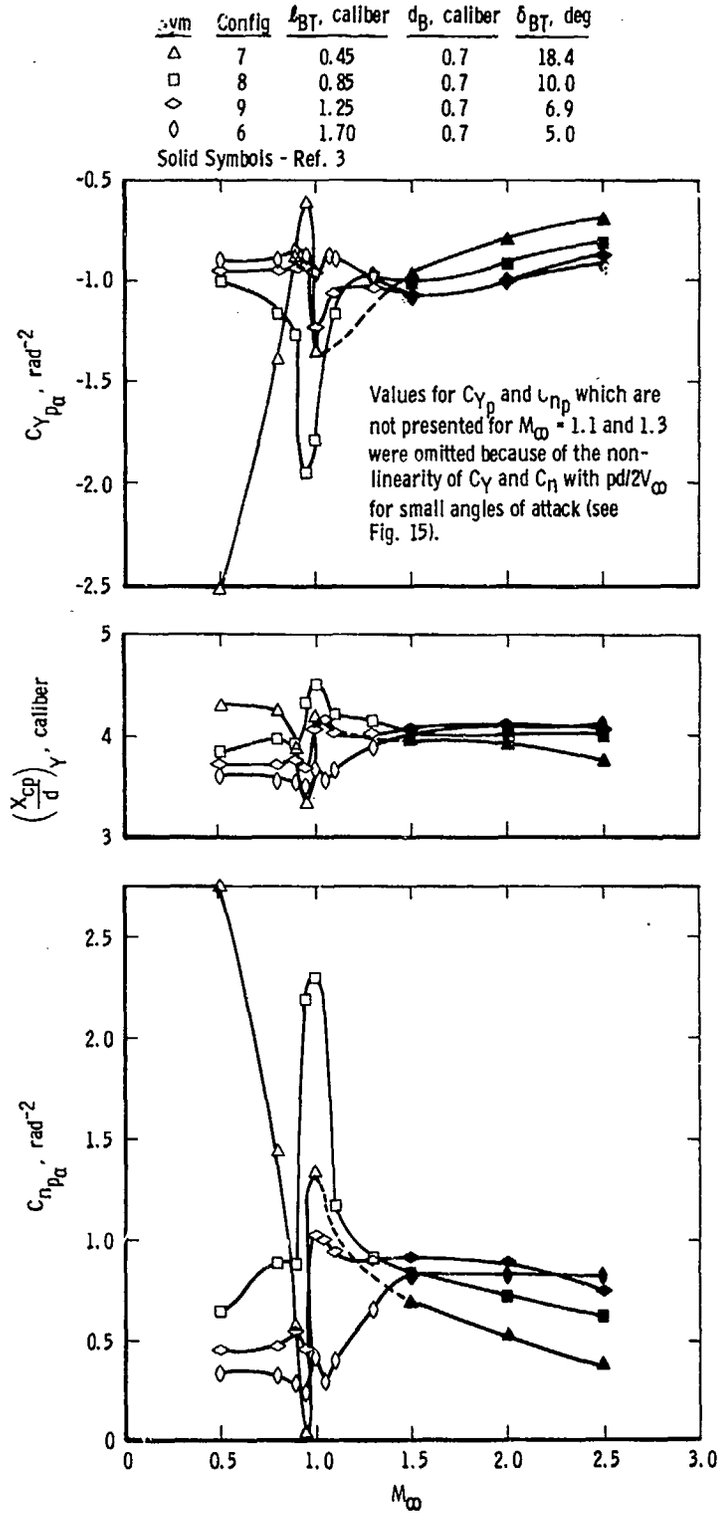

c. Effect of boattail length with a constant base diameter

Figure 19. Concluded.

Table 1. Test Summary

Configuration	Boattail Length (ℓ_{BT}), calibers	Boattail Angle (δ_{BT}), deg	Base Diameter (d_B), calibers	M_∞ (Re = 4 x 10^6/ft)							
				0.50	0.80	0.90	0.95	1.00	1.05	1.10	1.30
0	0	0	1.0000	x	x	x	x	x		x	x
1	1.00	2.5	0.9126	x	x	x	x	x		x	x
2	1.00	5.0	0.8249	x	x	x	x	x		x	x
3	1.00	7.5	0.7366	x	x*	x	x	x*		x	x*
4	0.50	5.0	0.9124	x	x	x	x	x		x	x
5	1.35	5.0	0.7637	x	x	x	x	x		x	x
6	1.70	5.0	0.7024	x	x	x	x	x	x	x	x
7	0.45	18.4	0.7000	x	x	x	x	x		x	x
8	0.85	10.0	0.7000	x	x	x	x	x		x	x
9	1.25	6.9	0.7000	x	x	x	x	x	x	x	x

*Also tested at Re = 2.4 x 10^6/ft

NOMENCLATURE

A	Reference area, model maximum cross-sectional area, 23.715 in.^{2}
C_m	Pitching-moment coefficient, pitching moment/$q_\infty Ad$
C_{m_α}	Pitching-moment coefficient derivative at $\alpha = 0$, $\partial C_m/\partial\alpha$, per deg
C_N	Normal-force coefficient, normal force/$q_\infty A$
C_{N_α}	Normal-force coefficient derivative at $\alpha = 0$, $\partial C_N/\partial\alpha$, per deg
C_n	Yawing (Magnus)-moment coefficient, yawing moment/$q_\infty Ad$ (see Fig. 2)
C_{n_p}	Magnus-moment spin derivative coefficient for $(pd/2V_\infty) < 0.15$ when $\alpha < 4$ deg and for $(pd/2V_\infty) < 0.1$ when $\alpha \geq 4$ deg, $\partial C_n/\partial(pd/2V_\infty)$, per radian
$C_{n_{p_\alpha}}$	Magnus-moment coefficient derivative at $\alpha = 0$, $\partial^2 C_n/\partial(pd/2V_\infty)\partial\alpha$, per radian^2
C_Y	Side (Magnus)-force coefficient, side force/$q_\infty A$ (see Fig. 2)
C_{Y_p}	Magnus-force spin derivative coefficient for $(pd/2V_\infty) < 0.15$ when $\alpha < 4$ deg and for $(pd/2V_\infty) < 0.1$ when $\alpha \geq 4$ deg, $\partial C_Y/\partial(pd/2V_\infty)$, per radian
$C_{Y_{p_\alpha}}$	Magnus-force coefficient derivative at $\alpha = 0$, $\partial^2 C_Y/\partial(pd/2V_\infty)\partial\alpha$, per radian^2

d	Reference diameter, model maximum diameter, 5.495 in.
d_B	Base diameter, calibers (note: one caliber = 5.495 in.)
ℓ	Model length, 28.662 in.
ℓ_{BT}	Boattail length, calibers (note: one caliber = 5.495 in.)
ℓ_c	Length of cylindrical section, calibers (note; one caliber = 5.495 in.)
M_∞	Free-stream Mach number
p	Model spin rate (positive, clockwise viewing from the base), radians/sec
p_o	Tunnel stilling chamber pressure, psia
$pd/2V_\infty$	Spin parameter, radians
q_∞	Free-stream dynamic pressure, psia
Re	Free-stream unit Reynolds number, ft^{-1}
Re_ℓ	Free-stream Reynolds number based on model length (ℓ)
T_o	Tunnel stilling chamber temperature, °R
V_∞	Free-stream velocity, ft/sec
$(X_{cp}/d)_N$	Center of pressure in the pitch plane in calibers from the nose (note: caliber = 5.495 in.), $X_{MR} - (C_{m_\alpha}/C_{N_\alpha})_{\alpha=0}$

$(X_{cp}/d)_Y$	Magnus center of pressure in calibers from the nose (note: caliber = 5.495 in.), $X_{MR} - \left(Cn_{p_\alpha} / Cy_{p_\alpha}\right)_{\alpha=0}$
X_{MR}	Moment reference point in calibers from the nose, 3.216 calibers
α	Angle of attack, deg
δ_{BT}	Boattail angle, deg